Model-based investigation of nitrogen and oxygen cycles in the oxygen minimum zone of the eastern tropical South Pacific

Dissertation

zur Erlangung des Doktorgrades

der Mathematisch-Naturwissenschaftlichen Fakultät

der Christian-Albrechts-Universität

zu Kiel

vorgelegt von

Bei Su

Kiel, 2015

Referent: Prof. Dr. Andreas Oschlies
Korreferent: Dr. Markus Pahlow

Tag der mündlichen Prüfung: 29. 06. 2015

Zum Druck genehmigt: 29. 06. 2015

gez. Prof. Dr. Wolfgang J. Duschl, Dekan

Contents

Summary

Nitrogen is an essential nutrient for controlling marine primary production. Its cycling in the ocean is tightly associated with primary gain and loss processes, including nitrogen fixation, atmospheric deposition, water-column and benthic denitrification, and anaerobic ammonium oxidation (anammox). Oxygen minimum zones (OMZs) in the ocean are usually defined to be water columns with O_2 concentration below 20 µmol kg^{-1}. OMZs currently account for only about 8 % of the global ocean area, but could be responsible for as much as 30–50 % of the total fixed-N loss, mainly in form of N_2, into the atmosphere by denitrification or anammox. The eastern tropical South Pacific (ETSP), encompassing one of the permanent OMZs in the ocean, is responsible for about 10% of all fish catch in the global ocean. The NO_3^- and O_2 circulation and budget in this region have a high scientific relevance. This dissertation employs both 2-D box modelling and 3-D coupled phyisical-biogeochemical modelling to better understand important NO_3^- and O_2 cycles and budgets in the ETSP.

A simple steady-state box model of a coastal OMZ by Canfield [2006] shows that a positive feedback between N_2 fixation and denitrification could strip the OMZ of all fixed nitrogen when N_2 fixation is permitted to restore the nitrate : phosphate ratio to Redfield proportions in the surface ocean. Observed concentrations of fixed-N (nitrate plus nitrite) in OMZ waters, however, typically range from about 15 to 40 μmol kg^{-1}. We develop a 2-D prognostic box model to examine under which conditions the observed situation of an essentially complete drawdown of subsurface oxygen and an incomplete drawdown of nitrate can be reproduced for the case of the ETSP. The optimum model configuration indicates that the fixed-N inventory can be stabilized at non-zero levels in the ETSP OMZ only if the remineralization rate via denitrification is slower than that via aerobic respiration. For the current notion of nitrogen fixation being favoured in N-deficit waters, the water column of the ETSP could be a small net source of nitrate.

Both atmospheric deposition and benthic remineralization influence the marine nitrogen cycle, and hence ultimately also marine primary production. With the optimum configuration of the 2-D prognostic model, the biological and biogeochemical responses of the ETSP to these processes are analysed. Sensitivity analyses of the local response to both atmospheric deposition and benthic remineralization indicate a nitrogen-balancing mechanism in the ETSP, which tends to keep a balanced nitrogen inventory, e.g., nitrogen input by atmospheric deposition is counteracted by decreasing nitrogen fixation; NO_3^- loss via benthic denitrification is partly compensated by increased nitrogen fixation; enhanced nitrogen fixation by phosphate regeneration is partly removed by the stronger water-column denitrification. Even though the water column of our model domain acts as a NO_3^- source, considering benthic denitrification, the ETSP could become a NO_3^- sink.

Based on the important role of the southern boundary on the oxygen and nutrient contents of

the ETSP found in the box model, a configuration of the same region is built with the high-resolution hydrodynamic model ROMS (*Regional Ocean Modelling System*) [Shchepetkin and McWilliams, 2005], coupled with the biogeochemical model PISCES (*Pelagic Interaction Scheme for Carbon and Ecosystem Studies*) [Aumont and Bopp, 2006]. A validation against in situ observations shows a realistic simulation of the horizontal and vertical oxygen and nutrient distributions by the standard configuration. In the idealised model configurations, designed to investigate the role of southern boundary conditions on the oxygen, nitrate and phosphate variations of the ETSP, the southern boundary is found to have a significant influence on their contents and distributions. Lateral fluxes indicate that our model domain is gaining O_2 and losing NO_3^- and PO_4^{3-} through the southern boundary. The southern boundary is found to have a more significant influence on O_2 concentration of the deep layer than the upper layer, suggesting a pathway of deep northward intrusion of well-oxygenated southern waters. The Southern Ocean is thought to be sensitive to global warming due to reductions in deep convection, resulting in significant decrease in O_2 concentrations. This study might give some insights into the impacts of Southern Ocean variations under climate change on the O_2 and nutrient changes of the ETSP.

The mechanisms of the stabilised nitrogen inventory in the OMZ of the ETSP are investigated in the box model, i.e., reduced remineralization rate under suboxic conditions is responsible for the essentially complete drawdown of subsurface oxygen and an incomplete drawdown of nitrate, and the nitrogen fixation and water-column denitrification adjust to counteract the additional nitrogen input via nitrogen deposition and nitrogen removal via benthic denitrification. In the high-resolution coupled physical-biogeochemical model, the stabilised nitrogen inventory is observed in the OMZ of the ETSP even though the remineralisation rates of denitrification and aerobic respiration are identical. Dissolved organic matter (DOM) is found to be exported out of the model domain, which could explain the stabilised nitrogen inventory, because DOM cycling is thought to be capable of promoting the spacial decoupling of nitrogen fixation and denitrification, and allowing for negative feedbacks stabilising the nitrogen inventory [Landolfi et al., 2013].

Zusammenfassung

Stickstoff ist ein essentieller Nährstoff in der Kontrolle der marinen Primärproduktion. Seine Zirkulation im Ozean ist eng mit primären Zuwachs- und Verlustprozessen wie Stickstofffixierung, atmosphärischer Deposition, Denitrifizierung in der Wassersäule und benthischer Denitrifizierung, und anaerober Ammoniumoxidation (anammox), verbunden. Sauerstoffminimumzonen (OMZs) im Ozean sind für gewöhnlich als Wassersäulen, in denen die O_2-Konzentration unter 20 µmol kg^{-1} liegt, definiert. Aktuell erstrecken sich OMZs nur über 8 % der globalen Ozeanfläche, sie könnten jedoch für bis zu 30–50 % des gesamten Verlustes an fixiertem Stickstoff an die Atmosphäre, hauptsächlich in Form von N_2, durch Denitrifizierung oder anammox verantwortlich sein. Aus dem östlichen tropischen Südpazifik (ETSP), wo sich eine der permanenten OMZs im Ozean befindet, stammen über 10% der globalen Fischereierträge. NO_3^-- und O_2-Zirkulation und -Haushalt in dieser Region haben hohe wissenschaftliche Relevanz. Diese Dissertation verwendet sowohl 2-D box modelling als auch 3-D gekoppelte physikalisch-biogeochemische Modellierung um wichtige NO_3^-- und O_2-Kreisläufe und -Etats im ETSP besser zu verstehen.

Ein einfaches steady-state Box-Modell einer küstennahen OMZ von Canfield [2006] zeigt, dass eine positive Rückkopplung zwischen Stickstofffixierung und Denitrifizierung den gesamten fixierten Stickstoff aus der OMZ herausziehen könnte, wenn es der Stickstofffixierung erlaubt ist, das Nitrat:Phosphat Verhältnis zu Redfield Verhältnissen im Oberflächenozean wiederherzustellen. Beobachtete Konzentrationen fixierten Stickstoffes (Nitrat plus Nitrit) in OMZ-Gewässern erstrecken sich jedoch typischerweise über einen Bereich von 15 bis 40 μmol L^{-1}. Wir entwickeln ein prognostisches 2-D Box-Modell um zu untersuchen, unter welchen Bedingungen die beobachtete Situation einer im Wesentlichen totalen Absenkung des Sauerstoffs unter der Oberfläche und einer unvollständigen Absenkung des Nitrats für den Fall des ETSP reproduziert werden kann. Die optimale Modellkonfiguration weist darauf hin, dass der Etat des fixierten Stickstoffs in der ETSP OMZ nur dann auf von Null verschiedenen Niveaus stabilisiert werden kann, wenn die Remineralisierungsrate durch Denitrifizierung kleiner ist als die durch aerobe Atmung. Nach der aktuellen Auffassung, dass Stickstofffixierung in N-defizitären Gewässern begünstigt wird, könnte die Wassersäule des ETSP eine kleine Nitrat-Nettoquelle sein.

Sowohl atmosphärische Deposition als auch benthische Remineralisierung beeinflussen den marinen Stickstoffkreislauf und damit letztendlich auch die marine Primärproduktion. Mit der optimalen Konfiguration des prognostischen 2-D Modells werden die biologischen und biogeochemischen Reaktionen des ETSP auf diese Prozesse analysiert. Sensitivitätsanalysen der lokalen Reaktion auf atmosphärische Deposition und benthische Remineralisierung zeigen einen stickstoff-ausgleichenden Mechanismus im ETSP auf, der dazu tendiert, den Stickstoffetat im Gleichgewicht zu halten: dem Stickstoffeintrag durch atmosphärische Deposition wird zum Beispiel durch abnehmende Stickstofffixierung entgegengewirkt; der NO_3^- Verlust durch

benthische Denitrifizierung wird teilweise durch gesteigerte Stickstofffixierung kompensiert; die erhöhte Stickstofffixierung durch Phosphatregeneration wird teilweise durch stärkere Denitrifizierung in der Wassersäule beseitigt. Obwohl die Wassersäule in unserem Modell eine NO_3^--Quelle darstellt, könnte der ETSP, betrachtet man benthische Denitrifizierung, eine NO_3^--Senke sein.

Basierend auf der Entdeckung der wichtigen Rolle des südlichen Ozeans auf den Sauerstoff- und Nährstoffgehalt des ETSP durch das Box-Modell, wird eine Konfiguration der selben Region mit dem hochauflösenden hydrodynamischen Modell ROMS (*Regional Ocean Modelling System*) [Shchepetkin and McWilliams, 2005], gekoppelt mit dem biogeochemischen Modell PISCES (*Pelagic Interaction Scheme for Carbon and Ecosystem Studies*) [Aumont and Bopp, 2006], erstellt. Eine Validierung gegen in situ Beobachtungen zeigt eine realistische Simulation der vertikalen und horizontalen Verteilungen von Sauerstoff und Nährstoffen durch die Standardkonfiguration. In den idealisierten Modellkonfigurationen, die zur Untersuchung der Rolle der südlichen Randbedingungen auf die Sauerstoff-, Nitrat- und Phosphatvariationen des ETSP entwickelt wurden, zeigt sich, dass der südliche Gebietsrand einen signifikanten Einfluss auf deren Gehalt und Verteilungen hat. Die lateralen Flüsse weisen darauf hin, dass unser Modellgebiet O_2 durch den südlichen Rand erhält und dort NO_3^- sowie $PO_4{}^{3-}$ verliert. Es stellt sich heraus, dass der südliche Rand einen signifikanteren Einfluss auf die O_2-Konzentrationen in der tieferen Schicht als in der oberen Schicht hat. Dies weist auf einen nordwärts gerichteten Eintragsweg von sauerstoffreichem südlichem Wasser hin. Es wird angenommen, dass der südliche Ozean durch Reduktion in der tiefen Konvektion, die in einer signifikanten Abnahme der O_2-Konzentrationen resultiert, empfindlich auf die globale Erwärmung reagiert. Diese Studie könnte Einsichten in die Auswirkungen von Veränderungen im südlichen Ozean durch die zukünftige Klimaveränderung auf die O_2 und Nährstoffvariationen im ETSP geben.

Die Mechanismen des stabilisierten Stickstoffinventars in der OMZ des ETSP werden im Box-Modell untersucht, dass heißt, die reduzierte Remineralisierungsrate unter suboxischen Bedingungen ist für den im Wesentlichen totalen Verbrauch des Sauerstoffs unter der Oberfläche und den unvollständigen Verbrauch des Nitrats verantwortlich, und die Stickstofffixierung und Denitrifizierung in der Wassersäule regulieren sich dahingehend, den zusätzlichen Stickstoffeintrag via Stickstoffdeposition und Stickstoffentfernung via benthische Denitrifizierung auszugleichen. Im hochauflösenden gekoppelten physikalisch-biogeochemischen Modell wird das stabilisierte Stickstoffinventar in der OMZ des ETSP trotz einer identischen Remineralisierungsrate von Denitrifizierung und aerober Respiration beobachtet. Gelöste organische Stoffe (DOM) werden aus dem Modellgebiet exportiert, wodurch das stabilisierte Stickstoffinventar erklärt werden könnte, da die DOM-Zirkulation als geeignet dafür angesehen wird, die räumliche Entkopplung von Stickstofffixierung und Denitrifizierung zu fördern, und so negative Rückkopplungen, die zur Stabilisierung des Stickstoffinventars führen, zu ermöglichen [Landolfi et al., 2013].

Chapter 1

Introduction

1.1 The nitrogen cycle in the ocean

1.1.1 The importance of fixed-nitrogen for primary production in the ocean

Nitrogen is an essential component of cells and enzymes responsible for synthetic and metabolic processes of organisms. In the ocean, bioavailable fixed-nitrogen is considered an essential nutrient for marine primary production. Due to the fixed-nitrogen loss via denitrification or anammox in form of N_2 or N_2O in O_2-deficit environments, fixed-N is a primary limiting nutrient in the ocean.

1.1.2 Nitrogen species and their transformations in the ocean

In the ocean, nitrogen exists in more chemical forms than most other elements. Most transformations among different species are undertaken by marine organism as part of their metabolism, either to take up nitrogen for organism structure, or to obtain energy for metabolism [Gruber, 2008a]. There are five relatively stable states in the marine environment: the fixed nitrate (NO_3^-), nitrite (NO_2^-), nitrous oxide (N_2O), and ammonium (NH_4^+); and unfixed dinitrogen (N_2). All of these inorganic species are available for non-diazotrophic phytoplankton except N_2 as the most abundant species, which is only available for diazotrophic phytoplankton. There are also many organic compounds in the ocean containing nitrogen, most of which are in the form of amino-groups.

The main transformations among different species are summarised in Figure. 1.1. In the euphoric zone, where there is enough light to support photosynthesis, the assimilation of NH_4^+ and NO_3^- to form organic nitrogen performed by marine phytoplankton is the dominant process in the marine nitrogen cycle. This can satisfy their nitrogen demand and fuel the marine

primary production [Gruber, 2008a]. Phytoplankton are thought to preferentially take up NH_4^+, because its assimilation is more energy-efficient. N_2 fixation by diazotrophic phytoplankton is the main process in the ocean to transform N_2 to bioavailable fixed-Nitrogen.

The organic matter of phytoplankton, which can be transferred to zooplankton and higher-trophic levels in the marine food web, is mainly returned to the environment by remineralization. Under oxic conditions, the organic matter is remineralized to NH_4^+ initially (named "ammonification"), and then oxidised to NO_3^- through nitrification. The remineriliza tion processes for organic nitrogen under anoxic conditions are more diverse and difficult to quantify. Denitrification is thought to be the canonical pathway responsible for anaerobic remineralisation, transferring bioavailable NO_3^- to biounavailable N_2 (Eq. 1.1) [Falkowski, 1997]. Anammox was discovered later as another new pathway responsible for the production of N_2 in the ocean (Eq. 1.2) [Kuypers et al., 2003]. N_2O (not shown in Fig. 1.1), a strong greenhouse gas which is thought to be 200 times more potent than CO_2, acts as an intermediary for both nitrification and denitrification, but the the relative contributions of these two processes are still debated [Jin and Gruber, 2003].

$$C_{106}H_{175}O_{42}N_{16}P + 104HNO_3 = 106CO_2 + 60N_2 + H_3PO_4 + 138H_2O \tag{1.1}$$

$$NO_2^- + NH_4^+ = N_2 + 2H_2O \tag{1.2}$$

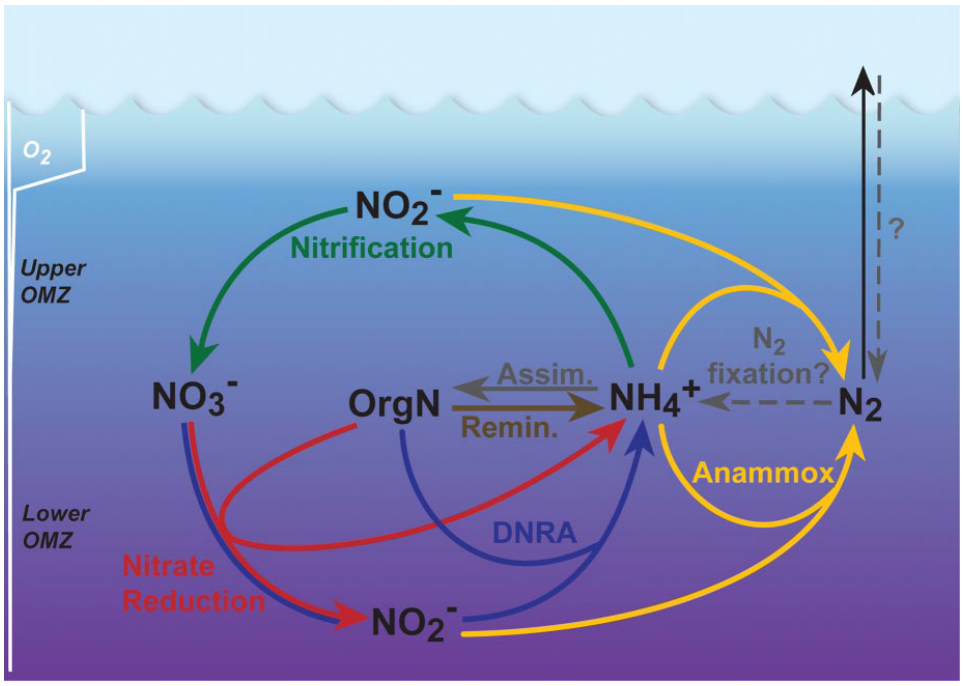

Figure 1.1: Schematic summary of nitrogen cycle in the ocean [Lam et al., 2009].

1.1.3 Distribution of fixed-nitrogen in the ocean

Global scale

The distribution of different fixed-nitrogen species in the ocean is mainly connected to the biological processes and the physical circulation. Many data exist for profiles of NO_3^- and NO_2^-, but only sparse data for NH_4^+.

The vertical profile of NO_3^- follows a prevalent pattern of depletion at the surface and repletion in the deep ocean, which is due to biological uptake by phytoplankton in the surface ocean and remineralization at depth (left graph of Fig. 1.2). Different from NO_3^-, NO_2^- and NH_4^+ concentrations reach maxima at about 50 to 80 meter (lower or bottom part of the euphoric zone), and then decrease rapidly below (left graph of Fig. 1.2). For NO_2^-, the maximum occurs at the bottom of euphotic zone or below (right graph of Fig. 1.2), where light is low enough to prevent nitrification limitation and NO_2^- is produced during nitrification. The NH_4^+ maximum is at the deeper part of euphotic zone where there is rapid recycling of organic matter (OM) via remineralization, liberating much of NH_4^+ (right graph of Fig. 1.2). At the lower part of euphotic zone, photosynthesis may be limited partly by irradiance making generation of NH_4^+ exceed its consumption.

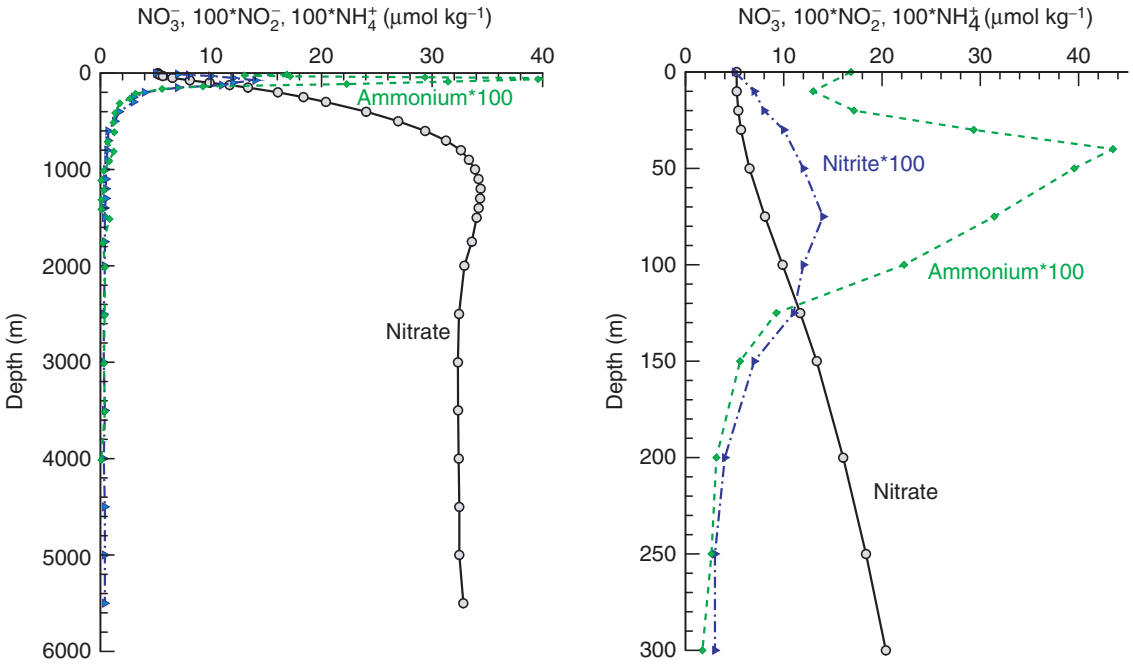

Figure 1.2: Global mean profile of fixed-nitrogen for the entire water volume and top 300 meter [Gruber, 2008a].

The NO_3^- concentration in the surface ocean is extremely low except in the low-latitude upwelling regions, including the Southern Ocean, part of the North Pacific and the equatorial

Pacific. Nitrate, together with other nutrients, is upwelled into the surface ocean in the upwelling regions, which can support high primary production. However, even though there is enough fixed-nitrogen in the surface ocean of the three regions mentioned above, there are still low-chlorophyll concentrations there. These are referred as High-Nutrients Low-Chlorophyll (HNLC) regions. The micronutrient iron is thought to be the main limiting factor in HNLC regions [Aumont and Bopp, 2006, Okin et al., 2011]. NO_2^- and NH_4^+ concentrations in the ocean are almost three orders of magnitude lower than that of NO_3^-. Thus, we mainly focus on NO_3^- in our work.

Eastern Tropical South Pacific (ETSP)

The ETSP hosts one of the major permanent OMZs in the ocean. Due to the high rate of organic matter decomposition and insufficient ventilation, the oxygen minimum zone ensues, concomitant with fixed-N loss in form of N_2 or N_2O by denitrification or anammox. Even though there is fixed-N loss in the O_2-deficit region, the NO_3^- concentration in the ETSP ranges roughly from 15 to 45 µmol kg^{-1}[Codispoti and Christensen, 1985, Chang et al., 2010].

Usually, NH_4^+ concentrations are almost undetectable in coastal upwelling regions except in some parts of the lower euphotic zone and the bottom water of the continental shelf. Uniquely, there is a relatively large amount of NH_4^+ provided by excretion from anchovy in the upwelling region off Peru [Gruber, 2008b]. The relative high concentration of NH_4^+ can also be caused by the dissimilatory nitrate reduction to ammonium (DNRA) in the sediment [Bohlen et al., 2012].

1.1.4 Fixed-N budget in the ocean

Nitrogen is thought to be the proximate limiting nutrient for growth of phytoplankton, thus, the nitrogen budget and its spatio-temporal distribution are crucial for marine primary production. The fixed-N inventory in the ocean is determined by the differences between sources and sinks. Due to the large-scale of the different processes and lack of enough measurements, various biogeochemical models coupled with hydrodynamic models are employed to estimate the quantity of different sources and sinks of fixed-nitrogen besides in-situ observations. Here we outline the most known sinks and sources estimated from both models and observations.

Sources

N_2 fixation

In the last decades, tremendous progress has been made in quantifying N_2 fixation rates and organisms responsible for fixing atmospheric N_2 both in sediments and the pelagic ocean [Carpenter, 1983, Capone et al., 1997, Montoya et al., 2004]. Macrophyte communities, microbial

mats and coral reef associated habits are found to be responsible for benthic nitrogen fixation. In the water column, early research mainly focused on cyanobacterium *Trichodesmium* [Karl et al., 2002], however, subsequent discoveries have shown that unicellular coccoid cyanobacteria, and certain diatom- or dinoflagellate-symbiont cyanobacteria can also express nitroganase, enriching the diversity of N_2 fixers [Carpenter and Capone, 2008, Montoya et al., 2004, Foster and Zehr, 2006]. Since oceanic nitrogen fixation is also affected by temperature, light, oxygen, turbulence, trace metals and inorganic nutrients (e.g. phosphate), estimating its rate is a huge challenge.

Due to the large spatial and temporal variability and continuing discoveries of new species responsible for N_2 fixation, there are still considerable uncertainties in the estimates for the global and large-scale regional rates of N_2 fixation. The estimated global rates have increased from about 5 $\mathrm{Tg\,N\,yr^{-1}}$ to about 300 $\mathrm{Tg\,N\,yr^{-1}}$ [Capone and Budin, 1982, Brandes and Devol, 2002]. Most recent biogeochemical model results indicate a range of 100-300 $\mathrm{Tg\,N\,yr^{-1}}$, which results from insufficiently constrained biogeochemical parameters [Codispoti et al., 2001, Gruber, 2004, Deutsch et al., 2007, DeVries et al., 2012]. It is also difficult to estimate the N_2 fixation rate in upwelling regions such as the ETSP, the ETNP and the Arabian Sea. New measurement methods and discoveries of new species for N_2 fixation will probably allow better constraints for the oceanic N_2-fixaion rate [Foster et al., 2011, Großkopf et al., 2012] .

Atmospheric nitrogen deposition

In the last few decades, a number of investigations have been carried out on the role of atmospheric fixed-nitrogen input into the ocean on marine biogeochemical cycles [Duce, 1986, Duce et al., 1991, Krishnamurthy et al., 2007, 2010, Okin et al., 2011]. Duce et al. [2008] indicate that the anthropogenic nitrogen deposition input is rapidly approaching the global oceanic estimates for N_2 fixation, arising from an order of magnitude lower than N_2 fixation at the pre-industrial stage. However, the response of nitrogen-fixation and denitrification to atmospheric nitrogen deposition remains an open question. Inorganic nitrogen, from fossil fuel combustion, biomass burning, soil emission and breakdown of urea from domestic animals [Warneck, 1988], dominates atmospheric nitrogen inputs into the global ocean [Paerl and Whitall, 1999]. The species of nitrogen from deposition of Lamarque et al. [2011] only include inorganic NOy and NHx. The magnitude of dissolved organic nitrogen (DON) deposition is not clear due to lack of observations [Cornella et al., 2003, Duce et al., 2008, Zamora et al., 2011]. Even though phytoplankton can take up DON [Seitzinger and Sanders, 1999, Duarte et al., 2006, Duce et al., 2008], the contribution of DON to total nitrogen deposition is still debated [Duce et al., 2008, Zamora et al., 2009] and the distribution, bioavailability and lifetime are also not clear. Therefore, including DON deposition in the analysis is still challenging.

Riverine discharge

A significant quantity of nitrogen from land, mainly from fertilizer use, fossil fuel combustion and biological nitrogen fixation, is transported from the continents via rivers into the coastal

oceans [Boyer et al., 2006]. The riverine nitrogen discharge into the ocean includes dissolved inorganic nitrogen (DIN), dissolved organic nitrogen (DON) and particulate nitrogen (PN). There is a large uncertainty in quantifying riverine nitrogen input into the ocean at global and regional scales due to the coarse resolution of available data, land characteristics and associated assumptions about their hydraulic characteristics, vague nitrogen transportation processes and insufficient measurements for riverine nitrogen loads [Boyer et al., 2006]. Based on current comprehensive assumptions and empirical models, the global riverine nitrogen input is estimated from 40 to 66 Tg N yr^{-1} [Green et al., 2004, Seitzinger et al., 2005].

The integrated model of Seitzinger et al. [2010] indicates that south Asia is a region responsible for major riverine nitrogen export to the coastal ocean, however, south America together with Africa show the largest increases in DIN input in the past 30 years and in the coming 30 years. The ETSP will probably receive more riverine nitrogen input in the future and riverine nitrogen input will account for more contribution to nitrogen sources in ETSP.

Sinks

In the global marine environment, water-column denitrification and anammox in OMZs, together with benthic denitrification, determine the magnitude of fixed-nitrogen loss, in which benthic denitrification is considered a major fixed-nitrogen loss process [Codispoti et al., 2001, Galloway et al., 2004, Gruber, 2004, Codispoti, 2007, Somes et al., 2013].

Water-column denitrification and anammox

OMZs play an important role in the global marine fixed-nitrogen budget as they are sites responsible for a large fraction of total marine fixed-N loss [Canfield, 2006]. The relative contribution of heterotrophic denitrification and autotrophic anammox to the total oceanic fixed-nitrogen sink remains debated [Kuypers et al., 2005, Lam et al., 2009, Ward et al., 2009]. Even though autotrophic anammox has been suggested to be responsible for most of the fixed-N loss in the ETSP [Lam et al., 2009, Kalvelage et al., 2013], anammox is ultimately driven by the flux of organic matter into the OMZ as heterotrophic remineralization of organic matter supplies the necessary substrates for it [Koeve and Kähler, 2010, Kalvelage et al., 2013]. Thus, heterotrophic denitrification is considered as the major fixed-nitrogen loss process in the present study.

Whether canonical denitrification or anammox is dominant in marine fixed-nitrogen loss still remains uncertain, since they require and happen in the same environmental conditions. Most estimates for total N-loss in the water column based on models and in-situ observations lie between 50–150 Tg N yr^{-1} [Gruber, 2004, Codispoti, 2007].

Benthic denitrification

A high rain rate to the sediment can drive microorganisms to use up all O_2 and result in an anaerobic sediment environment, which provides conditions for fixed-nitrogen loss. Continental shelves and the upper continental slopes are thought to be the most important sites for benthic fixed-nitrogen loss [Christensen et al., 1987, Devol, 1991]. Bohlen et al. [2011] found that the anaerobic continental shelf and upper continental slope of the ETSP across a section at 11°S are sites of fixed-nitrogen recycling rather than nitrogen loss, because of relatively low rates of denitrification and high rates of NH_4^+ release from Dissimilatory Nitrate Reduction to Ammonium (DNRA). Besides, the contribution of open-ocean sediments is still uncertain. Because of the large uncertainties, the global benthic denitrification rate is estimated in a large range from about 60 [Codispoti and Christensen, 1985] to more than 300 Tg N yr^{-1} [Codispoti, 2007].

1.1.5 The sensitivity of the marine nitrogen-cycle to phosphate in the ocean

Compared with the nitrogen cycle, the phosphorus cycle in the ocean is relatively simple, because P has no gas phase and only one valence (+5) in its compound forms. The main global sources of P into the ocean are thought to be river runoff, atmospheric deposition and volcanic sources, among which river runoff is thought to be most significant. Sedimentary burial is the dominant loss pathway for P. In the sediment under anoxic conditions, P regeneration provides extra inorganic P release into the water column from the sediment [Wallmann, 2010].

Both N and P are essential macronutrients for growth of phytoplankton in the ocean. According to the classical Redfield ratio, the N:P stochiometry 16 is regarded as the criteria to differentiate between N limitation and P limitation in the ocean [Redfield, 1934]. A ratio less that 16 is assumed to indicate N limitation, and a ratio larger than 16 is assumed to indicate P limitation. There are debates about which nutrient, P or N, controls primary production in the ocean. The geological viewpoints support that P is the limiting nutrient because N can be supplied by nitrogen fixation when it limits the growth of phytoplankton and the residence time of P is much longer than that of N in the ocean [Ruttenberg, 2003]. Fixed-nitrogen is thought to be the limiting nutrient by biologists because there is a relatively low N:P ratio in many surface ocean regions and nitrogen enrichment experiments do enhance primary production there [Falkowski et al., 1998, Garcia et al., 2010b]. Tyrrell [1999] uses a model to indicate that N is the proximate limiting nutrient in the ocean, while P is considered as the ultimate limiting nutrients for primary production. There is evidence that P is the limiting nutrient for nitrogen fixation in the North Atlantic and North Pacific [Karl et al., 1997, Wu et al., 2000], thus, the addition of P into these regions could enhance the biological fixed-nitrogen input into ocean.

P regeneration has been found on the continental shelf off California and off the Perivian coast, where anoxic bottom water enhances P release from sediments receiving a high rain rate [Ingall and Jahnke, 1994]. The enhanced release of P from the sediment can also enhance primary

production, which could in turn stimulate oxygen depletion in bottom waters significantly, thereby providing further P addition for primary production [Ingall et al., 1993]. The intensification of anoxic conditions in the coastal ocean due to anoxic P regeneration could also have significant influence on the nitrogen cycle in these regions.

1.2 Oxygen minimum zones (OMZs) in the ocean

1.2.1 Definition and Characteristics

Since the expression of "OMZ" appeared in Cline and Richards [1972], Oxygen minimum zones (OMZs), characterized as O_2-deficit water columns, receive much attention in the present ocean research. Commonly, an OMZ is defined as water with O_2 concentration less than 20 µmol kg^{-1}, but this threshold is still a matter of debate [Paulmier and Ruiz-Pino, 2009, references therein]. For example, it has been suggested that denitrification, which is O_2-dependent, can be the criterion for defining the extent of an OMZ [Paulmier and Ruiz-Pino, 2009].

1.2.2 OMZ distribution in the ocean

Using the global World Ocean Atlas 2005 (WOA2005) O_2 climatology, four major tropical OMZs in the open ocean have been described by Paulmier and Ruiz-Pino [2009]: the eastern tropical South Pacific (ETSP) and eastern tropical North Pacific (ETNP), in the Pacific Ocean; the Arabian Sea (AS) and Bay of Bengal (BB), in the Indian Ocean (Fig. 1.3). More recently, the eastern sub-tropical North Pacific ($25 - 52°N$) has been identified as another permanent deep OMZ. Two additional seasonal OMZs at high latitudes have also been identified: the western Bering Sea and the Gulf of Alaska. The total ocean area and volume occupied by the most intense OMZs (O_2<20 µmol kg^{-1}) have been evaluated by WOA 2005 data analysis [Paulmier and Ruiz-Pino, 2009]: 30.4 ±3 million km^2 and 102±15 million km^3, accounting for, 8% and 1% of the global ocean area and volume respectively.

Paulmier et al. [2006] demonstrate that there are at least three layers in the structure of OMZs when analyzing the OMZ in the ETSP off Chile: the oxycline with an extremely high O_2 gradient, the core with O_2 concentration less than 20 µmol kg^{-1}, and a deep O_2 gradient. The oxycline is thought to be the region where most intensive remineralization occurs [Brandes et al., 2007]. The structure of the OMZ-core is diverse. The core of the OMZ in the eastern tropical Pacific is thought to lie between 150 and 400 meter, with an oxygen minimum of 0.1 µmol kg^{-1} [Karstensen et al., 2008]. The OMZ core of the Indian Ocean corresponds to depths between 100 and 650 meter and reaches O_2 values as low as 0.3 µmol kg^{-1} [Morrison et al.,

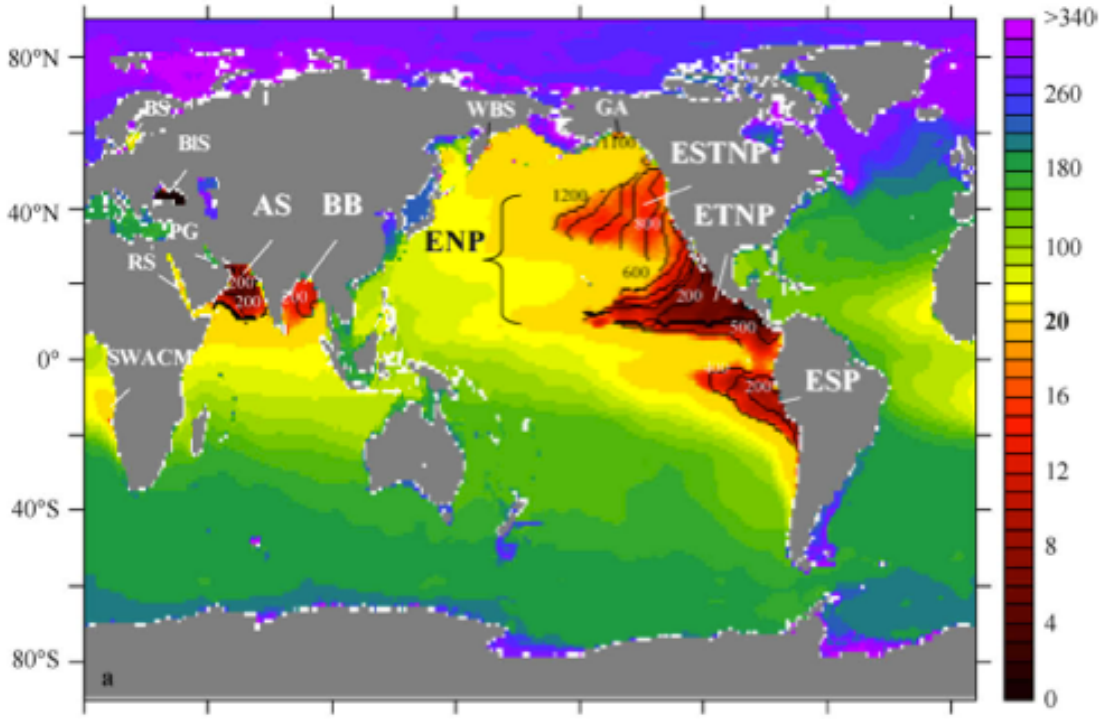

Figure 1.3: OMZs distribution in the ocean [Paulmier and Ruiz-Pino, 2009].

1999]. There is no suboxic zone (<20 µmol kg^{-1}) in Atlantic Ocean, where the O_2 concentration minimum corresponds to a depth of about 420 and 400 meter, respectively, in the North and South Atlantic (O_2>40 µmol kg^{-1} in the north; >20 µmol kg^{-1} in the south, except in some areas over the continental margin where O_2 reaches 17–18 µmol kg^{-1}).

1.2.3 Importance of OMZs and their significance for the marine nitrogen cycle

The intensity of perturbations of OMZs and their potential influence on the marine biogeochemical cycle and ecosystems depend on their extent, which can vary in response to climate change, such as lower ventilation due to stratification and decrease of O_2 solubility at higher temperature, and natural or anthropogenic perturbations through limiting nutrient inputs by upwelling, river input or atmospheric dust deposition [Stramma et al., 2008]. These are the keys to understanding the present unbalanced or balanced nitrogen cycle and the role of the ocean in sequestering atmospheric greenhouse gases [Codispoti, 2007, DeVries et al., 2012], since the O_2-deficit in the marine environment is essential for the anaerobic bacteria which can convert fixed-N to N_2 or N_2O via denitrification or anaerobic ammonium oxidation (anammox) [Devol, 2003, Kuypers et al., 2003]. Under O_2-deficit conditions, NO_3^- can replace O_2 as electron acceptor in decomposition of organic matter in denitrification, in which NO_3^- is reduced to N_2 [Devol, 2003]. The bacteria responsible for anammox (e.g., bacteria from the Planctomycetales

order) can oxidize NH_4^+ directly to N_2 with NO_2^- as the electron acceptor [Kuypers et al., 2003].

1.2.4 The oxygen minimum zone of the ETSP

The Humboldt Current System is the most productive eastern boundary current system. This work focuses on the northern part of the Humboldt Current System, the ETSP off Peru, hosting one of the most significant permanent OMZs. The ETSP upwelling region is known as one of the most productive systems of the world ocean, where high export production is decomposed in the water column below, consuming dissolved oxygen. Combined with sluggish ventilation, the high O_2 demand produces the sub-surface OMZ of the ETSP[Hellya and Levin, 2004]. In oxygen-depleted regions, NO_3^- is converted to N_2O or N_2 by canonical denitrification or anammox, thus resulting in a nitrate deficit relative to the Redfield equivalent of phosphate [Codispoti and Christensen, 1985].

Figure 1.4 is a schematic summary of the current systems in the eastern tropical Pacific. Due to the remarkable characteristic of the Peru Current System (PCS) being in proximity and directly connected to the equatorial ocean, the Equatorial Current System (ECS) can not be excluded when the PCS is discussed.

The surface of the PCS is dominated by the Peru Coastal Current (PCC), which is equatorward, with a width of 500-1000 km from the coast [Strub et al., 1998]. The PCC is directly associated with coastal upwelling, thus featuring cold and salty water. It feeds the South Equatorial Current (SEC), which is the westward surface current of the ECS. There is a poleward flow below the PCC dominating the subsurface layer (Fig. 1.4). The Peru-Chile Under Current (PCUC) can extend from 50m to 700m along the western coast of South American with depth increasing toward the south, transporting salty water rich in nutrients and extremely low in O_2 [Wyrtki, 1963, Penven et al., 2005, and references therein]. The PCUC is thought to originate from the eastward Equatorial Under Current (EUC), which splits when arriving at the American landmass. Both the primary South Subsurface Countercurrent (pSSCC) and secondary South Subsurface Countercurrent (sSSCC) could be complementary sources of the PCUC [Lukas, 1986, Montes et al., 2010]. Since the PCUC is thought to be one of the major sources of the upwelled water in the ETSP, its oxygen and nutrient contents are important for the study of the upwelling region and the OMZ below [Penven et al., 2005, and references therein]. The connection between the PCUC and the equatorial eastward subsurface currents (EUC, pSSCC, sSSCC), especially with respect to oxygen and nutrients, is very important for understanding the formation of the OMZ in the ETSP. However, Montes et al. [2010] indicate in a high-resolution regional model that only about 30% of the PCUC is fed by the three subsurface equatorial currents (EUC, pSSCC, sSSCC), among which only the two SSCC contribute substantially. The remaining part of the PCUC comes from an alongshore recirculation associated with flows below and from the southern part of the domain, south of 9°S [Montes et al.,

2010].

Another surface current belonging to the PCS, the offshore Peru Oceanic Current (POC) extends from the surface to a depth of 700m and veers eastward around 15–20°S [Wyrtki, 1963, Penven et al., 2005]. Offshore of the PCC and the PCUC, the Peru-Chile Counter Current (PCCC) is featured by warm water originating from the split of EUC, and ranges between 80°W–84°W and 8°S–35°S [Huyer et al., 1991, Penven et al., 2005]. The PCCC flows southward and reaches a maximum speed of $0.1\,\mathrm{m\,s^{-1}}$ at 50m depth [Huyer et al., 1991]. So far, the connection and exchanges of nutrient and oxygen between the PCCC and the PCUC are not clear.

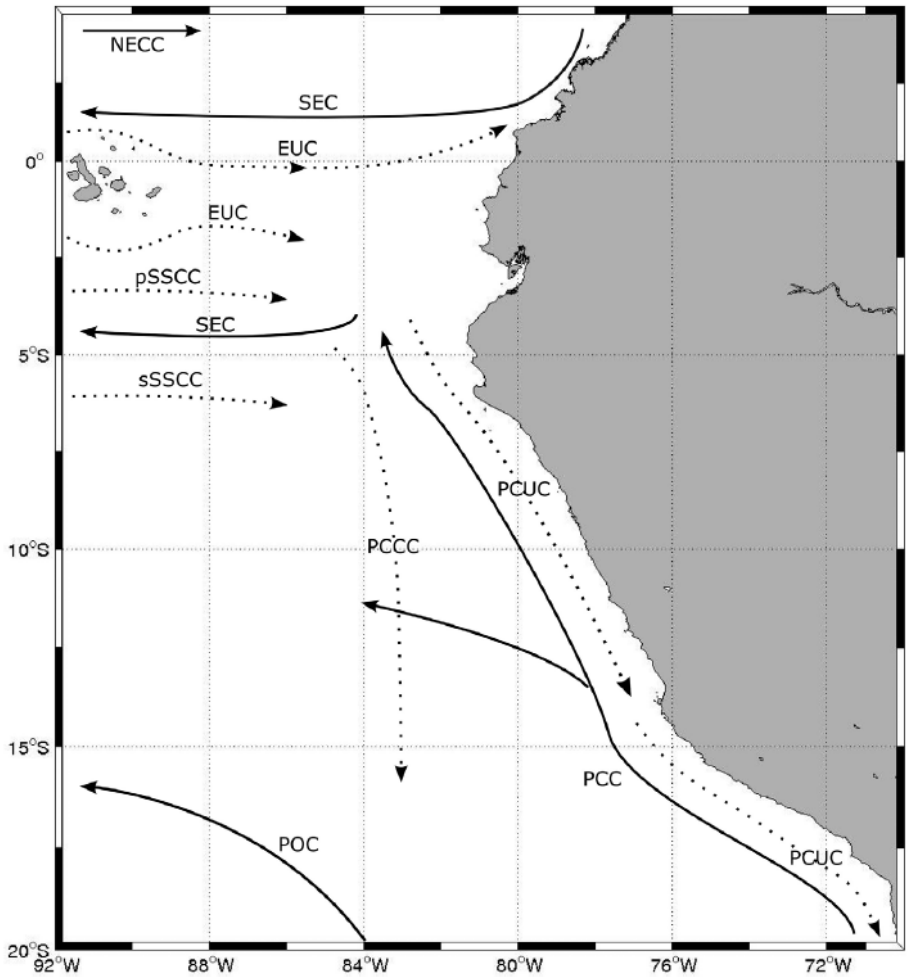

Figure 1.4: Oceanic circulation scheme for the ester tropical Pacific [Montes et al., 2010, and references therein]. Solid lines indicate the surface currents and dotted lines represent subsurface currents. NECC: North Equatorial Countercurrent; SEC: South Equatorial Current; EUC: Equatorial Undercurrent; pSSCC: primary South Subsurface Countercurrent; sSSCC: secondary Southern Subsurface Countercurrent; PCC: Peru Coastal Current; POC: Peru Oceanic Current; PCUC: Peru-Chile Undercurrent; and PCCC: Peru-Chile Countercurrent.

1.3 Models

Two modelling approaches are applied in this dissertation to explore the nitrogen cycle in the OMZ of the ETSP: a fully prognostic 5-box model coupled with a simplified biogeochemical model and the 3-D dynamical regional model ROMS (*Regional Ocean Modelling System*) coupled with PISCES (*Pelagic Interaction Scheme for Carbon and Ecosystem Studies*).

1.3.1 Box model

Even though there are lots of state-of-the-art global circulation models (GCM) available, box models are still popular tools applied to study global and regional marine biogeochemical cycles [Shaffer and Sarmiento, 1995, Tyrrell, 1999, Deutsch et al., 2004, Canfield, 2006, Mills and Arrigo, 2010, Eugster and Gruber, 2012, DeVries et al., 2012], due to their ability to capture the most important first-order characteristics of the system and computational efficiency required for thousands of sensitivity or calibration experiments. Recently, a dynamic 5-box model of the ETSP was presented by Mills and Arrigo [2010] to explore the impact of stoichiometry of dissolved nitrogen and phosphorus utilization by phytoplankton on the magnitude and distribution of nitrogen fixation. Eugster and Gruber [2012] used the 14-box model of Deutsch et al. [2004] to estimate the global marine nitrogen budget mainly determined by the magnitude of N_2-fixation and denitrification.

We developed Canfield's [2006] box model into a fully prognostic box model of NO_3^-, ${PO_4}^{3-}$ and O_2 cycles in a coastal upwelling region and an adjacent ocean basin. Different from Canfield's [2006] model, which includes only the dynamics of the OMZ with all the biogeochemical tracers prescribed in the surrounding waters, our box model represents local as well as spatially-separated feedbacks between the relatively small OMZ and the much larger open-ocean basin. The physical dynamics of our model system is governed by vertical and horizontal mixing and advection, which are calibrated with $\Delta^{14}C$ data from GLODAP [Key et al., 2004].

A simplified biogeochemical model is incorporated, including two phytoplankton species: ordinary phytoplankton, which require both NO_3^- and ${PO_4}^{3-}$ for growth, and nitrogen fixers, which can grow only if ${PO_4}^{3-}$ is available in the ambient environment. There are complex N-cycle biogeochemical models with increasing numbers of compartments developed [Laws et al., 2000, Fennel et al., 2006]. But there are still some suggestions that modellers should stick with simple NPZ and NPZD model, rather than try to 'parameterize'additional food web complexity [Steele, 1998, Pahlow and Vézina, 2003]. In the box model, we keep our biogeochemical model as simple as possible to match the simple physical dynamics.

1.3.2 3-D model

The 3-D model employed in this dissertation is the Reginal Ocean Modelling System (ROMS-AGRIF) [Shchepetkin and McWilliams, 2005] coupled with the biogeochemical model PISCES [Aumont and Bopp, 2006].

ROMS is a new generation ocean circulation model that has been specially designed for accurate simulations of regional systems. A split-explicit, free surface, terrain-following vertical coordinates ocean model which solves the primitive equations of Navier Stokes in the presence of rotation characterises ROMS [Shchepetkin and McWilliams, 2005]. Different from many other oceanic general circulation models, ROMS has sigma vertical coordinate, which is designed to enhance resolution near the sea surface and employs a mode-splitting algorithm to separate the natural time-scale between barotropic and baroclinic processes, by solving the vertically-integrated barotropic momentum equations [Shchepetkin and McWilliams, 2009, Penven et al., 2010].

This work requires a biogeochemical model which can simulate the O_2, NO_3^- and ${PO_4}^{3-}$ cycles of the ETSP, include the explicit processes for the marine nitrogen cycle in the OMZ (denitrification), and also nitrogen-fixation. PISCES, derived from the Hamburg Model of Carbon Cycle (version 5, HAMOCC5), is adequate to reproduce the biogeochemical processes required for the simulation of the ETSP.

PISCES is a biogeochemical model which simulates marine biogeochemical productivity and describes the biogeochemical cycles of carbon and the main nutrients (P, N, Si, Fe) [Aumont and Bopp, 2006]. It includes two phytoplankton types, which correspond to nanophytoplankton and diatoms, and two zooplankton size classes that represent microzooplankton and mesozooplankton. The limiting nutrients for phytoplankton growth include: NO_3^- and NH_4^+, ${PO_4}^{3-}$, Si and Fe. There are three non-living compartments: semi-labile dissolved organic matter, small and big sinking particles. The model also simulates dissolved inorganic carbon, total alkalinity and dissolved oxygen [Aumont et al., 2003]. All the parameters for this region are according to Echevin et al. [2014].

The biogeochemical processes related to the nitrogen cycle include nitrogen fixation, denitrification, nitrification and ammonification in PISCES [Aumont and Bopp, 2006]. Diazotrophic phytoplankton can fix N_2 under the following conditions: 1) water temperature is above $20\,^{\circ}C$, 2) there is insufficient fixed-N in the environment, 3) iron is available. Nitrogen fixation is only restricted to the sea surface and annual total nitrogen fixation should balance denitrification to ensure nitrogen conservation in the model domain. Denitrification ensues when oxygen concentration is under 6 $\mu mol\,kg^{-1}$. Nitrification represents the conversion of NH_4^+ to NO_3^- due to bacterial activity, which is assumed to be photoinhibited and O_2 concentration dependent. Ammonification is responsible for the remineralization of particulate organic matter and dissolved organic matter to NH_4^+.

1.4 Overview of the thesis and author contributions

Nitrogen is an essential nutrient for phytoplankton in the ocean, thus, the bioavailable fixed-nitrogen budget is an essential control on the potential of the ocean to sequester atmospheric CO_2 via the marine biological pump. The nitrogen budget in the ocean is determined by the main sources, i.e., nitrogen fixation and atmospheric deposition, and sinks, including denitrification and anammox. O_2 concentration is an important control on the marine nitrogen cycle, because NO_3^- is the second electron acceptor after O_2 for the remineralization of organic matter. In suboxic conditions, biological fixed-nitrogen is lost via denitrification or anammox. Due to the current climate warming, O_2 concentration in the ocean is thought to be decreasing due to lower solubility and intensified stratification, which could also have an impact on the marine nitrogen cycle. This dissertation concentrates mainly on the nitrogen and O_2 cycles of the eastern tropical South Pacific and its OMZ.

Chapter 2 examines under which conditions the observed situation of an essentially complete drawdown of subsurface oxygen and an incomplete drawdown of nitrate can be reproduced for the case of the ETSP OMZ. It reveals that the fixed-N inventory can be stabilized at non-zero levels only if the remineralization rate via denitrification is slower than that via aerobic respiration. This conclusion is drawn by developing a fully prognostic box model of NO_3^-, ${PO_4}^{3-}$ and O_2 cycles in the coastal upwelling of the ETSP and its adjacent ocean basin. Model results also demonstrate that the water column of the ETSP is a NO_3^- source. This chapter is published in the journal *Biogeosciences* (citation: B. Su, M. Pahlow, H. Wagner, and A. Oschlies, What prevents nitrogen depletion in the oxygen minimum zone of the eastern tropical South Pacific?, *Biogeosciences*, 12, 1113–1130, doi:10.5194/bg-12-1113-2015). BS developed the fully dynamic 5-box prognostic model from the Canfield [2006] model based on the initial idea provided by AO. BS performed all experiments, calculations and analysis with the help of MP. BS wrote the manuscript, with guidance and comments from all co-authors.

Chapter 3 investigates the sensitivity of the nitrogen cycle in the ETSP to nitrogen deposition and benthic remineralization, employing the optimum configuration developed by Su et al. [2015]. The local response to both atmospheric deposition and benthic remineralization is examined in the sensitivity analyses. The results indicate a nitrogen-balancing mechanism in the ETSP, which tends to keep a balanced nitrogen inventory, i.e., nitrogen input by atmospheric deposition is counteracted by decreasing nitrogen fixation; NO_3^- loss via benthic denitrification is partly compensated by increased nitrogen fixation; enhanced nitrogen fixation by phosphate regeneration is partly removed by the stronger water-column denitrification. Even though the water column in our model domain acts as a NO_3^- source, the ETSP including benthic denitrification might become a NO_3^- sink. This chapter is a submitted manuscript entitled "Box-modelling the impacts of atmospheric nitrogen deposition and benthic remineralization on the nitrogen cycle of the eastern tropical South Pacific" by B. Su, M. Pahlow and A. Oschlies. BS performed all the data analysis, calculation and sensitivity experiments based on the initial

idea provided by AO. BS wrote the manuscript with the guidance and comments from MP and AO.

In chapter 4, a configuration of the ETSP OMZ is built employing the 3-D hydrodynamic model ROMS coupled with the biogeochemical model PISCES. Three experimental model configurations are performed to investigate the influence of southern boundary conditions on the O_2 and nutrient distributions of the model domain. This chapter is a manuscript in preparation with the title "Coupled physical/biogeochemical modeling of the oxygen minimum zone of the eastern tropical South Pacific: sensitivity to the southern boundary conditions" by B. Su, Y. José, I. Montes, M. Pahlow, and A. Oschlies. BS conceived the idea and designed the experiments with the guidance of AO and IM. BS performed all experiments, calculations and analyses with help of YJ and MP. BS wrote the manuscript with comments and english improvement provided by the co-authors.

In Chapter 5, the main results of the thesis are summarised. The mechanism responsible for the stabilised nitrogen inventory in the ROMS-PISCES model and the influence of interannual variabilities (i.e., ENSO) on the dynamics of the OMZ and the nitrogen balance will be investigated as outlook on future research. To have a better understanding of the full nitrogen cycle in the ETSP, coupling the benthic remineralization into ROMS-PISCES will be another future research direction.

Chapter 2

What prevents nitrogen depletion in the oxygen minimum zone of the eastern tropical South Pacific?

Bei Su[1], Markus Pahlow[1], Hannes Wagner[1], and Andreas Oschlies[1]

[1]GEOMAR Helmholtz-Zentrum für Ozeanforschung Kiel, Marine Biogeochemical Modelling, Düsternbrooker Weg 20, 24105 Kiel, Germany.

Correspondence to: B. Su (bsu@geomar.de)

Biogeosciences

Received: 11 June 2014 – Published in Biogeosciences Discussion: 18 July 2014

Revised: 19 December 2014 – Accepted: 27 January 2015 – Published: 24 February 2015

Abstract Local coupling between nitrogen fixation and denitrification in current biogeochemical models could result in runaway feedback in open-ocean oxygen minimum zones (OMZs), eventually stripping OMZ waters of all fixed nitrogen. This feedback does not seem to operate at full strength in the ocean, as nitrate does not generally become depleted in open-ocean OMZs. To explore in detail the possible mechanisms that prevent nitrogen depletion in the OMZ of the eastern tropical South Pacific (ETSP), we develop a box model with fully prognostic cycles of carbon, nutrients and oxygen in the upwelling region and its adjacent open ocean. Ocean circulation is calibrated with $\Delta^{14}C$ data of the ETSP. The sensitivity of the simulated nitrogen cycle to nutrient and oxygen exchange and ventilation from outside the model domain and to remineralization scales inside an OMZ is analysed. For the entire range of model configurations explored, we find that the fixed-N inventory can be stabilized at non-zero levels in the ETSP OMZ only if the remineralization rate via denitrification is slower than that via aerobic respiration. In our optimum model configuration, lateral oxygen supply into the model domain is required at rates sufficient to oxidize at least about one fifth of the export production in the model domain to prevent anoxia in the deep ocean. Under these conditions, our model is in line with the view of phosphate as the ultimate limiting nutrient for phytoplankton, and implies that for the current notion of nitrogen fixation being favoured in N-deficit waters, the water column of the ETSP could even be a small net source of nitrate.

2.1 Introduction

The oceanic fixed nitrogen (fixed-N) budget is an essential control on the potential of the ocean to sequester atmospheric CO_2 via the marine biological pump. Denitrification is generally recognized as a major loss of fixed nitrogen, whereas the balance of the global oceanic nitrogen budget remains controversial. Accordingly, estimates derived from both field data and model analyses for the global oceanic fixed-N budget range from sources roughly balancing sinks [Gruber and Sarmiento, 1997, Gruber, 2004, Eugster and Gruber, 2012, DeVries et al., 2013] to a rather large net deficit between 140 and 234 Tg N yr^{-1} [Codispoti et al., 2001, Galloway et al., 2004, Codispoti, 2007].

One of the main uncertainties in the global marine nitrogen budget is the extent of nitrogen loss via denitrification and anaerobic ammonium oxidation (anammox) in oxygen minimum zones (OMZs), located in tropical coastal upwelling regions. Coastal upwelling zones are often associated with very high primary production. Subsequent decomposition of sinking organic matter leads to high levels of oxygen consumption in subsurface waters. Under conditions of sluggish circulation, oxygen-poor source waters, or lack of exchange with oxygenated surface waters, OMZs can develop, usually at intermediate depths of about 200–700 m [Bethoux, 1989, Capone and Knapp, 2007]. An OMZ is commonly defined as a water body with an O_2 concentration below 20 μmol L^{-1} [Paulmier and Ruiz-Pino, 2009]. The four major open-ocean OMZs

are in the eastern North Pacific (ENP), the eastern tropical South Pacific (ETSP), the Arabian Sea, and the Bay of Bengal. OMZs currently account for only about 8 % of the global ocean area but observations of intense denitrification and anammox in the OMZs indicate that they could be responsible for 30–50 % of the total fixed-N loss [Gruber and Sarmiento, 1997, Codispoti et al., 2001, Dalsgaard et al., 2005, Paulmier and Ruiz-Pino, 2009].

Canfield [2006] used a simple steady-state box model of a coastal OMZ to show that a positive feedback between N_2 fixation and denitrification could strip the OMZ of all fixed nitrogen when N_2 fixation was permitted to restore the nitrate : phosphate ratio to Redfield proportions in the surface ocean. Observed concentrations of fixed-N (nitrate plus nitrite) in OMZ waters, however, typically range from about 15 to 40 μmol L^{-1} [Codispoti and Richards, 1976, Codispoti and Packard, 1980, Morrison et al., 1998, Voss et al., 2001]. A possible explanation for the relatively high nitrate concentrations even in the suboxic core of open-ocean OMZs could be low levels of nitrogen fixation in the overlying surface waters [Landolfi et al., 2013]. However, recent interpretations of observed fixed-N deficits relative to the Redfield equivalent of phosphorus point to high rates of nitrogen fixation closely related to the upwelling of nitrogen-deficit waters along the South American coast [Deutsch et al., 2007]. Although alternative explanations for these nutrient patterns have been proposed in models [Mills and Arrigo, 2010], direct measurements have confirmed the occurrence of nitrogen fixation in and above the OMZ of the ETSP [Fernandez et al., 2011]. Global biogeochemical models also generally predict substantial rates of N_2 fixation in the nitrate-deficit waters of the upwelling region of the ETSP that, if not compensated for by some ad hoc slow-down of remineralization in suboxic conditions, lead to a complete draw-down of nitrate in the OMZ [Moore and Doney, 2007, Schmittner et al., 2008]. The question of how non-zero nitrate concentrations can be maintained in the OMZ thus still awaits a mechanistic answer.

The computational efficiency of box models makes them suitable for sensitivity analyses requiring thousands of model evaluations. In spite of its simplicity, Canfield's (2006) box model is also able to capture the most important first-order interactions among ocean circulation, nitrogen fixation, denitrification and OMZs. However, Canfield's model was limited in its power to investigate the influence of open ocean nutrients and oxygen conditions on the upwelling region, because its dynamics were restricted to the OMZ, where all biogeochemical tracers were prescribed in the surrounding waters. Based on Canfield's (2006) steady-state formulation with prescribed oxygen and nutrient concentrations at all depths outside the OMZ, we here present a fully prognostic box model of NO_3^-, PO_4^{3-} and O_2 cycles in a coastal upwelling region and an adjacent ocean basin. We employ this model to examine under which conditions the observed situation of an essentially complete drawdown of subsurface oxygen and an incomplete drawdown of nitrate can be reproduced for the case of the ETSP. Sensitivity experiments explore how nutrient exchange and oxygen ventilation from the southern boundary influence the nitrogen budget within the model domain.

By including a prognostic description not only of conditions within the OMZ, but also in the water surrounding it, we aim to represent local as well as spatially separated feedbacks between the relatively small OMZ and the much larger open-ocean basin. The model describes net primary and export production by ordinary and N_2-fixing phytoplankton, as well as aerobic and anaerobic remineralization. The latter is generally associated with nitrogen loss, commonly attributed to denitrification [Codispoti, 1995]. Anammox has recently been reported as another major pathway for fixed-N removal [Kuypers et al., 2005, Hamersley et al., 2007, Molina and Farás, 2009], but the relative contributions of anammox and denitrification are still a matter of debate [Ward et al., 2009, Bulow et al., 2010]. In our model, we do not explicitly resolve the different inorganic nitrogen species and pragmatically consider all loss of fixed-N via anaerobic remineralization as denitrification. In Canfield's (2006) model, most of the physical model parameters were constrained by observations from suboxic upwelling zones in the Arabian Sea and the eastern tropical North and South Pacific. The physical dynamics of our model system are governed by vertical and horizontal mixing and advection, which are calibrated with Δ^{14}C data of the ETSP from GLODAP [Global Ocean Data Analysis Project, Key et al., 2004].

2.2 Model description

Figure 2.1 shows the model structure, consisting of five boxes representing an upwelling region and an adjacent ocean basin. The U box represents the upper upwelling region. The UM box is the underlying OMZ, where suboxia is expected to develop. The S box represents the surface ocean away from the upwelling zone. Below the S box sits the I box, which represents water of intermediate depth and exchanges water with UM. D is the deep box, which represents water deeper than 500 m. When the UM, I or D boxes become suboxic, denitrification (Denif) will ensue to remineralize the exported organic matter, causing a loss of nitrate (the only form of fixed inorganic nitrogen in our model).

Prognostic tracers represent NO_3^-, PO_4^{3-}, O_2, ^{14}C and the biomass of ordinary and N_2-fixing phytoplankton, respectively (Table 2.1). The rate of concentration change of a tracer, X_i, in box i is composed of physical transport, Transport(X_i), and a sources-minus-sinks term, SMS(X_i), which represents the effects of biotic processes, air–sea gas exchange and, in the case of ^{14}C, radioactive decay on the tracer concentration (Eq. 2.1).

$$\frac{\mathrm{d}X_i}{\mathrm{d}t} = \frac{\mathrm{Transport}(X_i) + \mathrm{SMS}(X_i)}{V_i}$$

$$i \in [\mathrm{U, S, UM, I, D}], \tag{2.1}$$

where U, S, UM, I and D refer to the model boxes defined above and V_i to the corresponding

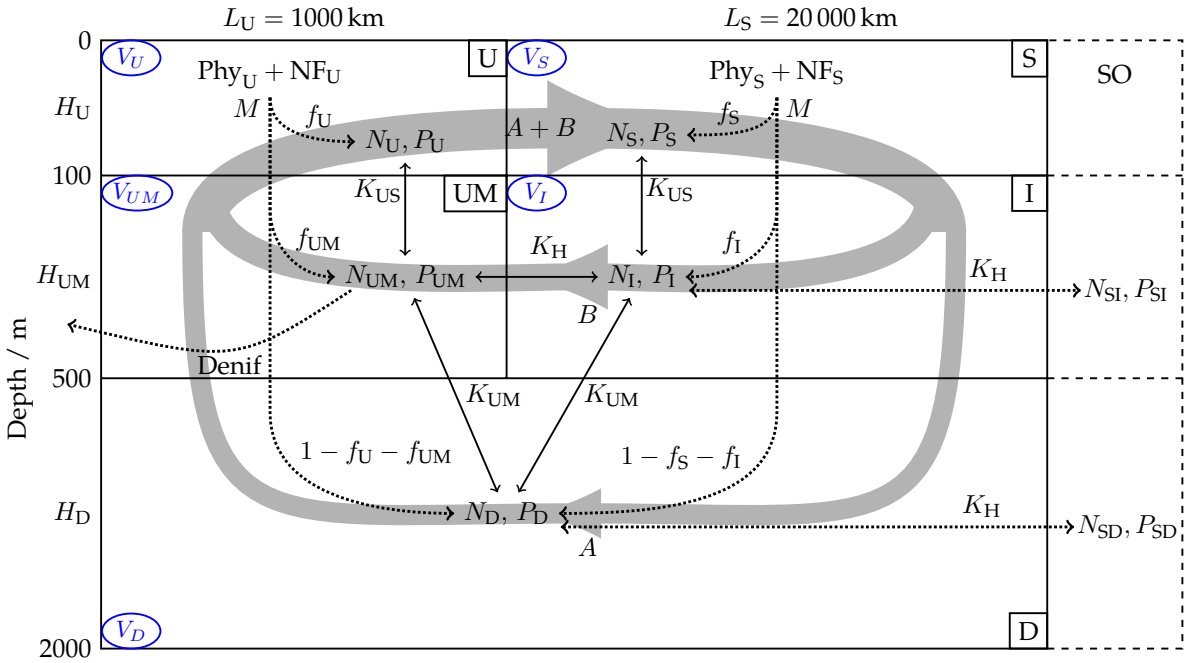

Figure 2.1: Model structure and configurations. The model domain comprises five active boxes representing the top 100 m of an upwelling region (U), the underlying oxygen minimum zone (UM), and an adjacent open-ocean basin divided into a surface (S) and an intermediate-depth box (I). A deep box (D) underlies both the upwelling region and the open ocean. The large-scale circulation is represented by deep (A) and shallow (B) convection (thick grey lines). Mixing between boxes is implemented via mixing coefficients (K). Remineralization derived from net primary production by ordinary (Phy) and diazotrophic (NF) phytoplankton in the surface boxes consumes oxygen. Under anoxic conditions remineralization is fuelled by anaerobic remineralization (Denif). The model can be configured to exchange nutrients and oxygen with the southern subtropical ocean (right, denoted as "SO"). See Table 2.3 for symbol definitions and text for details.

volumes (Fig. 2.1).

2.2.1 Transport model

Advection represents the large-scale circulation and is indicated in Fig. 2.1 by wide grey lines. L_U and L_S are the horizontal scales of the upwelling region and the open ocean, and H_U, H_{UM} and H_D refer to the thickness of the respective boxes. The volumes V_i of the boxes are defined in this 2-D model by $V_i = H_i \times L_i$. K_{US}, K_{UM} and K_H are the coefficients of mixing between different boxes. A and B represent the deep and shallow large-scale circulation. The upwelling intensity into box U is given by $A+B$. The tracer transport equations for the standard configuration are given in Appendix A (Eqs. 2.12–2.16). All parameters are defined in Tables 2.2 and 2.3.

Variables	Units	Description	Equation
Phy_i	$\mu\mathrm{mol\,N\,kg^{-1}}$	Ordinary phytoplankton in box i	Eq. (2.2)
NF_i	$\mu\mathrm{mol\,N\,kg^{-1}}$	Nitrogen fixers in box i	Eq. (2.3)
N_i	$\mu\mathrm{mol\,N\,kg^{-1}}$	Nitrate concentration in box i	Eq. (2.7)
$\mathrm{N}_{\mathrm{avg}}$	$\mu\mathrm{mol\,N\,kg^{-1}}$	Average nitrogen concentration	[a]
P_i	$\mu\mathrm{mol\,P\,kg^{-1}}$	Phosphate concentration in box i	Eq. (2.8)
$\mathrm{P}_{\mathrm{avg}}$	$\mu\mathrm{mol\,P\,kg^{-1}}$	Average phosphorus concentration	[b]
O_{2i}	$\mu\mathrm{mol\,kg^{-1}}$	Oxygen concentration in box i	Eq. (2.9)

$$^{\mathrm{a}}\mathrm{N}_{\mathrm{avg}} = \frac{(\mathrm{N_U}+\mathrm{Phy_U}+\mathrm{NF_U})\cdot V_\mathrm{U}+\mathrm{N_{UM}}\cdot V_\mathrm{UM}+(\mathrm{N_S}+\mathrm{Phy_S}+\mathrm{NF_S})\cdot V_\mathrm{S}+\mathrm{N_I}\cdot V_\mathrm{I}+\mathrm{N_D}\cdot V_\mathrm{D}}{V_\mathrm{U}+V_\mathrm{UM}+V_\mathrm{S}+V_\mathrm{I}+V_\mathrm{D}}$$

$$^{\mathrm{b}}\mathrm{P}_{\mathrm{avg}} = \frac{\left(\mathrm{P_U}+\frac{\mathrm{Phy_U}+\mathrm{NF_U}}{r_\mathrm{P}}\right)\cdot V_\mathrm{U}+\mathrm{P_{UM}}\cdot V_\mathrm{UM}+\left(\mathrm{P_S}+\frac{\mathrm{Phy_S}+\mathrm{NF_S}}{r_\mathrm{P}}\right)\cdot V_\mathrm{S}+\mathrm{P_I}\cdot V_\mathrm{I}+\mathrm{P_D}\cdot V_\mathrm{D}}{V_\mathrm{U}+V_\mathrm{UM}+V_\mathrm{S}+V_\mathrm{I}+V_\mathrm{D}}$$

Table 2.1: Model variables.

Configuration	**STD**	VD	VID	Units
			VIDRD	
	RD	VDRD	OB	
Parameter			**OBRD**	
K_US	8.44	3.37	3.41	$\mathrm{m\,yr^{-1}}$
K_UM	1.59	0.40	0.58	$\mathrm{m\,yr^{-1}}$
K_H	47 799	50 475	42 938	$\mathrm{m\,yr^{-1}}$
A	7.20	7.30	7.22	$\mathrm{m\,yr^{-1}}$
B	18.01	19.60	23.07	$\mathrm{m\,yr^{-1}}$
g_U	9.87	8.89	9.88	$\mathrm{m\,yr^{-1}}$
g_S	2.94	1.42	1.46	$\mathrm{m\,yr^{-1}}$

Configurations in bold are the main configurations.

Table 2.2: Parameters of the physical model configurations. Detailed explanations for these parameters are given in Table 2.3.

2.2.2 Biogeochemical model

The ecological model is composed of two phytoplankton types, ordinary phytoplankton, Phy, and nitrogen fixers, NF. The SMS terms for phytoplankton are obtained as the difference between net primary production (NPP) and mortality (M):

$$\mathrm{SMS}(\mathrm{Phy}_i) = (\mathrm{NPP}^{\mathrm{Phy}_i} - \mathrm{M}^{\mathrm{Phy}_i}) \cdot V_i \quad i \in [\mathrm{U}, \mathrm{S}] \tag{2.2}$$

$$\mathrm{SMS}(\mathrm{NF}_i) = (\mathrm{NPP}^{\mathrm{NF}_i} - \mathrm{M}^{\mathrm{NF}_i}) \cdot V_i \quad i \in [\mathrm{U}, \mathrm{S}]. \tag{2.3}$$

Growth of ordinary phytoplankton is described by a Liebig-type dependence on the nitrate and phosphate limitation terms (Eq. 2.4),

$$\mathrm{NPP}^{\mathrm{Phy}_i} = \mu \cdot \min\left(\frac{\mathrm{N}_i}{\mathrm{N}_i + \mathrm{N}_\mathrm{h}}, \frac{\mathrm{P}_i}{\mathrm{P}_i + \mathrm{P}_\mathrm{h}}\right) \cdot \mathrm{Phy}_i \quad i \in [\mathrm{U}, \mathrm{S}] \tag{2.4}$$

$$\mathrm{NPP}^{\mathrm{NF}_i} = \mu_{\mathrm{NF}} \cdot \frac{\mathrm{P}_i}{\mathrm{P}_i + \mathrm{P}_\mathrm{h}} \cdot \mathrm{NF}_i \quad i \in [\mathrm{U}, \mathrm{S}] \tag{2.5}$$

where i is the model box, μ and μ_{NF} are the maximum growth rates of Phy_i and NF_i, respectively. N_i and P_i are nitrate and phosphate concentrations, and N_h and P_h are half-saturation concentrations for nitrate and phosphate. Considering possible viral lysis, phytoplankton aggregation, or a feedback between zooplankton grazing and phytoplankton concentration, a quadratic mortality term is adopted for both Phy and NF in all model configurations (Eq. 2.6).

$$\mathrm{M}^{\mathrm{Phy}_i} = M_\mathrm{q} \cdot \mathrm{Phy}_i^2 \qquad \mathrm{M}^{\mathrm{NF}_i} = M_\mathrm{q} \cdot \mathrm{NF}_i^2. \tag{2.6}$$

Table 2.3: Model parameters.

Parameter	Description	Units	Value	Range(reference)
$\mathrm{r_a}$	O2-used/NO3-produced during organic carbon(OC) oxidation	—	10.6	8.6–10.6[a]
$\mathrm{r_c}$	C/N ratio of OC oxidation	—	6.63	6.63–7.31[a]
$\mathrm{f_U}$	Remineralization ratio in U	—	20%	[b]
$\mathrm{f_S}$	Remineralization ratio in S	—	20%	[b]
$\mathrm{f_{UM}}$	Remineralization ratio in UM	—	70%	[b]
$\mathrm{f_I}$	Remineralization ratio in I	—	70%	[b]

Table 2.3: (continued)

Parameter	Description	Units	Value	Range(reference)
r_{den}	OC/NO_3^- in denitrification	—	1.02	1.02[a]
r_p	N/P released in OC oxidation	—	16	15–16[a]
μ	Maximum growth rate of Phy	yr^{-1}	91.5	36.5–1861.5[c]
μ_{NF}	Maximum growth rate of NF	yr^{-1}	30.5[e]	65.7–438[d]
M_q	Quadratic mortality	$yr^{-1}(\mu mol\ N\ kg^{-1})^{-1}$	18.25	3.65–18.25[f]
N_h	Nitrate half saturation constant	$\mu mol\ N\ kg^{-1}$	0.5	0.5[g]
P_h	Phosphate half saturation constant	$\mu mol\ P\ kg^{-1}$	0.03125	0.03[h]
L_x	Length of box x	m	see Fig. 2.1	–
H_x	Depth of box x	m	see Fig. 2.1	–
K_H	Horizontal exchange	$m\ yr^{-1}$	[n]	157.68–56765[a]
K_{US}	Vertical mixing between surface and intermediate depth	$m\ yr^{-1}$	[n]	0.79–31.54[a]
K_{UM}	Vertical mixing between intermediate depth and deep ocean	$m\ yr^{-1}$	[n]	0.21–7.88[a]
A+B	Upwelling rates	$m\ yr^{-1}$	[n]	23.7–630.7[a]
O_{2U}	Oxygen concentration in U	$\mu mol\ kg^{-1}$	159.54[i]	–
O_{2S}	Oxygen concentration in S	$\mu mol\ kg^{-1}$	198.11[i]	–
g_U	Gas exchange coefficient for U	$m\ yr^{-1}$	[l]	–
g_S	Gas exchange coefficient for S	$m\ yr^{-1}$	[l]	–
λ	Radioactive decay rate for ^{14}C	yr^{-1}	1.21×10^{-4}	1.21×10^{-4} [j]
N_{SD}	Southern boundary nitrate concentration at depth of D	$\mu mol\ N\ kg^{-1}$	32.65	[k]
N_{SI}	Southern boundary nitrate concentration at depth of I	$\mu mol\ N\ kg^{-1}$	10.93	[k]

Table 2.3: (continued)

Parameter	Description	Units	Value	Range[reference]
P_{SD}	Southern boundary phosphate concentration at depth of D	μmol N kg^{-1}	2.30	[k]
P_{SI}	Southern boundary phosphate concentration at depth of I	μmol N kg^{-1}	0.84	[k]
O_{2SD}	Southern boundary oxygen concentration at depth of D	μmol N kg^{-1}	181.37	[k]
O_{2SI}	Southern boundary oxygen concentration at depth of I	μmol N kg^{-1}	217.98	[k]

[a]Ranges for r_a, r_c, r_{den}, K_{US}, K_{UM},K_H, A and B are the same as in Canfield [2006].

[b]The fraction of regeneration above 500 m has been estimated between 92% [Suess, 1980] and 97% [Martin et al., 1987]. According to Canfield [2006], most likely 60-70% of the export production is remineralised in the OMZ. Thus, we define 20% and 70% of export production remineralised in the surface boxes and intermediate boxes respectively.

[c]Furnas [1990]

[d]Robarts and Zohary [1987], [Capone et al., 1997]

[e]Temperature-corrected maximum growth rate of NF [Breitbarth et al., 2007].

[f]Palmer and Totterdell [2001];[Schmittner et al., 2008]

[g]Eppley et al. [1969]

[h]McAllister et al. [1964]

[i]Average 0-100m O_2 concentrations of the corresponding areas from World Ocean Atlas (2009)

[j]Libby [1956]

[k]Averages of the corresponding areas from World Ocean Atlas (2009)

[l]These parameter values are defined in Table 2.2.

Both Phy and NF require phosphate, whereas nitrate is required in addition to phosphate only by Phy, and NF can fix N_2 as long as $PO_4{}^{3-}$ is available (Eqs. 2.4, 2.5). While the ability to utilize organic P has been proposed as an advantage of diazotrophs [Houlton et al., 2008, Ye et al., 2012], ordinary phytoplankton can also use DOP [e.g. Chu, 1946, Cotner, Jr. and Wetzel, 1992] and a clear advantage of diazotrophs over ordinary phytoplankton in the presence of DOP

has never been demonstrated. Thus, we treat all available P to phytoplankton operationally as PO_4^{3-} and assume that all organic phosphate is remineralized to PO_4^{3-} directly. N_2 fixers are given a lower maximum growth rate (μ_{NF}, Eq. 2.5), which is $1/3$ of the maximum growth rate of ordinary phytoplankton (μ), to account for the high cost of nitrogen fixation [LaRoche and Breitbarth, 2005]. The dependence of NF on iron is not explicitly considered in this model [Mills et al., 2004]. Both types use nitrogen and phosphorus in the Redfield ratio of $16 : 1$ [Redfield et al., 1963].

Sensitivity experiments are also performed with a configuration where nitrogen fixers preferentially use nitrate when available and cover only the residual nitrogen demand via N_2 fixation, denoted as facultative N_2-fixation, but overall results are found to be virtually unchanged (Appendix B).

Dead phytoplankton is immediately remineralized in the surface layer and underlying boxes according to the respective remineralization fraction f_i of box i. Remineralization occurs preferentially via aerobic respiration, with anaerobic remineralization and the associated nitrogen loss setting in only when all O_2 has been consumed by aerobic respiration. Phytoplankton growth and aerobic remineralization together with denitrification and, once all inorganic nitrogen is consumed, remineralization via sulfate reduction define the SMS terms of the nitrogen and phosphorus cycles:

$$\mathrm{SMS}(\mathrm{N}_i) = -\mathrm{NPP}^{\mathrm{Phy}_i} \cdot V_i + \mathrm{Rem}_i^{\mathrm{N}} - \mathrm{Denif}_i \tag{2.7}$$

$$\mathrm{SMS}(\mathrm{P}_i) = -\frac{(\mathrm{NPP}^{\mathrm{Phy}_i} + \mathrm{NPP}^{\mathrm{NF}_i}) \cdot V_i}{r_{\mathrm{P}}} + \mathrm{Rem}_i^{\mathrm{P}} \tag{2.8}$$

where the remineralization (Rem) and denitrification (Denif) terms are defined in Appendix C.

O_2 is set constant in the surface ocean boxes U and S, which are in immediate contact with the atmosphere, but varies as a function of transport and respiration in the UM, I and D boxes. Thus, the aerobic respiration terms (Res_i) are only needed in the interior boxes UM, I and D:

$$\mathrm{SMS}(\mathrm{O}_{2i}) = -\mathrm{Res}_i \quad i \in [\mathrm{UM, I, D}] \tag{2.9}$$

where Res is defined in Appendix C (Eq. 2.30). Note that aerobic respiration will, in general, also take place in anoxic model boxes, where it utilizes the O_2 transported from adjacent boxes, before anaerobic respiration starts. All model runs are initialized with O_2, NO_3^- and PO_4^{3-} annual data from the World Ocean Atlas 2009 [Garcia et al., 2010a,b], averaged over the regions indicated in Table 2.4.

Box	Lat(S)	Lon(W)	Depth(m)	Data[a]
U	5–15	80–90	0–100	–72.39
UM	5–15	80–90	100–500	–93.28
S	0–20	90–190	0–100	–62.21
I	0–20	90–190	100–500	–81.02
D	0–20	80–190	500–2000	–160.30
SI[b]	20–40	90–190	100–500	–71.02
SD[b]	20–40	80–190	500–2000	–134.4

[a]GLODAP "natural ^{14}C" data averaged over the respective regions.

[b]SI and SD represent the southern boundary outside the I and D boxes, respectively.

Table 2.4: Δ^{14}C (in ‰) data from GLODAP used for calibration of the model physical parameters.

2.2.3 Model calibration

In the present work, the prescribed transport among the different boxes in terms of advection and mixing was calibrated by fitting the modelled Δ^{14}C distribution to the GLODAP "pre-bomb" Δ^{14}C distribution of the eastern tropical South Pacific (Key et al., 2004; Table 2.4). The ^{13}C fractionation-corrected ratio of ^{14}C/^{12}C, Δ^{14}C, is commonly used in ocean modelling to evaluate and calibrate model physics [Toggweiler et al., 1989, Shaffer and Sarmiento, 1995] because it tends to cancel the effect of the biotic downward transport of ^{14}C with the rain of organic particles produced by marine organisms. For practical reasons, we employ the arbitrary scale introduced by Shaffer and Sarmiento [1995] to represent Δ^{14}C, and define $\widehat{\Delta^{14}\mathrm{C}}$. $\widehat{\Delta^{14}\mathrm{C}}$ can be converted to Δ^{14}C units as follows:

$$\Delta^{14}\mathrm{C} = 1000(\widehat{\Delta^{14}\mathrm{C}} - 1)‰ \tag{2.10}$$

The ^{14}C dynamics in the model includes input from the atmosphere at the sea surface and radioactive decay with decay rate $\lambda = 1.21 \times 10^{-4}\,\mathrm{yr}^{-1}$ within the model domain. The SMS term for $\widehat{\Delta^{14}\mathrm{C}}$ is thus given by:

$$\mathrm{SMS}(\widehat{\Delta^{14}\mathrm{C}_i}) = (\frac{g_i(\widehat{\Delta^{14}\mathrm{C}_a} - \widehat{\Delta^{14}\mathrm{C}_i})}{H_i} - \lambda\widehat{\Delta^{14}\mathrm{C}_i}) \cdot V_i \quad i \in [\mathrm{U, UM, S, I, D}] \tag{2.11}$$

where $\widehat{\Delta^{14}C}_i$ is the value of $\widehat{\Delta^{14}C}$ in box i, $\widehat{\Delta^{14}C}_a$ is the atmospheric $\widehat{\Delta^{14}C}$, and g_i is the gas exchange rate. For $i \in$ [UM, I, D], $g_i = 0$. We assume that the $\Delta^{14}C$ of the preindustrial atmosphere, $\Delta^{14}C_a$, is 0 ‰. Therefore, $\widehat{\Delta^{14}C}_a$ is 1. Model configurations with an open southern boundary also include ^{14}C exchange with the adjacent subtropical ocean. We also investigate how sensitive our main conclusions are to the uncertainty in the $\Delta^{14}C$ data. Table 2.4 shows the $\Delta^{14}C$ values used for the calibrations of the different model configurations. Transport and SMS terms for $\widehat{^{14}C}$ constitute a system of 5 linear equations with 7 parameters, including 5 transport parameters, A, B, K_{US}, K_{UM}, K_H, and 2 air–sea $\widehat{^{14}C}$ exchange coefficients, g_U and g_S. After setting g_U and g_S, the 5 equations can be inverted to solve for the transport parameters. A detailed description of the inversion scheme is provided in Appendix D.

2.2.4 Model configurations

The above transport and biogeochemical formulations define the standard (STD) configuration, where the transport and biogeochemical models are applied without exchange with the southern boundary ("SO" in Fig. 2.1). Fixed fractions f_i of net primary production in U and S are remineralized in the U, UM, S and I boxes, with the remainder being remineralized in D (Fig. 2.1). Nutrient regeneration is assumed to be instantaneous.

In order to investigate the relationships between the different biotic and physical processes and the nitrogen cycle in an OMZ, we introduce seven additional model configurations. The main differences to the STD configuration are shown in Table 2.5.

(1) In the Reduced-denitrification (RD) configuration, denitrification in the OMZ is reduced to $1/5$ of the rate of the STD configuration following the procedure applied in the global biogeochemical circulation model by Schmittner et al. [2008]. When oxygen is exhausted in the OMZ, denitrification within the UM box will be responsible for only $1/5$ of the remaining organic matter remineralization and the remainder will be remineralized in the D box (Eqs. 2.27 and 2.28). (2) The Ventilation-D (VD) configuration modifies the STD configuration in that the southern boundary of the model domain is partially opened to allow ventilation of O_2 and ^{14}C (but not NO_3^- and PO_4^{3-}) to the D box from the southern subtropical ocean (Eq. 2.18). The circulation parameters were recalibrated to account for ventilation of ^{14}C from the south. Ventilation is simulated by applying lateral mixing with the subtropical oligotrophic ocean tracer reservoirs with prescribed ^{14}C and O_2 concentrations inferred from observations. All other biogeochemical processes within the model domain are kept the same as in the STD configuration. (3) In the Ventilation-D + Reduced-denitrification (VDRD) configuration, the reduced denitrification rate is applied in the VD configuration. (4) In the Ventilation-ID (VID) configuration, the partially open southern boundary is extended to allow ventilation of O_2 and ^{14}C also into the I box from the subtropical ocean (Eq. 2.17). Again, circulation parameters are recalibrated against observed $\Delta^{14}C$ taking into account the ^{14}C exchange between the subtropical

ocean and the I and D boxes. (5) In the Ventilation-ID + Reduced-denitrification (VIDRD) configuration, the reduced denitrification rate is also applied in the VID configuration. (6) In the Open-boundary (OB) configuration, nutrient mixing is added to the VID configuration to allow for the exchange of nutrients between the I and D boxes and the subtropical ocean. (7) In the Open-boundary + Reduced-denitrification (OBRD) configuration, the reduced-denitrification rate is again added to the OB configuration. The physical transports of NO_3^- and ${PO_4}^{3-}$ for the I and D boxes in the last six configurations are represented by Eqs. (2.17) and (2.18) in Appendix A.

2.2.5 Sensitivity experiments

Two sensitivity experiments are performed for each of the VID and OB configurations to explore the possibilities for preventing NO_3^- depletion in the OMZ: (a) different reduced remineralization rates (f_{UM}) and (b) facultative N_2-fixation (see Appendix E).

For the OBRD configuration, three sensitivity experiments are performed to investigate our model sensitivity to variable physical transports and biogeochemical tracer concentrations: (1) the mixing rate with the southern boundary, K_{H}, is reduced for individual tracers (nutrients, oxygen) or combinations thereof from full rates to zero. (2) Simulations are repeated with individual circulation parameters varied by $\pm 50\,\%$ to explore the sensitivity with respect to the circulation parameters of the box model. (3) The sensitivity of NO_3^- and O_2 concentrations in the OMZ to different physical parameters derived from variations of the $\Delta^{14}C$ data and O_2 concentrations in the U-box is also examined.

The literature ranges in Table 2.3 provide only a rough guide for the biogeochemical parameters. The sensitivity of r_{p}, μ, μ_{NF}, $\mathrm{N_h}$ and $\mathrm{P_h}$ is tested in the OBRD configuration by changing each of them according to the literature range. The effects of changing the remineralization fractions f_{U}, f_{UM}, f_{S}, and f_{I} are examined by redistributing remineralization between the U and UM, and S and I boxes. These sensitivity experiments will be discussed in Sect. 3.3 below.

2.3 Results

The physical circulation parameters calibrated with $\Delta^{14}C$ are given in Table 2.2. The resulting circulation is comparable with our expectations for the upwelling region of the eastern tropical South Pacific. The parameters of the biogeochemical model are shown in Table 2.3.

Configuration	Abbreviation	Reduced denitrification rate	O_2, ^{14}C ventilation of D	O_2, ^{14}C ventilation of I	NO_3^-, PO_4^{3-} exchange of D and I
Standard	**STD**				
Reduced-denitrification	**RD**	+			
Ventilation-D	VD		+		
Ventilation-D+Reduced-denitrification	VDRD	+	+		
Ventilation-ID	VID		+	+	
Ventilation-ID+Reduced-denitrification	**VIDRD**	+	+	+	
Open-boundary	OB		+	+	+
Open-boundary+ Reduced-denitrification	**OBRD**	+	+	+	+

Table 2.5: Summary of model configurations. "+" means that the modification applies to this configuration. The configurations in bold are the main configurations in the text, while the others are the sensitivity configurations described in Appendix E. STD is defined in Sects. 2.2 and 2.3; in RD, a reduced denitrification rate is applied; VD indicates that the southern boundary of the model domain is partially opened to allow ventilation of O_2 and ^{14}C (but not NO_3^- and PO_4^{3-}) to the D box; VDRD is the configuration when a reduced denitrification rate is applied in VD; VID differs from VD only in that the partially open southern boundary is extended to allow ventilation of O_2 and ^{14}C also into the I box; VIDRD is the configuration when a reduced denitrification rate is applied in VID; in OB, nutrient (NO_3^- and PO_4^{3-}) mixing is added to VID; OBRD is the configuration in which the reduced denitrification rate is added to OB.

2.3.1 Biogeochemical tracer concentrations

Nutrient and oxygen concentrations in the upwelling region (boxes U and UM) are influenced by physical exchange with regions outside the upwelling zone (boxes I and D) and subsequent remineralization of exported organic matter. The results for biogeochemical tracer concentrations of the STD, RD, VIDRD and OBRD configurations are shown in Fig. 2.2 and will be used to develop our main conclusions, whereas those of the VD, VDRD, VID and OB configurations are also included in Fig. 2.3 and described in Appendix E.

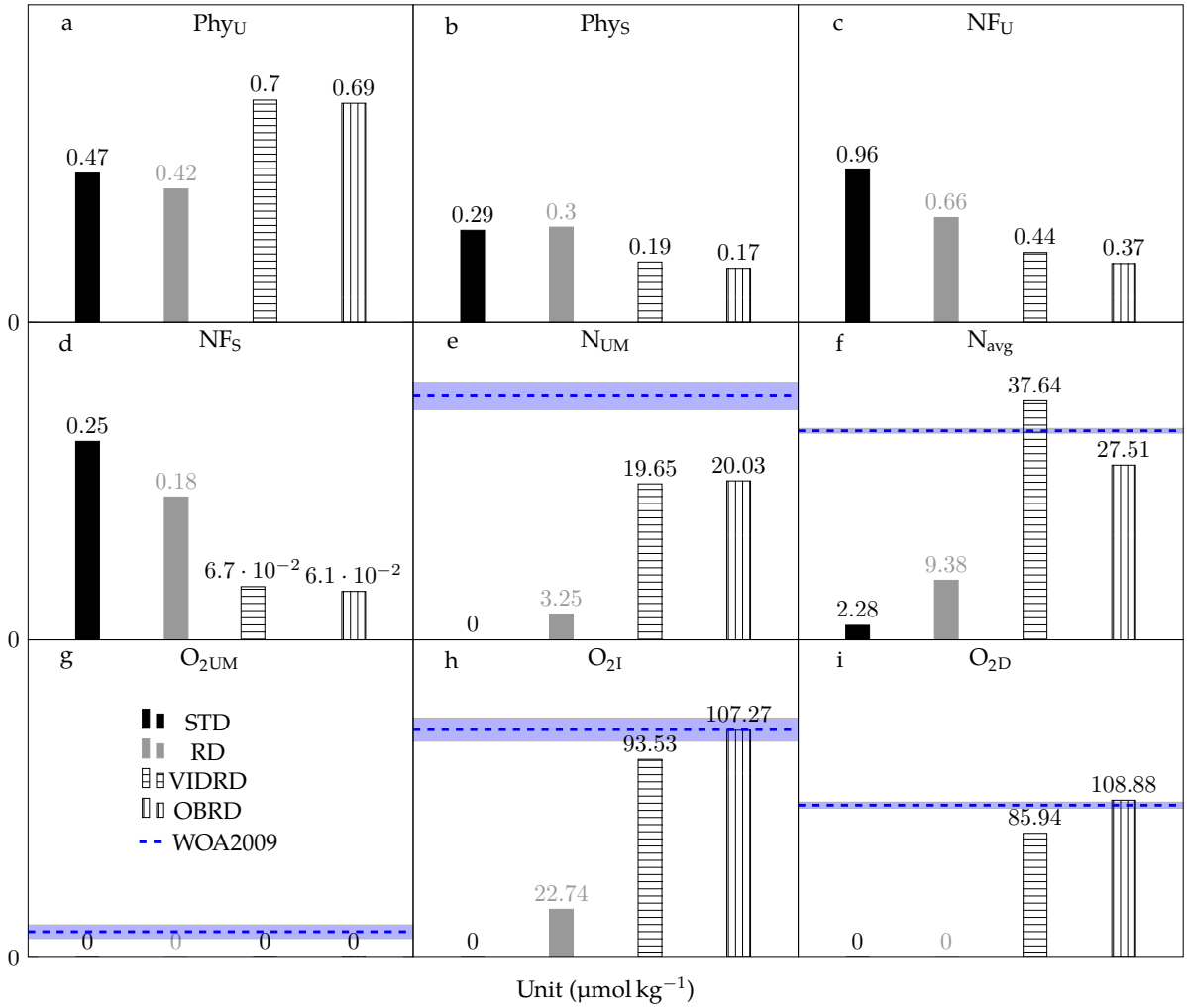

Figure 2.2: Simulated steady-state phytoplankton, nutrient and oxygen concentrations for the main model configurations defined in Tables 2.5 and 2.2. Each panel uses a linear scale of the y axis starting at zero. Dashed blue lines represent the averages of the WOA2009 nitrate and oxygen data for the corresponding boxes, and the light blue shadings refer to the 95 % confidence intervals; however, there are no data for Phy_U, Phy_S, NF_U and NF_S.

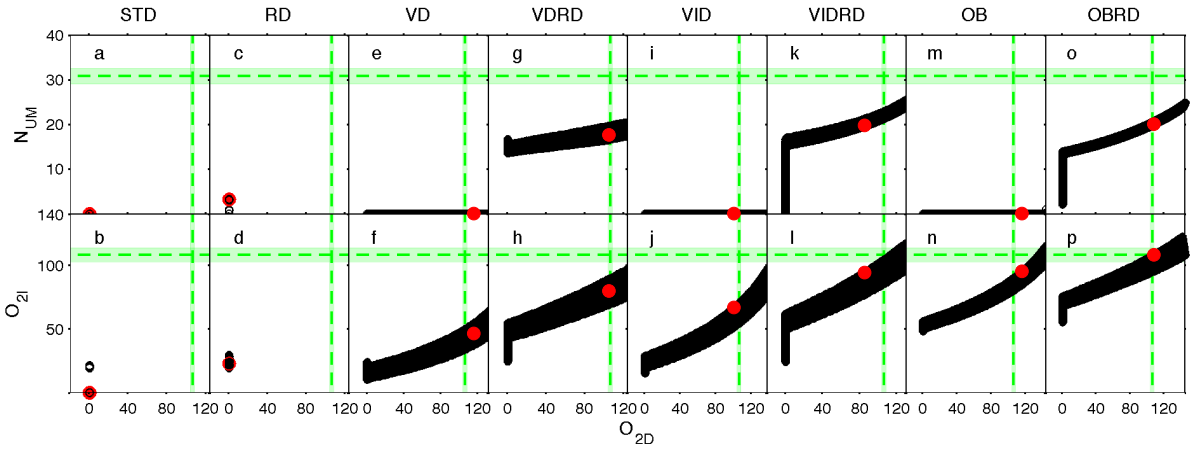

Figure 2.3: NO_3^- concentration in the OMZ and O_2 concentration in the I box for all combinations of g_U and g_S resulting in all transport parameters being inside the literature range as given in Table 2.3. The x axis is the O_2 concentration in the D box. The red dot in each panel is the selected suite of physical transport parameters which fit the biogeochemical data best in each model configuration. The horizontal green dashed lines represent the averages of the WOA2009 data for N_{UM} and O_{2I}, and the vertical green dashed lines denote the averages of the WOA2009 data for O_{2D}. The light green shadings show the 95 % confidence intervals of the WOA2009 data.

In the STD configuration, NO_3^- levels in the UM box are quickly exhausted by denitrification in the UM box (black bars in Fig. 2.2), where decomposition of exported organic matter consumes all O_2 entering the UM box via advection and diffusion, and all NO_3^- entering via physical transport and remineralization of exported organic matter. O_2 is also depleted in the D box, owing to weak ventilation. This results in over 90 % of the initial nitrate being lost from the model domain by denitrification once the model has reached steady state. The large nitrate deficit with respect to phosphate in the upwelling waters results in nitrogen fixers becoming dominant in the U box despite having a lower maximum growth rate than ordinary phytoplankton (black bars in Fig. 2.2a, c).

In the RD configuration, complete NO_3^- exhaustion in the UM box is prevented (grey bars in Fig. 2.2). There is some observational evidence for the efficiency of decomposition of organic matter driven by denitrification in some high-productivity areas being lower than for respiratory processes in the presence of sufficient dissolved oxygen [Liu and Kaplan, 1984, Devol and Hartnett, 2001, Van Mooy et al., 2002]. In our model, this mechanism helps prevent NO_3^- depletion in the OMZ because less nitrate is consumed by denitrification during the passage of the particles through the OMZ. However, the NO_3^- concentration in the UM box is only 3.25 μmol kg^{-1}, far less than the literature range of about 15 to 40 μmol L^{-1}. The additional organic matter now passing through the OMZ must be remineralized in the D box, which still becomes anoxic in this configuration. Even though the RD configuration fails to simulate the realistic biogeochemical tracer concentrations in the OMZ and its adjacent ocean, it reveals a

possible mechanism for preventing NO_3^- depletion in the OMZ.

While a reduced remineralization rate under suboxic conditions appears to be a prerequisite for maintaining non-zero nitrate in the OMZ (Fig. 2.3), we find that ventilation of O_2 from the lateral subtropical ocean into the model domain is essential for preventing anoxic conditions in the D box. But even ventilation of O_2 into both I and D boxes fails to prevent NO_3^- depletion in the UM box in the VID configuration (Fig. 2.3i). After reducing the denitrification rate in the OMZ, which is the configuration denoted as VIDRD, NO_3^- depletion is prevented (bars with horizontal lines in Fig. 2.2). Compared to the RD configuration, NO_3^- concentration in the UM box is in a realistic range (15–40 μmol kg^{-1}) for the OMZ, and O_2 concentrations in the I and D boxes are also closer to the WOA2009 data, but still about 15.0 and 22.7 % lower than the observations (blue dashed lines in Fig. 2.2).

In the OBRD configuration, nutrients are exchanged in addition to O_2 between the subtropical ocean and the I and D boxes, together with reducing the denitrification rate under suboxic conditions. N_{UM} depletion is prevented and N_{UM} approaches a concentration of 20 μmol kg^{-1} at steady state (bars with horizontal lines in Fig. 2.2). The UM box is suboxic and the O_2 concentrations in the I and D boxes agree very well with the WOA2009 data (blue dashed lines in Fig. 2.2). Overall, the tracer distributions simulated by the OBRD configuration agree best with the observations.

In the sensitivity configuration OB, where only nutrients are exchanged in addition to O_2 between the subtropical ocean and the I and D boxes, nitrate is still exhausted in the OMZ (Fig. 2.3m).

2.3.2 Biogeochemical fluxes

For the biogeochemical fluxes, we focus on the STD, RD, VIDRD and OBRD configurations (configurations in bold in Table 2.5), since they show most clearly the mechanisms responsible for preventing NO_3^- depletion in the OMZ (Fig. 2.4). Denitrification rates are much higher in the STD than in the RD configuration (black and grey bars in Fig. 2.4, respectively), even though the physical parameters are the same in the two configurations, leading to nitrate exhaustion in the UM box of the STD but not in the RD configuration. In both VIDRD and OBRD configurations, NO_3^- depletion is prevented (bars with horizontal and vertical lines in Fig. 2.2e). Denitrification is weaker in the OBRD than in the VIDRD configuration (bars with horizontal lines in Fig. 2.4), even though the physical parameters are the same in both, keeping more NO_3^- in the UM-box in the OBRD configuration. Aerobic respiration in the UM box continues even when the UM box is anoxic. It consumes all O_2 entering the UM box via the various physical transport processes and thereby oxidizes about 8.7, 64, 85 and 92 % of the organic matter remineralized (denitrification + aerobic respiration) in the UM box in all four configurations, STD,

RD, VIDRD and OBRD, respectively. Aerobic respiration is increased in the OBRD configuration compared with the VIDRD configuration (92 % vs. 85 %) at the expense of denitrification.

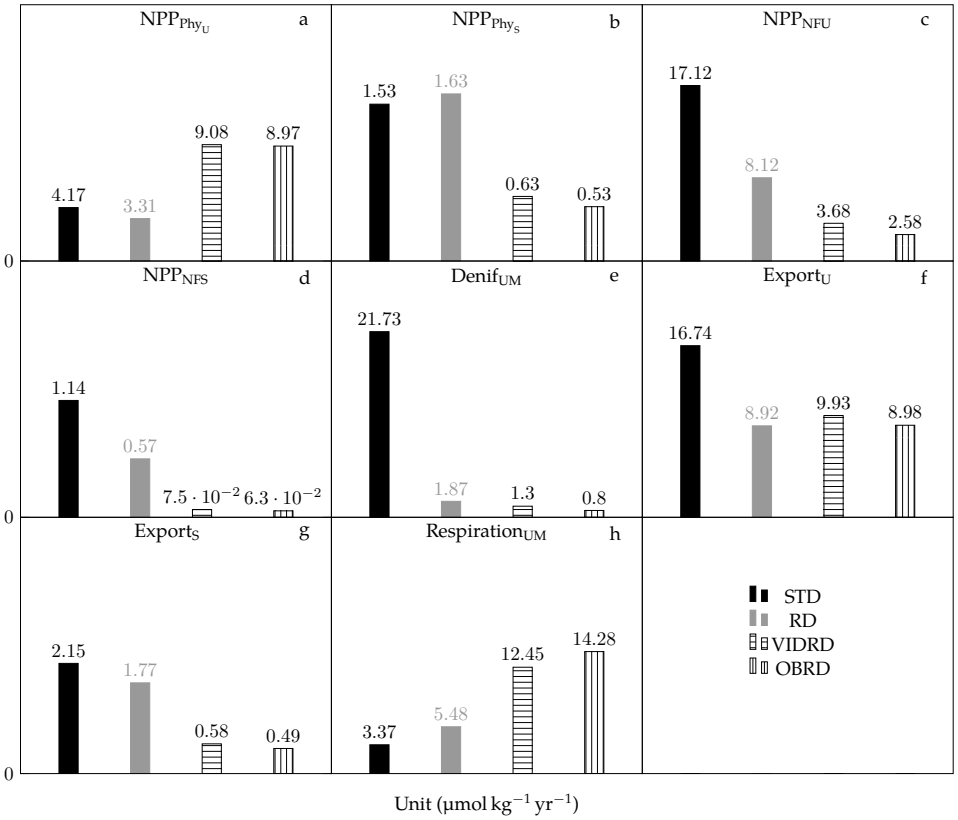

Figure 2.4: Simulated steady-state biogeochemical fluxes for the main model configurations defined in Tables 2.5 and 2.2. NPP_{PhyU}, NPP_{PhyS}, NPP_{NFU} and NPP_{NFS} represent the net primary production rates of Phy_U, Phy_S, NF_U and NF_S, respectively. $Denif_{UM}$ indicates the nitrogen loss rate by anaerobic remineralization in the UM box. $Export_U$ and $Export_S$ represent the export production rate out of U and S. $Respiration_{UM}$ represents aerobic respiration rate in the UM box. Note that all panels are in units of nitrogen except **(h)**, which is in units of O_2. Each panel uses a differrent linear scale for the y axis starting at zero.

Compared with the VIDRD configuration, total PO_4^{3-} in the model domain decreases by about 28 % in the OBRD configuration at steady state, and the net PO_4^{3-} flux out of the I box and the corresponding net flux of PO_4^{3-} from the subtropical ocean into the D box causes a 9.6 % decrease in organic matter exported into the UM box. This explains why NO_3^- concentrations in the OMZ and O_2 concentrations in the I and D boxes are slightly higher (bars with vertical lines in Fig. 2.2). Restricting, in a hypothetical sensitivity experiment, exchange with the subtropical oligotrophic ocean to NO_3^- and O_2 does not result in higher O_2 concentrations in the I and D boxes, because PO_4^{3-} is conserved and export production does not change substantially. Restricting, on the other hand, exchange to PO_4^{3-} and O_2 depresses production and organic matter decomposition by almost the same amount as in the model run that exchanges NO_3^-, PO_4^{3-} and O_2, and succeeds in driving O_{2I} and O_{2D} concentrations closer to the observations

(not shown). Thus, opening the model boundary to PO_4^{3-} and O_2 helps to improve the model results with respect to those of the VIDRD configuration that do not exchange PO_4^{3-} across the southern boundary.

2.3.3 Model sensitivity

In sensitivity experiments of the OBRD configurations, designed to elucidate the importance of the influence of the subtropical ocean on the model domain, we reduce the mixing rates (K_H) of O_2, NO_3^- and PO_4^{3-} across the southern boundary in different combinations (two of them are shown in Fig. 2.5). Total net primary production (NPP) is the same when varying the mixing rate of either only O_2 or O_2 together with NO_3^-, as long as the PO_4^{3-} exchange rate with the subtropical ocean remains unchanged (dotted lines in Fig. 2.5b). The reason is that changes in nitrate exchange with the subtropical ocean are compensated for by changes in denitrification and nitrogen fixation. This implies that NPP is, at steady state, determined only by phosphate availability. Once the total NPP of NF and Phy is determined by PO_4^{3-} supply, aerobic respiration will increase with increasing O_2 supply, while anaerobic remineralization will decrease (solid and dashed lines in Fig. 2.5c). Comparing simulations that vary the mixing rate of O_2 together with that of PO_4^{3-}, with simulations that vary the mixing rate of O_2 together with that of NO_3^- and PO_4^{3-} (dotted lines in Fig. 2.5g) reveals that the combined NPP of Phy and NF decreases with decreasing PO_4^{3-} inventory at low mixing rates and increases with increasing PO_4^{3-} inventory at high mixing rates, irrespective of NO_3^- mixing rate.

It turns out that NO_3^- depletion in the OMZ is prevented in the four sensitivity experiments of Fig. 2.5 no matter how much O_2 is supplied from the subtropical ocean into the model domain. But anoxia in the D box can only be prevented if the external O_2 supply can oxidize more than about 20 % export production in the model domain (solid lines in Fig. 2.5e, j). This ratio can vary according to the size of S box. It increases for a smaller S box, because a smaller S box leads to less downward O_2 supply from the surface box into the lower model domain and more lateral ventilation is needed, and vice versa (not shown). These experiments also reveal an interesting link among the O_2 supply from the subtropical ocean, the nitrate concentration in the OMZ, and the NO_3^- flux between the model domain and surrounding ocean. As soon as the O_2 supply from the subtropical ocean accounts for about 17.5 % of the respiratory O_2 consumption, the model domain turns into a small net source of NO_3^- (dashed lines in the first row of Fig. 2.5). Once anoxia is prevented in the D box, the nitrate concentration in the OMZ (UM box) increases quite strongly from about 15 μmol kg^{-1} to reach about 20 μmol kg^{-1} at full mixing strength.

The conclusion that the model domain is a small pelagic net NO_3^- source in the OBRD configuration does not change when individual physical transport parameters vary by up to ± 50 % (Fig. 2.6). Varying biogeochemical parameters also does not affect this conclusion. The finding

that the model domain is a net NO_3^- source is also tenable for all suites of physical transport parameters in the literature range for which the D-box is oxic (Fig. 2.7).

The oxygen concentrations in the I and D boxes increase in sensitivity model runs with physical parameters calibrated from increased ^{14}C concentrations (lower water mass age, figure not shown). NO_3^- depletion is prevented in the OMZ in the OBRD configuration within the range of about $\pm 10\,\%$ around the default ventilation intensity (Fig. 2.8a). The UM box remains anoxic when $\Delta^{14}C$ is varied within this range, which indicates that this mechanism for preventing NO_3^- depletion in the OMZ may be robust against modest changes in the regional ocean circulation patterns. Meanwhile, NO_3^- and O_2 in the UM box are quite insensitive to the O_2 concentration in the U-box for this configuration (Fig. 2.8b).

Varying biogeochemical parameters affects individual model predictions but not our main conclusions. The strongest effects are those of varying the N : P ratio r_P and the remineralization fractions (f_U, f_{UM}, f_S and f_I) (Fig. 2.6). Lowering r_P to 12 increases N_{UM} by about 35 %, but cannot change the strength of our model domain as a net NO_3^- source. Increasing r_P to 20 decreases N_{UM} by about 18 %, but triples the strength of our model domain as a NO_3^- source. However, observations indicate that r_P for the ETSP is more likely to be higher than lower compared to the Redfield N : P ratio of 16 [Franz et al., 2012]. Increasing the maximum growth rate of NF, μ_{NF}, to $1/2\mu$, the maximum growth rate of Phy, results in higher N_{UM} concentrations and our model domain being a larger NO_3^- source. Intuitively, decreasing μ_{NF} to $1/4\mu$ results in lower N_{UM} concentrations and our model domain becoming a smaller NO_3^- source. Varying the NO_3^- half saturation constant, N_h, results in virtually unchanged results. N_{UM} increases when changing remineralization fractions in the intermediate boxes (f_{UM} and f_I) from 70 to 50 and 30 %, respectively, effectively lowering export production via lowering the export ratio. Nevertheless, the qualitative behaviour of the model remains the same in these sensitivity experiments.

2.4 Discussion and conclusions

Nitrogen is often considered to be the primary limiting nutrient in marine upwelling regions with OMZs [Cline and Richards, 1972, Codispoti and Christensen, 1985, Morrison et al., 1998, Voss et al., 2001], where denitrification rates can be high and are generally thought to cause a major loss of NO_3^- from the world's oceans. The nitrogen deficit is commonly assumed to

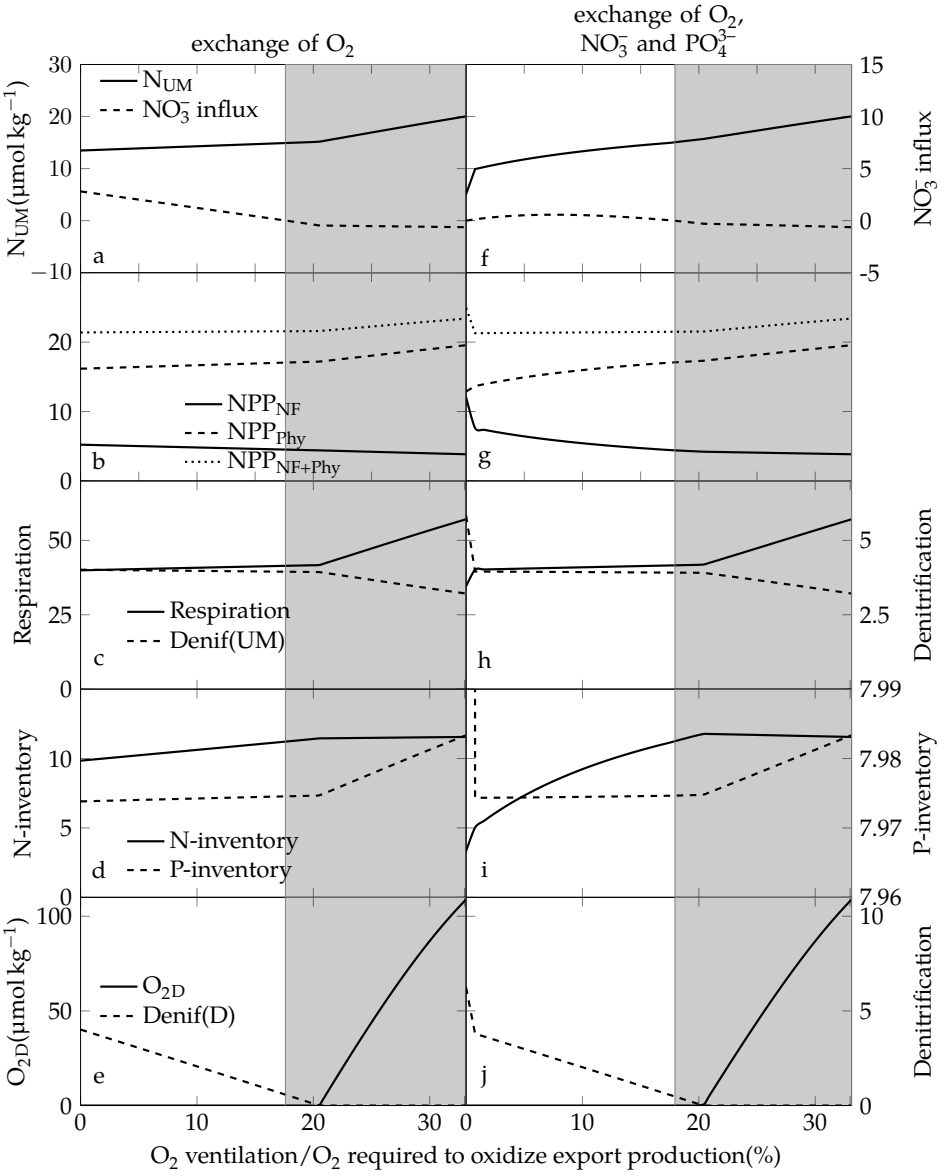

Figure 2.5: Dependence of biogeochemical processes on the exchange of O_2, NO_3^- and $PO_4{}^{3-}$ with the subtropical ocean through the southern boundaries of the I and D boxes. The x axes indicate the contribution of O_2 supplied from the subtropical ocean relative to that required to oxidize all export production from the surface ocean (boxes U and S). **(a–e)** only O_2 exchanged through the southern boundaries is reduced; **(f–j)** exchange of O_2, NO_3^- and $PO_4{}^{3-}$ is reduced. N_{UM} is NO_3^- concentration in the UM box and NO_3^- influx is the NO_3^- flux through the southern boundary (positive into model domain). NPP_{Phy}, NPP_{NF} and NPP_{NF+Phy} are net primary production by ordinary phytoplankton, nitrogen fixers, and the sum of both in the surface ocean. Respiration and Denif (UM) represent O_2 consumption by aerobic remineralization and NO_3^- removal by anaerobic remineralization, respectively, in the UM box. N-inventory and P-inventory are the total nitrogen and phosphorus inventories in the model domain, including all organic and inorganic species. O_{2D} and Denif (D) represent O_2 concentration and NO_3^- removal by anaerobic remineralization in the D box. Units of all variables are 10^{11} μmol yr^{-1} m^{-1} except for N_{UM} and O_{2D}, which are given in μmol kg^{-1}, and N-inventory and P-inventory, which are 10^{11} μmol m^{-1}. The shaded area denotes the parameter range for which the model domain is a net source of NO_3^-.

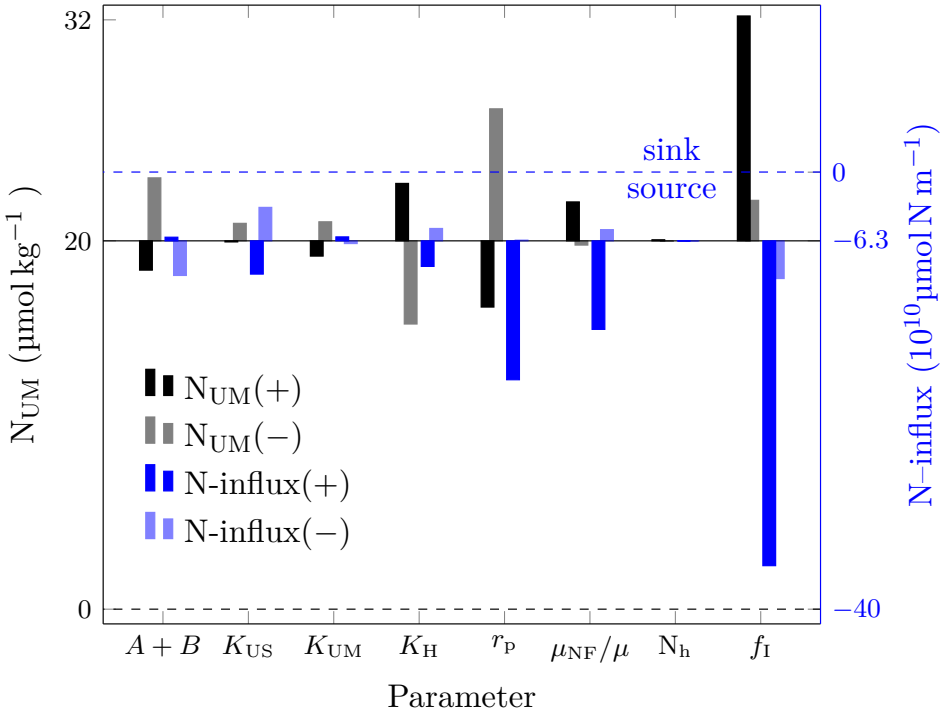

Figure 2.6: Sensitivity of NO_3^- concentration in the OMZ (N_{UM}) and the net NO_3^- flux out of the model domain to variations of the individual parameters describing ocean transport and biogeochemical processes (see Tables 2.2, 2.3 and Fig. 2.1 for a description of the parameters). Black and blue bars represent changes in N_{UM} and N-influx, respectively. "+" and "−" indicate the response to increased and decreased parameters. Physical circulation parameters are varied by $\pm 50\,\%$. r_P is varied between 12 and 20. μ_{NF}/μ is varied between $1/4$ and $1/2$. N_h varies between 0.3 and 0.9 μmol kg^{-1}. For f_i, "+" indicates $f_U = f_S = 60\,\%$ and $f_{UM} = f_I = 30\,\%$, and "−" means 40 % and 50 %, respectively.

stimulate N_2 fixation, both in observational estimates of N_2 fixation [Deutsch et al., 2007, Monteiro et al., 2010] and in current descriptions of N_2 fixation in biogeochemical models [Moore and Doney, 2007, Schmittner et al., 2008]. However, if N_2 fixation is tightly linked to nitrogen loss processes, denitrification of organic matter derived from N_2 fixation can consume more nitrogen than was fixed via N_2 fixation and thereby lead to a vicious cycle of runaway nitrogen loss [Landolfi et al., 2013]. This has been found to lead to total depletion of NO_3^- in the OMZ of box models [Canfield, 2006] and global biogeochemical circulation models [Moore and Doney, 2007, Schmittner et al., 2008]. For our fully prognostic 5-box model, we have identified the mechanisms capable of arresting the runaway nitrogen loss that can result from a close coupling of nitrogen fixation and denitrification [Landolfi et al., 2013] and maintaining realistic non-zero NO_3^- concentrations in open-ocean OMZs of the ETSP: reduced NO_3^- consumption by denitrification owing to slower remineralization under suboxic compared to oxic conditions, coupled with lateral ventilation of oxygen and, to some extent, nutrients with the subtropics.

In this work, the model configuration with reduced denitrification rate, and lateral ventilation and nutrient exchange (OBRD configuration) performs best with respect to the observations,

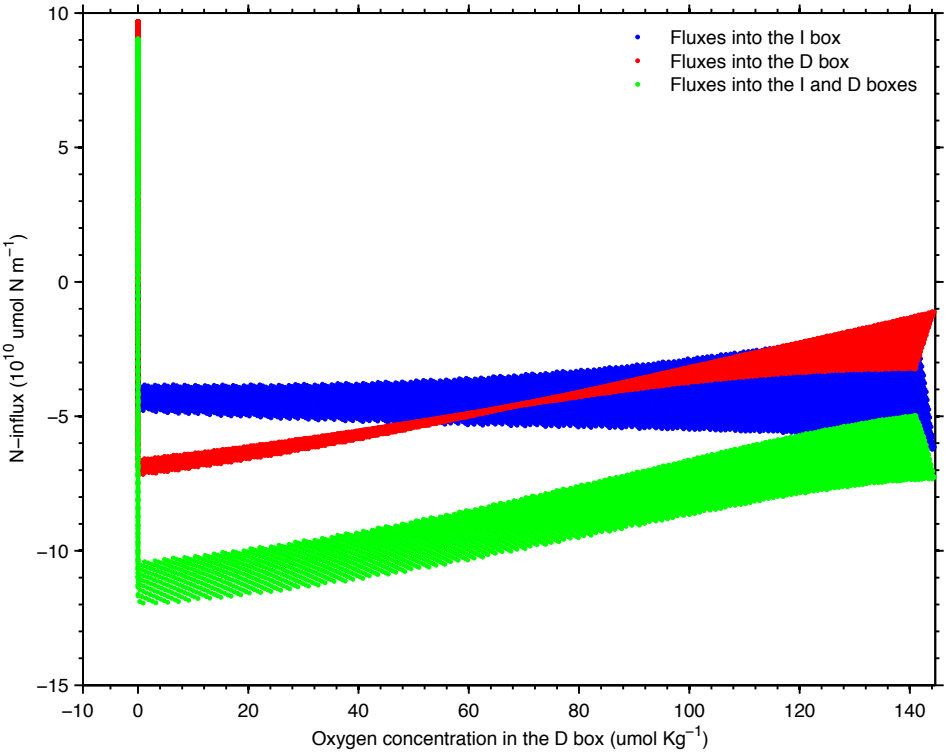

Figure 2.7: Lateral NO_3^- input into the model domain of the OBRD configuration as a function of the oxygen concentration in the D box. "Fluxes into the I box" represents lateral NO_3^- input into the I box; "fluxes into the D box" represents lateral NO_3^- input into the D box; "fluxes into the I and D boxes" is the sum of the above two processes. Note that only the I and D boxes can exchange O_2 or nutrients with the region outside of the model domain. In this figure, negative values indicate that the model is a NO_3^- source, and positive values that the model is a NO_3^- sink instead.

whereas reduced rates of denitrification alone lead to unrealistic O_2 depletion in the deep waters, and reduced rates of denitrification combined with only O_2 ventilation in the D, or both I and D boxes still underestimate the WOA2009 data for O_2 in the I and D boxes. By allowing for exchange of O_2 and nutrients with the subtropical ocean in the OBRD configuration, the delicate balance between sufficient O_2 supply required for maintaining high levels of aerobic respiration and sufficient ${PO_4}^{3-}$ loss through the open boundary appears fulfilled. Compared with other box models [Shaffer and Sarmiento, 1995, Tyrrell, 1999, Deutsch et al., 2004, Canfield, 2006, Mills and Arrigo, 2010, Eugster and Gruber, 2012, DeVries et al., 2012], the box model we use here explicitly employs both a reduced-denitrification rate and an open boundary condition, which seems to be a prerequisite for the ability to simulate realistic nitrate conditions in the OMZ and oxygen concentrations in the adjacent ocean.

The NO_3^- loss by denitrification in the OMZ of the OBRD configuration is compared with that of other model-based and observational estimates in Table 2.6. Our simulated denitrification is consistent with the results of Somes et al. [2010] and DeVries et al. [2013] for the ETSP, lower

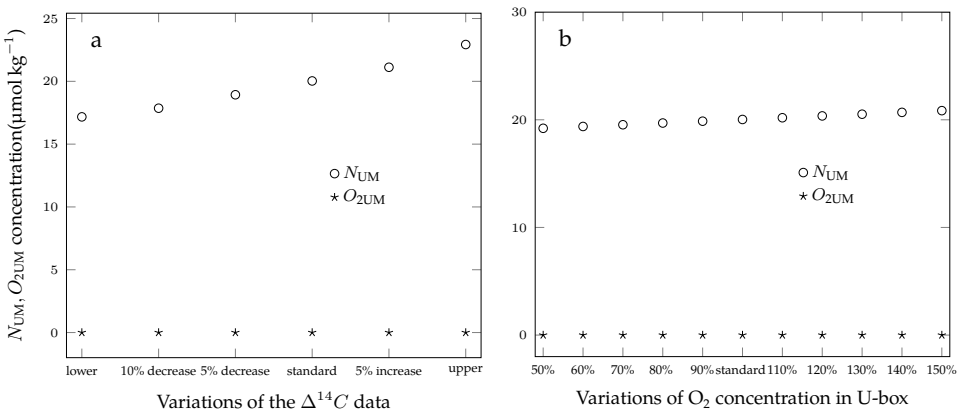

Figure 2.8: NO_3^- and O_2 concentrations in the OBRD configuration for different physical parameters derived from variations of the Δ^{14}C data **(a)** and O_2 concentration in the U box **(b)**. **(a)** Decrease and increase mean that Δ^{14}C values in all boxes are reduced or increased simultaneously. **(b)** Values of the x axis denote the variations of O_2 concentration in the U box relative to the standard. The standard run in each figure is the OBRD configuration with physical parameters defined in Table 2.2.

than the estimate of Bianchi et al. [2012] and Kalvelage et al. [2013], but higher than that of Mills and Arrigo [2010]. However, the estimated denitrification by Bianchi et al. [2012] represents that of the entire South Pacific but not only the ETSP. The Kalvelage et al. (2013) model has much higher fixed-N influx into the OMZ via physical transport than our model, which could compensate for their more intense NO_3^- loss by denitrification.

Data/models	Denitrification (Tg N yr^{-1})
OBRD configuration	5.0[c]
Kalvelage et al. [2013][a]	10.2[c]
T. DeVries et al. (2013, pers. comm.)[b]	7.0 ± 2.0[c]
Bianchi et al. [2012][a]	17.6[d]
C. Somes et al. (2010, pers. comm.)[b]	5.8[c]
Mills and Arrigo [2010][b]	1.9[c,*]

Table 2.6: Denitrification comparison with model-based and observational estimates. [a] Observational estimate; [b] model results; [c] ETSP; [d] entire South Pacific; * OMZ value extrapolated to the UM box of our model.

Phosphate turns out to be the ultimate limiting nutrient in our model (Fig. 2.5), and hence determines the nitrogen content of the OMZ. This strong control of the N cycle by phosphate is similar to the findings of previous models [e.g. Lenton and Watson, 2000, Canfield, 2006],

where the occurrence and extent of oceanic anoxia was also tightly linked to phosphate supply. These studies explicitly assumed that N_2 fixation acts to restore surface-oceanic dissolved inorganic N : P ratio towards the Redfield ratio. By contrast, we do not prescribe the effect of nitrogen fixation on surface inorganic nutrients, and the finding of phosphate as the ultimate limiting nutrient is obtained regardless of whether NF responds directly to the N : P ratio in the surface ocean or whether NF is inhibited by the presence of NO_3^- (see Appendix B).

Even though our model indicates only a weak dependence of simulated NO_3^- concentrations in the OMZ on the lateral O_2 supply from the subtropical ocean, O_2 depletion in the adjacent ocean can be prevented only when the O_2 supply from the subtropical ocean accounts for more than 20 % of the O_2 required to oxidize export production from the surface ocean of our model domain (U and S boxes). This value only varies between about 17 and 23 %, when the size of the S box varies by ± 50 %, indicating that our above conclusion is rather insensitive to our choice of model domain. The O_2 supply from the subtropical ocean might be also linked to the balance of the regional fixed-N cycle. In the most realistic (OBRD) configuration, the balance of water-column denitrification and nitrogen fixation is tightly linked to the nitrate concentration in the OMZ: if the model domain acts as a sink for NO_3^-, nitrate concentrations in the OMZ do not exceed about 15 μmol kg^{-1}, i.e. the lower limit of current observations, 15 to 40 μmol kg^{-1} [Codispoti and Richards, 1976, Codispoti and Packard, 1980, Morrison et al., 1998, Voss et al., 2001]. Nitrate concentrations close to those commonly found in OMZs are predicted only when nitrogen fixation exceeds water-column denitrification and the ocean basin containing the OMZ becomes a net source of NO_3^- (Fig. 2.5a, f).

There are no specific data or model results focusing on the water-column nitrogen balance of the ETSP. Our simulations using a parameterization where nitrogen fixation is inhibited by the presence of nitrate yield very similar results, only with slightly reduced nitrogen fixation resulting in a somewhat reduced (by ≤ 15 %) nitrogen source for strong enough lateral oxygen supply. Ganachaud and Wunsch [2002] estimated a net northward NO_3^- transport of 270 ± 170 kmol s^{-1} (119.2$\pm$75.1 Tg N yr^{-1}) across 17°S into the ETSP in a geostrophic inverse box model, which indicates that the ETSP is a net nitrogen sink, but their estimate included benthic denitrification, which is not accounted for in our current analysis. In a model-guided analysis, DeVries et al. [2012] predicted water-column denitrification rates of 21–33 Tg N yr^{-1} by simulating the distribution of observed dissolved N_2 gas produced by denitrifying bacteria. From an ocean circulation-biogeochemical model-based analysis of nutrient concentrations and transport rates, Deutsch et al. [2007] estimated nitrogen fixation rates in the Pacific Ocean of about 95 Tg N yr^{-1}, half of which was speculated to occur in the ETSP. From these estimates, we cannot rule out that the water column of the ETSP is a net source of NO_3^-, which would be consistent with our results obtained in the OBRD configuration. More recently, Eugster and Gruber [2012] probabilistically estimated nitrogen fixation and water-column and benthic denitrification separately in their box model, which appears to be consistent with our results as their results also indicate that the water column of the Indo-Pacific is a large fixed-N source.

Based on our model results, we conclude that reduced NO_3^- consumption by denitrification owing to slower remineralization under suboxic conditions together with lateral transport is essential to arrest the vicious cycle of runaway fixed-N loss in the OMZ. More research is needed to better constrain the model parameters, in particular the upwelling transport and the difference between the organic matter remineralization rate via aerobic respiration and anaerobic denitrification.

2.5 Appendix A

Physical transports of a tracer X among the boxes U, UM, S, I and D are defined for the STD configuration as follows:

$$\text{Transport}(X_\text{U}) = (X_{UM} - X_U)(A + B + K_\text{US}) \cdot L_\text{U} \tag{2.12}$$

$$\begin{aligned}\text{Transport}(X_\text{UM}) = {} & [AX_D + BX_\text{I} - X_{UM}(A + B) + K_\text{US}(X_U - X_{UM})] \cdot L_\text{U} \\ & + K_\text{UM}(X_D - X_{UM}) \cdot L_\text{U} + K_\text{H}(X_I - X_{UM}) \cdot H_\text{UM}\end{aligned} \tag{2.13}$$

$$\text{Transport}(X_\text{S}) = (A + B)(X_U - X_S) \cdot L_\text{U} + K_\text{US}(X_I - X_S) \cdot L_\text{S} \tag{2.14}$$

$$\begin{aligned}\text{Transport}(X_\text{I}) = {} & (A + B)(X_S - X_I) \cdot L_\text{U} + K_\text{H}(X_{UM} - X_I) \cdot H_\text{UM} \\ & + K_\text{US}(X_S - X_I) \cdot L_\text{S} + K_\text{UM}(X_D - X_I) \cdot L_\text{S}\end{aligned} \tag{2.15}$$

$$\text{Transport}(X_\text{D}) = A(X_I - X_D) \cdot L_\text{U} + K_\text{UM}(X_{UM} - X_D) \cdot L_\text{U} + K_\text{UM}(X_I - X_D) \cdot L_\text{S} \tag{2.16}$$

For the VD, VID and OB configurations, Eqs. 2.15 and 2.16 are modified to read:

$$\begin{aligned}\text{Transport}(X_\text{I}) = {} & (A + B)(X_S - X_I) \cdot L_\text{U} + K_\text{H}(X_{UM} - X_I) \cdot H_\text{UM} \\ & + K_\text{US}(X_S - X_I) \cdot L_\text{S} + K_\text{UM}(X_D - X_I) \cdot L_\text{S} \\ & + K_\text{H}(X_\text{SI} - X_\text{I}) \cdot H_\text{UM}\end{aligned} \tag{2.17}$$

$$\begin{aligned}\text{Transport}(X_\text{D}) = {} & A(X_I - X_D) \cdot L_\text{U} + K_\text{UM}(X_{UM} - X_D) \cdot L_\text{U} + K_\text{UM}(X_I - X_D) \cdot L_\text{S} \\ & + K_\text{H}(X_\text{SD} - X_\text{D}) \cdot H_\text{D}\end{aligned} \tag{2.18}$$

The transport equations (Eqs. 2.12, 2.14) are modified for Phy and NF because Phy and NF are assumed to be capable of regulating their buoyancy and exist only in U and S without being transported vertically between the U and UM or the S and I boxes.

2.6 Appendix B

It is well known from laboratory studies that diazotrophic phytoplankton can also utilize nitrate for growth, denoted as facultative N_2-fixation [e.g. Holl and Montoya, 2005]. Schmittner et al. [2008] introduced a formulation where nitrogen fixers preferentially use nitrate when available and cover only the residual nitrogen demand via N_2 fixation. In order to examine the behaviour of our model when nitrogen fixers (NF) preferentially use nitrate, nitrogen fixation is separated from diazotroph growth, as in Schmittner et al. [2008]:

$$\text{Nitrogen-fixation}_i = \left(1 - \frac{\text{N}}{\text{N} + \text{N}_\text{h}}\right) \cdot \text{NPP}^{\text{NF}_i} \quad i \in [\text{U, S}] \tag{2.19}$$

and Eq. (2.7) was modified to accommodate the additional nitrate uptake by NF as follows:

$$\begin{aligned} \text{SMS}(N_i) = (-\text{NPP}^{\text{Phy}_i} - (\text{NPP}^{\text{NF}_i} - \text{Nitrogen-fixation}_i)) \cdot V_i + \text{Rem}_i^{\text{N}} - \text{Denif}_i \\ i \in [\text{U, UM, S, I, D}] \end{aligned} \tag{2.20}$$

After incorporating Eqs. 2.19 and 2.20 in our all configurations described in Sect. 2.2, they behave very similarly compared to Fig. 2.2, except that Phy_U and Phy_S concentrations are somewhat lower because nitrogen fixers take up NO_3^- as well. Thus, we conclude that our results are robust with respect to assumptions about facultative N_2-fixation by diazotrophs.

2.7 Appendix C

The nitrogen cycle in this model includes nitrogen fixation, denitrification, inorganic nitrogen regeneration by remineralization, physical transport of NO_3^-, and transport of Phy and NF between the U and S boxes. The physical transport process of NO_3^- is the same as for other tracers. Rem_i^{N} represents nitrogen remineralization in box i with fixed fractions f_i of the net

primary production in the overlaying surface boxes.

$$\mathrm{Rem}_{\mathrm{U}}^{\mathrm{N}} = f_{\mathrm{U}} M(\mathrm{Phy}_{\mathrm{U}} + \mathrm{NF}_{\mathrm{U}}) \cdot H_{\mathrm{U}} \cdot L_{\mathrm{U}} \tag{2.21}$$

$$\mathrm{Rem}_{\mathrm{UM}}^{\mathrm{N}} = f_{\mathrm{UM}} M(\mathrm{Phy}_{\mathrm{U}} + \mathrm{NF}_{\mathrm{U}}) \cdot H_{\mathrm{U}} \cdot L_{\mathrm{U}} \tag{2.22}$$

$$\mathrm{Rem}_{\mathrm{S}}^{\mathrm{N}} = f_{\mathrm{S}} M(\mathrm{Phy}_{\mathrm{S}} + \mathrm{NF}_{\mathrm{S}}) \cdot H_{\mathrm{U}} \cdot L_{\mathrm{S}} \tag{2.23}$$

$$\mathrm{Rem}_{\mathrm{I}}^{\mathrm{N}} = f_{\mathrm{I}} M(\mathrm{Phy}_{\mathrm{S}} + \mathrm{NF}_{\mathrm{S}}) \cdot H_{\mathrm{U}} \cdot L_{\mathrm{S}} \tag{2.24}$$

$$\mathrm{Rem}_{\mathrm{D}}^{\mathrm{N}} = M\big[(1 - f_{\mathrm{U}} - f_{\mathrm{UM}})(\mathrm{Phy}_{\mathrm{U}} + \mathrm{NF}_{\mathrm{U}}) \cdot L_{\mathrm{U}} + (1 - f_{\mathrm{S}} - f_{\mathrm{I}})(\mathrm{Phy}_{\mathrm{S}} + \mathrm{NF}_{\mathrm{S}}) \cdot L_{\mathrm{S}}\big] \cdot H_{\mathrm{U}}. \tag{2.25}$$

Denitrification (Denif) is the nitrogen loss to N_2 when UM, I and D are anoxic. It is defined as:

$$\mathrm{Denif}_i = \max(\mathrm{Rem}_i^{\mathrm{N}} - \frac{\mathrm{Res}_i}{r_{\mathrm{a}}}, 0) \cdot \frac{r_{\mathrm{c}}}{r_{\mathrm{den}}} \quad i \in [\mathrm{UM, I, D}] \tag{2.26}$$

with the aerobic respiration term Res_i given below (Eq. 2.30). In the RD, VDRD, VIDRD and OBRD configurations, the equations for denitrification in the i box and remineralization in D are given by:

$$\mathrm{Denif}_i = \frac{1}{5} \cdot \max(\mathrm{Rem}_i^{\mathrm{N}} - \frac{\mathrm{Res}_i}{r_{\mathrm{a}}}, 0) \cdot \frac{r_{\mathrm{c}}}{r_{\mathrm{den}}} \quad i \in [\mathrm{UM, I}] \tag{2.27}$$

$$\begin{aligned}\mathrm{Rem}_{\mathrm{D}}^{\mathrm{N}} &= M\big[(1 - f_{\mathrm{U}} - f_{\mathrm{UM}})(\mathrm{Phy}_{\mathrm{U}} + \mathrm{NF}_{\mathrm{U}}) \cdot L_{\mathrm{U}} + (1 - f_{\mathrm{S}} - f_{\mathrm{I}})(\mathrm{Phy}_{\mathrm{S}} + \mathrm{NF}_{\mathrm{S}}) \cdot L_{\mathrm{S}}\big] \cdot H_{\mathrm{U}} \\ &\quad + 4 \cdot \frac{\mathrm{Denif}_i \cdot r_{\mathrm{den}}}{r_{\mathrm{c}}} \quad i \in [\mathrm{UM, I}].\end{aligned} \tag{2.28}$$

All the organic matter is composed according to the Redfield ratio, i.e. $\mathrm{C:N:P} = 106 : 16 : 1$. $\mathrm{Rem}_i^{\mathrm{P}}$ represents phosphate remineralization in box i, which is obtained by dividing $\mathrm{Rem}_i^{\mathrm{N}}$ by the Redfield N : P ratio, r_{p}:

$$\mathrm{Rem}_i^{\mathrm{P}} = \frac{\mathrm{Rem}_i^{\mathrm{N}}}{r_{\mathrm{p}}} \quad i \in [\mathrm{U, S, UM, I, D}]. \tag{2.29}$$

Respiration (Res_i) is considered in the intermediate and deep ocean. In the presence of sufficient oxygen or when oceanic circulation supplies enough O_2, organic matter will be preferentially oxidized by respiration. We use a ratio of $-\mathrm{O_2} : \mathrm{N} = 170 : 16$ during oxic remineralization of organic matter [Anderson and Sarmiento, 1994].

$$\mathrm{Res}_i = \begin{cases} r_{\mathrm{a}} \cdot \mathrm{Rem}_i^{\mathrm{N}} & \text{if} \quad \mathrm{O}_{2i} > 0 \\ \min\left(\mathrm{Transport}(\mathrm{O}_{2i}),\, r_{\mathrm{a}} \cdot \mathrm{Rem}_i^{\mathrm{N}}\right) & \text{if} \quad \mathrm{O}_{2i} = 0 \end{cases} \tag{2.30}$$

$$i \in [\mathrm{UM, I, D}].$$

2.8 Appendix D

Transport and SMS terms for $\widehat{^{14}\mathrm{C}}$ constitute a system of 5 linear equations including transport parameters A, B, K_{US}, K_{UM} and K_{H}, which are inverted from the $\Delta^{14}C$ values with air–sea $\Delta^{14}C$ exchange rates g_{U} and g_{S} for the U and S boxes, respectively as inputs. All possible combinations of values (with a step size of $0.01\,\mathrm{m\,yr^{-1}}$) for $\mathrm{g_U}$ and $\mathrm{g_S}$ are applied to derive the values for transport parameters A, B, K_{US}, K_{UM} and K_{H}. g_{U} and g_{S} are constrained in a two-step procedure. First, all combinations are determined which result in transport parameters in the literature range in Table 2.3. Finally, the combination giving the most realistic biogeochemical tracer concentrations (closest to observations) is chosen for the experiments in the main text (Fig. 2.3). This approach for determining the physical transport parameters is applied to obtain those in Table 2.2.

2.9 Appendix E

The VD, VDRD, VID and OB configurations are sensitivity configurations that we employ to explore the ability of several mechanisms for preventing nitrogen exhaustion in the OMZ. Even though all of them fail in simulating realistic biogeochemical tracer concentrations compared with observations, they reveal insights into the effects of the respective mechanisms.

The VD configuration, which differs from the STD configuration in supplying additional O_2 from the subtropical ocean into the D box, avoids anoxic deep waters, but fails to prevent nitrate exhaustion in the UM box (Fig. 2.3e, f). The I and D boxes are oxic at steady state, but NO_3^- is still exhausted by denitrification in the UM box. Comparing the oxygen concentrations of the RD and VD configurations, we conclude that ventilation helps to prevent oxygen depletion in the D box, but this mechanism alone cannot prevent eventual runaway denitrification in the UM box.

After incorporating reduced denitrification in the VDRD configuration, nitrate depletion is prevented and the I and D boxes are oxic (Fig. 2.3g, h). But the O_2 concentration in the I box is about 28 % lower than that of the WOA2009 data, which indicates that O_2 supply into the D-box only may not be sufficient to ventilate the model domain.

The VID configuration, which is modified from the VD configuration by including O_2 ventilation into the I box, fails to prevent NO_3^- depletion by denitrification in the OMZ (Fig. 2.3i, j).

In the OB configuration, nutrients are exchanged in addition to O_2 between the subtropical ocean and the I and D boxes. In this configuration, nitrate exhaustion in the OMZ is still not prevented, even though phytoplankton and nitrogen fixer concentrations are lower in the surface U and S boxes (Fig. 2.3m, n).

Two further sensitivity experiments were performed for each of the VID and OB configurations to explore how NO_3^- depletion in the UM box can be prevented. (1) Decreasing the fraction of export production remineralized in the UM box (f_{UM}) from 70 to 56 % makes NO_3^- persist in the UM box. Together with the 20 % remineralization in the U box, this implies that 76 % of the export production is remineralized in the upper 500 m of the ocean. However, the resulting NO_3^- concentration in the UM box is far below the literature range of about 15 to 40 μmol L^{-1}. (2) Facultative N_2-fixation inhibits nitrogen fixation in an environment with high NO_3^- concentrations, but fails to prevent NO_3^- depletion in the UM box.

The sensitivity with respect to the biogeochemical parameters (Sect. 2.5) is examined for all configurations. We only discuss the sensitivity of the OBRD configuration in Sect. 3.3, since the sensitivity experiments in all model configurations do not affect our main conclusion that fixed-N inventory can be stabilized at non-zero levels in the ETSP OMZ only if the remineralization rate via denitrification is slower than that via aerobic respiration. The model behaviour is very similar in all sensitivity experiments, with two exceptions. When μ_{NF} is raised to $1/2\mu$ and remineralization fractions in different boxes are rearranged to f_U=f_S=60% combined with f_{UM}=f_I=30%, the VDRD and VIDRD configurations reach a steady state only in combination with facultative N_2-fixation.

2.10 Acknowlegements

The authors wish to acknowledge funding from the CSC (Chinese Scholarship Council), Sonderforschungsbereich 754 “Climate-Biogeochemistry Interaction in the Tropical Ocean” (`www.sfb754.de`) supported by the Deutsche Forschungsgemeinschaft, the EU FP7 project CARBOCHANGE “Changes in carbon uptake and emissions by oceans in a changing climate” (Grant agreement no. 264879) and the Cluster of Excellence “The Future Ocean”, Kiel, Germany. The authors also wish to thank Ivonne Montes and Christopher Somes for the many helpful and inspiring discussions, and Christopher Somes and Tim DeVries for providing their model results of the ETSP. The very constructive comments that helped improve the manuscript from the two anonymous reviewers are highly appreciated.

Chapter 3

Box-modeling of the impacts of atmospheric nitrogen deposition and benthic remineralization on the nitrogen cycle of the eastern tropical South Pacific

Bei Su[1], Markus Pahlow[1], and Andreas Oschlies[1]

[1]GEOMAR Helmholtz-Zentrum für Ozeanforschung Kiel, Marine Biogeochemical Modelling, Düsternbrooker Weg 20, 24105 Kiel, Germany.

Correspondence to: B. Su (bsu@geomar.de)

Submitted to: ***Biogeosciences***

Abstract Both atmospheric deposition and benthic remineralization influence the marine nitrogen cycle, and hence ultimately also marine primary production. The biological and biogeochemical relations of the eastern tropical South Pacific (ETSP) to nitrogen deposition, benthic denitrification and phosphate regeneration are analysed in a prognostic box model of the oxygen, nitrogen and phosphorus cycles in the ETSP. In the model, atmospheric nitrogen deposition based on estimates for the years 2000-2009 is offset by half by reduced N_2 fixation, with the other half transported out of the model domain. Both model- and data-based benthic denitrification are found to trigger nitrogen fixation, partly compensating for the NO_3^- loss. Since phosphate is the ultimate limiting nutrient in the model, enhanced sedimentary phosphate regeneration under suboxic conditions stimulates primary production and subsequent export production and NO_3^- loss in the oxygen minimum zone (OMZ). A sensitivity analysis of the local response to both atmospheric deposition and benthic remineralization indicates dominant stabilizing feedbacks in the ETSP, which tend to keep a balanced nitrogen inventory, i.e., nitrogen input by atmospheric deposition is counteracted by decreasing nitrogen fixation; NO_3^- loss via benthic denitrification is partly compensated by increased nitrogen fixation; enhanced nitrogen fixation stimulated by phosphate regeneration is partly removed by the stronger water-column denitrification. Even though the water column in our model domain acts as a NO_3^- source, the ETSP including benthic denitrification might become a NO_3^- sink.

3.1 Introduction

Marine primary production (PP) by phytoplankton is a key factor controlling the strength of the oceanic biological carbon pump and the amount of CO_2 that is stored in the ocean [Gruber, 2004, Okin et al., 2011]. PP is controlled by light and nutrients, such as nitrogen, phosphorus or iron, necessary for the production of phytoplankton. These nutrients are supplied to the light-lit surface waters by upwelling, turbulent entrainment of subsurface water, riverine inputs, biological nitrogen fixation, atmospheric deposition and benthic remineralisation [Falkowski et al., 1998, Kasai et al., 2002, Duce et al., 2008, Bakun and Weeks, 2008, Moore and Braucher, 2008].

Nitrogen is often the limiting nutrient for phytoplankton in the ocean [Moore et al., 2013]. On the other hand, oceanic nitrogen is thought to adjust, via nitrogen gain and loss processes, to the marine phosphorus inventory on geological time scales, making phosphorus the ultimate limiting nutrient and nitrogen the proximate limiting nutrient [Tyrrell, 1999]. The ocean's nitrogen inventory has a turnover time of a few thousand years, being affected by relatively large interacting nitrogen sinks and sources. The exact mechanisms and timescales of the interactions are not well understood. Estimates of oceanic nitrogen fixation, the main fixed-N source into the ocean, vary from 106 to 330 $\mathrm{Tg\,N\,yr^{-1}}$ based on both in-situ observations and

models [Codispoti et al., 2001, Brandes and Devol, 2002, Gruber and Sarmiento, 2002, Gruber, 2004, Großkopf et al., 2012]. Water-column denitrification and anaerobic ammonium oxidation (anammox) in oxygen minimum zones (OMZs), accounting for 100–300 $\mathrm{Tg\,N\,yr^{-1}}$, and benthic denitrification, estimated as 95–300 $\mathrm{Tg\,N\,yr^{-1}}$, mainly determine the oceanic fixed-N sink [Gruber and Sarmiento, 2002, Gruber, 2004, Codispoti, 2007, Bohlen et al., 2012, Eugster and Gruber, 2012, DeVries et al., 2012]. Due to the large uncertainty in the major sources and sinks of the global nitrogen cycle, the balance of the nitrogen inventory in the ocean is still a matter of debate [Gruber, 2004, Codispoti, 2007, DeVries et al., 2012].

Phosphate can be the ultimate limiting nutrient on geological time scales even in regions with fixed nitrogen deficits with respect to the Redfield-equivalent of the phosphate concentration [Tyrrell, 1999, Su et al., 2015, Auguéres and Loreau, 2015]. The ocean's phosphorus budget has been suggested to be unbalanced in the modern ocean with sedimentary burial as the major sink exceeding phosphorus sources [Wallmann, 2010]. This condition might be alleviated by benthic phosphate regeneration, which can be enhanced under low-oxygen bottom waters (O_2<20 $\mu\mathrm{mol\,L^{-1}}$) [Slomp and Van Cappellen, 2007, Wallmann, 2010]. Input of bioavailable phosphorus into the ocean stimulates primary production, and decomposition of subsequent export production enhances O_2 consumption in the ocean, in turn increasing the volume of oceanic oxygen-deficit water and the fixed-N loss. Consequently, phosphate regeneration is expected to be enhanced by enlarging OMZs, possibly leading to a positive feedback loop [Van Cappellen and Ingall, 1994, Wallmann, 2003].

OMZs also play an important role in the global marine fixed-N budget as they are responsible for a large fraction of total marine fixed-N loss [Canfield, 2006]. The relative contribution of heterotrophic denitrification and autotrophic anammox to the total oceanic fixed-nitrogen sink remains debated [Lam et al., 2009, Ward et al., 2009]. Even though anammox has been observed to be a major fixed-N loss in eastern tropical South Pacific (ETSP) [Lam et al., 2009, Kalvelage et al., 2013], both denitrification and anammox are ultimately driven by the flux of organic matter into the OMZ [Koeve and Kähler, 2010, Kalvelage et al., 2013]. For simplicity, heterotrophic denitrification is considered the major fixed-N loss process in the present study. Continental shelves and the upper continental slopes are the most important sites for benthic fixed-N loss [Christensen et al., 1987, Devol, 1991]. However, Bohlen et al. [2011] found that the continental shelf and upper continental slope of the ETSP across a section at 11°S are sites of nitrogen recycling rather than fixed-N loss, because of relatively low rates of denitrification and high rates of NH_4^+ release from Dissimilatory Nitrate Reduction to Ammonium (DNRA). This illustrates that the NH_4^+ released from DNRA should be taken into account when the benthic fixed-N sink is estimated.

In the last few decades, a number of model and data based investigations have been carried out on the importance of atmospheric fixed-N input into the ocean for marine biogeochemical cycles [Duce, 1986, Duce et al., 1991, Krishnamurthy et al., 2007, 2010, Okin et al., 2011,

Mouriño-Carballido et al., 2012]. Duce et al. [2008] indicate that anthropogenic nitrogen deposition is rapidly approaching the global oceanic estimates for N_2 fixation, while preindustrial deposition was an order of magnitude lower than N_2 fixation. However, the response of nitrogen-fixation and denitrification to atmospheric nitrogen deposition remains an open question. Atmospheric nitrogen inputs into the global ocean are dominated by inorganic nitrogen from anthropogenic sources [Warneck, 1988, Paerl and Whitall, 1999]. The exact magnitude of organic nitrogen deposition is not clear due to a lack of observations [Cornella et al., 2003, Duce et al., 2008, Zamora et al., 2011]. Thus, the contribution of DON to total nitrogen deposition is still uncertain and the distribution, bioavailability and lifetime are also not clear [Seitzinger and Sanders, 1999, Duarte et al., 2006, Duce et al., 2008]. Therefore, DON deposition is excluded from our analysis.

Various biogeochemical models have addressed the effects and feedbacks between the major sources and sinks in the marine nitrogen cycle [Van Cappellen and Ingall, 1994, Deutsch et al., 2001, 2007, Krishnamurthy et al., 2007, Somes et al., 2013, Landolfi et al., 2013]. However, most of them have explored only a subset of the atmospheric, pelagic and benthic nitrogen sources and sinks. Using a conceptually simple and computationally efficient box model, we here attempt a synthesis considering all essential sources and sinks and their mutual interactions, with the only exception of riverine input, which is excluded from our model analysis because of its unknown and presumably minor role in the ETSP.

3.2 Model description

3.2.1 Circulation and biogeochemical model

The circulation model is the same as in Su et al. [2015], which is a prognostic 5-box model to explore the interactions among oceanic circulation, nitrogen fixation and water-column denitrification in the OMZ of the ETSP. Briefly, the physical parameters were calibrated to fit the average $\delta^{14}C$ of each box and biogeochemical parameters are constrained by literature data. All the simulations in this manuscript employ the Open-boundary + Reduced-denitrification (OBRD) configuration of Su et al. [2015], which allows for exchange of deep and intermediate ETSP waters with the southern subtropical ocean ("SO" in Fig. 3.1) and applies reduced remineralisation rates under suboxic conditions. The model domain consists of five boxes representing the water column of an upwelling region and an adjacent ocean basin. The U box represents the upper upwelling region. The UM box is the OMZ below, where suboxia is expected to develop. The S box represents the surface ocean away from the upwelling zone. Below the S box sits the I box, which represents water of intermediate depth and exchanges water with UM. D is the deep box, which represents water deeper than 500 m (model configuration shown in Fig. 3.1).

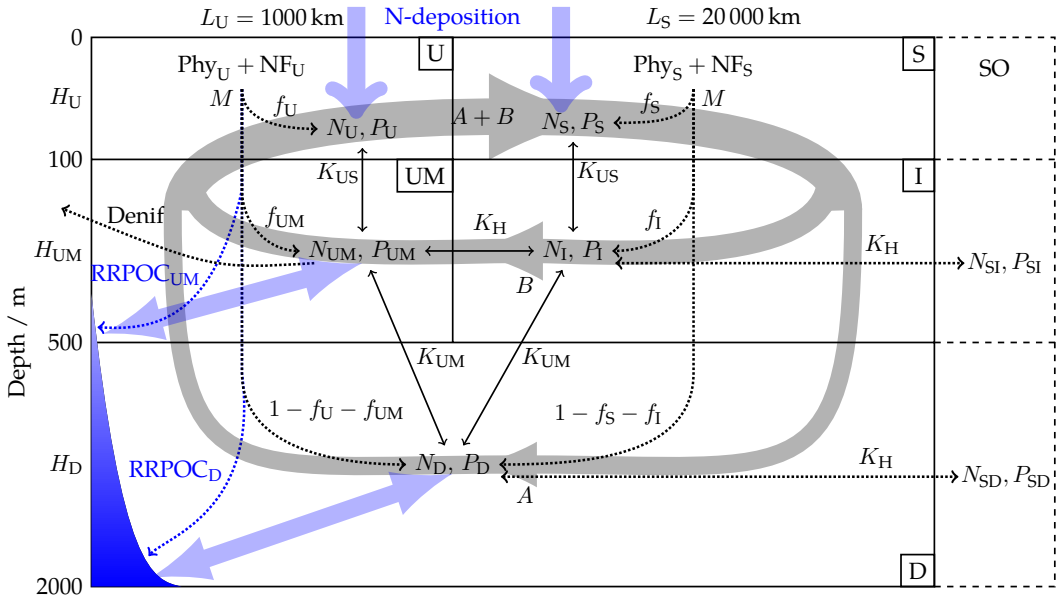

Figure 3.1: Model structure. The model domain comprises five boxes representing the top 100 m of an upwelling region (U), the underlying oxygen minimum zone (UM), and an adjacent open-ocean basin divided into a surface (S) and an intermediate-depth box (I). A deep box (D) underlies both the upwelling region and the open ocean. The large-scale circulation is represented by deep (A) and shallow (B) convection (thick grey lines). Mixing between boxes is implemented via mixing coefficients (K). Remineralisation derived from primary production by ordinary (Phy) and diazotrophic (NF) phytoplankton in the surface boxes consumes oxygen. Under anoxic conditions remineralisation is fueled by anaerobic remineralization (Denif). In the configuration employed in this study, the model domain exchanges nutrients and oxygen with the southern subtropical ocean (right, denoted as "SO''). Nitrogen deposition and benthic remineralization are included additionally to represent their influence on the local water-column nutrient concentrations (thick light blue arrows).

There are two phytoplankton types in the biogeochemical model, ordinary phytoplankton, Phy, and nitrogen fixers, NF, as defined in Su et al. [2015]. Both Phy and NF require phosphate, whereas nitrate is required in addition to phosphate only by Phy, and NF can fix N_2 as long as PO_4^{3-} is available. Dead phytoplankton is immediately remineralized in the surface layer and underlying boxes according to the pre-defined remineralization fractions. Remineralization occurs preferentially via aerobic respiration, with anaerobic denitrification and the associated nitrogen loss setting in only when all O_2 has been consumed by aerobic respiration. When oxygen is exhausted in the OMZ, remineralization is assumed to slow down by a factor of 5, and accordingly denitrification within the UM box is responsible for 1/5 of the remaining organic matter remineralization and the remainder will be remineralized in the D box.

In order to represent the nitrogen and phosphate fluxes across the water–sediment interface, remineralization of particulate organic carbon reaching the sediment (POC rain rate, RRPOC) is included additionally in the UM and D boxes. RRPOC is calculated according to the method

Configuration	Process				
	Model BD	Data BD	Model PR	Data PR	N-DEP
Control					
N-DEP					+
MBD	+				
MPR			+		
DBD		+			
DPR				+	
Synthesis configuration					
MBD+MPR (Syn1)	+		+		
DBD+DPR (Syn2)		+		+	
MBD+MPR+N-DEP (Syn3)	+		+		+
DBD+DPR+N-DEP (Syn4)		+		+	+

Table 3.1: Summary of model configurations. 'Model BD' and 'Data BD' represent model- and data-based benthic denitrification, respectively. 'Model PR' and 'Data PR' are model- and data-based benthic phosphate regeneration, respectively. 'N-DEP' represents the atmospheric nitrogen input into the surface ocean according to the estimate by Lamarque et al. [2011]. '+' indicates that the process is included.

introduced in Section 3.2.4, and we assume that all the POC is buried in the sediment.

3.2.2 Model configurations

The above descriptions define the control configuration. In order to investigate the model sensitivity to atmospheric nitrogen deposition and benthic remineralization, we employ another nine model configurations incorporating either a subset or all of these processes, which are summarized in Table 3.1. Detailed information of all processes is presented in Sections 3.2.3, 3.2.4 and 3.2.5.

3.2.3 Atmospheric nitrogen deposition

Years 2000–2009 levels of dry and wet inorganic nitrogen deposition following the RCP 4.5 scenario [Lamarque et al., 2011] are examined in our work. Inferred atmospheric inorganic nitrogen deposition rates are 0.081 and 1.4 $\mathrm{Tg\,N\,yr^{-1}}$ (73.1 and 64.9 $\mathrm{mg\,N\,m^{-2}\,yr^{-1}}$) for the U and S box, respectively. Note that the circulation remains constant in our model, and only

atmospheric nitrogen deposition fluxes are included as an additional annual nitrogen input into the surface (U and S) boxes.

Duce et al. [1991] estimated atmospheric dissolved inorganic phosphorus (DIP) input into the global ocean, which indicates high N/P (mole/mole) ratios of more than 100 on a global scale [Dentener et al., 2006, Duce et al., 2008, Mahowald et al., 2008], much higher than the average elemental N/P required by phytoplankton in the ocean. Thus, we do not explore the influence of atmospheric phosphorus deposition in our analysis.

3.2.4 Benthic denitrification

The empirical transfer function of Bohlen et al. [2012] is applied to predict benthic inorganic nitrogen loss (L_{DIN} in μmol N m^{-2} d^{-1}) through benthic denitrification, which can account for the net loss of dissolved inorganic nitrogen (DIN) from the sediment.

$$\mathrm{L_{DIN}} = (0.06 + 0.19 \times 0.99^{(\mathrm{O_2}-\mathrm{NO_3^-})_{\mathrm{bw}}}) \times \mathrm{RRPOC} \tag{3.1}$$

where NO_3^- and O_2 are bottom-water nitrate and oxygen concentrations in μmol kg^{-1}, and the rain rate (RRPOC) is in μmol C m^{-2} d^{-1}. Since the bottom-water NO_3^- and O_2 concentrations are well known in the ETSP, the uncertainty in our estimation of benthic denitrification comes mostly from uncertainties in the rain rate, which, in turn, depends on biological production, as a function of phytoplankton biomass and its physiological status. Simulated phytoplankton concentrations in the surface boxes of the model roughly agree with estimates by Behrenfeld et al. [2005] from Aqua-Modis satellite data and the Redfield C:N ratio (U-box: 1.06 μmol N kg^{-1} simulated vs. 0.68 μmol N kg^{-1} from Aqua-Modis; S-Box: 0.23 μmol N kg^{-1} simulated vs. 0.28 μmol N kg^{-1} from Aqua-Modis).

Model-based estimation of benthic denitrification

Fixed-N losses via benthic denitrification (L_{DIN}) in the UM and D boxes are obtained according to Eq. 3.1, with the respective simulated actual NO_3^- and O_2 concentrations taken as the bottom-water concentrations, and RRPOC is estimated from the export production out of the U and S boxes (EP_U and EP_S) and the Martin curve (Eq. 3.2) [Martin et al., 1987]:

$$\mathrm{RRPOC} = F \times \left(\frac{z}{100}\right)^{-b} \tag{3.2}$$

where RRPOC is the rain rate, F is the export production from both surface boxes, and z is the water depth. The bathymetry of the regions of the UM and D boxes is derived from ETOPO2 (`http://www.ngdc.noaa.gov/mgg/gdas/gd_designagrid.html`). We apply $b = 0.82$ in Eq. 3.2, which is the global average according to Berelson [2001] and also close to his estimate for the

	Sediment percentage (SD,%)	Average Martin curve value (AMC,%)
UM box	0.81	53.04
D box	2.25	12.51

Table 3.2: Sediment percentage and average Martin curve value used for the model-based estimation of benthic denitrification. "Sediment percentage" is the percentage of the surface areas of the UM and D boxes in contact with the sediment; "Average Martin curve value" represents the average of Martin curve fractions of export production reaching the sediment for each grid point of the topography data.

ETSP. An exponent of 0.4 for Eq. 3.2 in suboxic water is implied by Van Mooy et al. [2002]. Therefore, sensitivity experiments are performed with $b = 0.4$. From Eq. 3.2 and the fraction of the lower boundary of the respective box in contact with the seafloor, the RRPOC at the sediment surfaces of the UM and D boxes is calculated according to Eqs. 3.3 and 3.4:

$$\mathrm{RRPOC_{UM}} = \mathrm{EP_U} \times \mathrm{SD_{UM}} \times \mathrm{AMC_{UM}} \tag{3.3}$$

$$\mathrm{RRPOC_D} = (\mathrm{EP_U} + \mathrm{EP_S}) \times \mathrm{SD_D} \times \mathrm{AMC_D} \tag{3.4}$$

where $\mathrm{AMC_{UM}}$ and $\mathrm{AMC_D}$ are the average Martin-curve values corresponding to the actual water depth (z) in the grid of ETOPO2 respectively; $\mathrm{SD_{UM}}$ and $\mathrm{SD_D}$ represent the percentages in contact with the sediment in the UM and D boxes (Table 3.2).

Data-based estimation of benthic denitrification

For a second and independent estimate of $\mathrm{L_{DIN}}$, we combine observations from different datasets. O_2 and NO_3^- concentrations for our model domain are obtained from the annual objectively analyzed mean concentrations of the WOA 2009 $1° \times 1°$ data [Garcia et al., 2010a,b], and interpolated over the region of our model domain to match the resolutions of the other datasets.

RRPOC is estimated from primary production following Bohlen et al. [2012]. According to the carbon-based approach of Behrenfeld et al. [2005], average annual primary production is derived from photosynthetically available radiation (PAR), the diffuse attenuation coefficient at 490 nm (K490), chlorophyll a (Chl a) and mixed layer depth (MLD). PAR, K490 and Chl a are from the Aqua-Modis satellite data (2005–2010) (`http://oceancolor.gsfc.nasa.gov/`), and MLD is from the Fleet Numerical Meteorology and Oceanography Center (FNMOC, `http://www.public.navy.mil/fltfor/cnmoc/Pages/fnmoc_home.aspx`). Export production is estimated from primary production and sea-surface-temperature (SST) [Dunne et al., 2005],

where SST is from the WOA 2009 annual average $1^\circ \times 1^\circ$ temperature data [Locarnini et al., 2010]. The rate of particle transport at each grid cell to the seafloor is calculated using the Martin curve (Eq. 3.2) [Martin et al., 1987]. To obtain more accurate estimates for RRPOC of our regional box model, all data processed in this experiment are interpolated on a grid of $2' \times 2'$ in the UM box and $20' \times 20'$ in the D box, and the ETOPO2 data ($2' \times 2'$) are averaged within each $20' \times 20'$ grid cell in the D box. The Aqua-Modis data ($5' \times 5'$) and NO_3^- and O_2 concentrations from WOA 2009 dataset are interpolated or averaged horizontally to match these resolutions. The vertical resolution of the NO_3^- and O_2 concentrations are interpolated to resolve the bathmetry of the ETOPO2 data, and the NO_3^- and O_2 concentrations closest to the sediment are applied in Eq. 3.1 for the bottom water NO_3^- and O_2 concentrations.

Finally, the L_{DIN} derived from observational datasets are averaged over the regions represented by UM and D boxes to produce an annual NO_3^- loss term.

3.2.5 Phosphate regeneration

Phosphate regeneration is estimated according to Wallmann [2010] and Flögel et al. [2011] with both model- and data-based estimates for the rain rate. We estimate benthic PO_4^{3-} regeneration (resupply of benthic PO_4^{3-} into the water column, $\mathrm{Ben_{DP}}$) from the RRPOC degradation ratio (r_{REG}) and the POC burial rate in the sediments (BURPOC) according to:

$$\mathrm{Ben_{DPUM}} = \frac{\mathrm{RRPOC_{UM}} - \mathrm{BURPOC_{UM}}}{r_{\mathrm{REG}}} \tag{3.5}$$

$$\mathrm{Ben_{DPD}} = \min\left(\frac{\mathrm{RRPOC_{D}} - \mathrm{BURPOC_{D}}}{r_{\mathrm{REG}}}, \frac{\mathrm{RRPOC}}{106}\right) \tag{3.6}$$

where RRPOC is estimated with the methods described in sections 3.2.4 and 3.2.4. A minimum condition is introduced in the D-box to prevent $\mathrm{Ben_{DP}}$ exceeding the rain rate of particulate organic phosphate (RRPOP=RRPOC/106) to the deep ocean, but not for the UM box, because there are possible extra sources of RRPOP, such as inputs via weathering or eolian deposition, onto the continental shelf, which is contained in the UM box in our model.

BURPOC is estimated from Eq. 3.7 for the continental shelf (UM box) and Eq. 3.8 for the deep-sea sediment (D box), and r_{REG} is the C:P regeneration ratio estimated via Eq. 3.9 following the empirical relations of Wallmann [2010].

$$\mathrm{BURPOC_{UM}} = 0.14 \cdot \mathrm{RRPOC_{UM}^{1.11}} \tag{3.7}$$

$$\mathrm{BURPOC_{D}} = 0.014 \cdot \mathrm{RRPOC_{D}^{1.05}} \tag{3.8}$$

$$r_{\mathrm{REG}} = 123 + (-112) \times \exp(-\frac{\mathrm{O_2}}{32}) \tag{3.9}$$

where O_2 is the oxygen concentration in the ambient bottom water (in μmol kg^{-1}). r_{REG} in Eq. 3.9 is higher than the Redfield ratio in oxic water, resulting in preferential P burial under oxic conditions; it is much smaller than the Redfield ratio when O_2<20 μmol kg^{-1}, indicating excess phosphate release from the sediment under suboxic conditions.

3.2.6 Synthesis configurations

Nitrogen deposition, benthic denitrification and phosphate regeneration are integrated into the synthesis model configurations to explore the model sensitivity to each process and their mutual interactions in the ETSP. The configurations (Syn1 to Syn4) with different benthic processes and atmospheric inputs are summarized in Table 3.1.

3.2.7 Model sensitivity experiments

Since our model domain only includes the top 2000 meters of the water column, the sediments only account for a small portion of the whole sediment of the ETSP (Table. 3.2). A sensitivity experiment is performed with the assumption that all of the bottom of the D box is in contact with the sediment below 500m (high benthic denitrification (high-BD), or high phosphate regeneration (high-PR)) including all NO_3^- losses by benthic denitrification and phosphate release by phosphate regeneration of the sediment.

The original work of Martin et al. [1987] and Van Mooy et al. [2002] indicate a lower value for the exponent b of Eq. 3.2 in suboxic water. We perform an additional sensitivity experiment with b=0.4 according to the suggestion by Van Mooy et al. [2002], to explore the influence of benthic denitrification and phosphate regeneration under conditions of slower POC remineralization.

3.3 Results

3.3.1 Nitrogen deposition

Due to the low NO_3^- concentrations in the surface U and S boxes, the annual nitrogen input by atmospheric nitrogen deposition accounts for 63% and 10%, respectively, of nitrogen inventories of the U and S boxes. Fig. 3.2 indicates that the extra fixed-N input by nitrogen deposition reduces the growth of nitrogen fixers in the surface ocean by about 0.72–0.73 $\mathrm{Tg\,N\,yr^{-1}}$ (about 12% of total nitrogen fixation), which accounts for about 48% of the total fixed-N inputs into surface waters from atmospheric deposition ($1.5\,\mathrm{Tg\,N\,yr^{-1}}$). Water-column denitrification stays almost unchanged because the increase in export production (EP) of Phy is almost exactly compensated by the decrease in EP of NF, resulting in essentially unchanged total EP. As a result of the $\sim$50% of the nitrogen deposition not immediately compensated by a decline in nitrogen fixation, the model domain becomes a larger fixed-N source (Fig. 3.2). The N-loss through the lateral boundary increases from $0.93\,\mathrm{Tg\,N\,yr^{-1}}$ in the control configuration to $1.7\,\mathrm{Tg\,N\,yr^{-1}}$ in the configurations including nitrogen deposition, leading to about $0.78\,\mathrm{Tg\,N\,yr^{-1}}$ extra fixed-N loss from the model domain, i.e. about 50% of the total fixed-N input by nitrogen deposition. Thus, almost all the extra nitrogen input into the model domain via nitrogen deposition is offset by lower nitrogen fixation and nitrogen loss by lateral transport out of the model domain.

There is no significant influence of nitrogen deposition on the biogeochemical tracer concentrations of the model at steady state: ordinary phytoplankton (Phy) concentrations increase by 3% in the U box and even smaller changes occur in the S box, which can be attributed to the stronger nitrogen deficit in the region above the OMZ (U box) than in the open ocean (S box) (not shown). Largest changes are found for the concentration of nitrogen fixers (NF) that decrease by about 9% in the U box, counteracting the nitrogen input via nitrogen deposition (Fig. 3.3). Again in the S box, NF concentration stays almost unaltered (Fig. 3.3). There are also slight variations of the NO_3^- concentration in the UM box and of the O_2 concentrations in the I and D boxes (not shown).

3.3.2 Benthic denitrification

The data-derived benthic denitrification and phosphate regeneration in the UM and D boxes are shown in Table 3.3. The modeled net primary production (NPP) in the surface ocean above the UM and D boxes is, respectively, 1.4 and $0.87\,\mathrm{g\,C\,m^{-2}\,day^{-1}}$, indicating higher NPP in the coastal upwelling region and lower NPP in the open ocean adjacent to the upwelling region, which is consistent with the estimate by Behrenfeld et al. [2005]. Due to the small sediment area percentages, the annual nitrogen loss by benthic denitrification is 0.17 and $0.82\,\mathrm{Tg\,N\,yr^{-1}}$ in the UM and D boxes, accounting for only about 0.14% and 5.1×10^{-3}% per year, respectively,

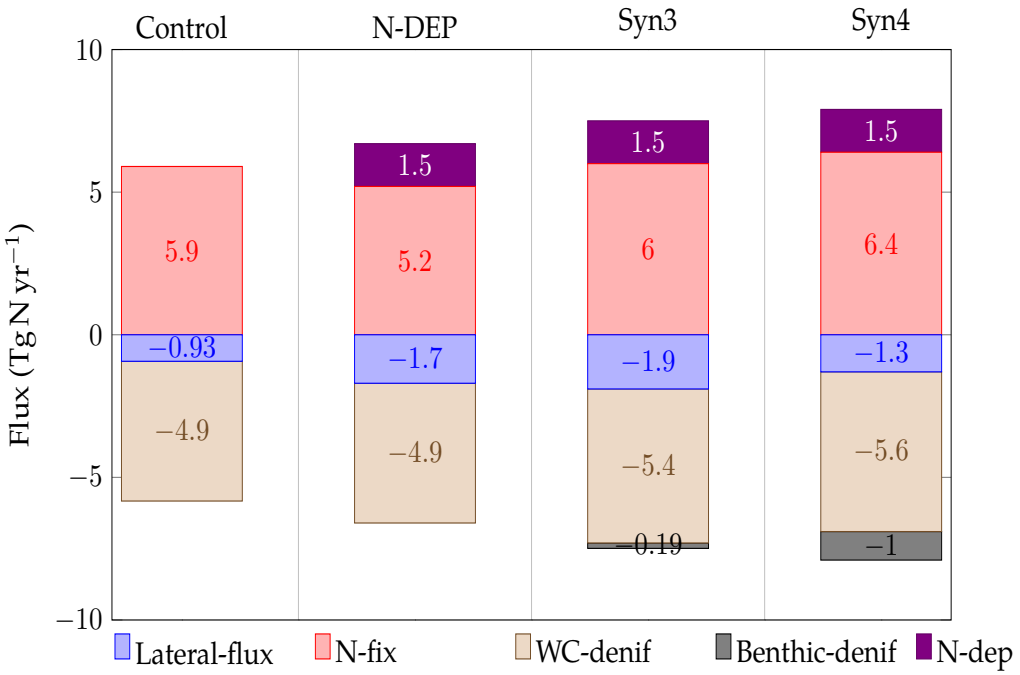

Figure 3.2: Nitrogen fluxes after including atmospheric nitrogen deposition in the control, Syn3 and Syn4 configurations defined in Table 3.1. Lateral-flux identifies the nitrogen efflux or influx through the southern boundary; N-fix represents the nitrogen fixation rate by NF; WC-denif is water-column denitrification; N-dep is the nitrogen input into surface ocean via nitrogen deposition.

	NPP	Rain rate	BD	PR
	(mg C m^{-2} day^{-1})		(Tg N yr^{-1})	(Tg P yr^{-1})
UM	1374.7	148.4	0.17	0.058
D	873.9	12.2	0.82	0.056
D (high-BD/PR)	873.9	12.2	8.8	0.56

Table 3.3: Fixed-N loss via benthic denitrification (BD) and phosphate release via phosphate regeneration (PR) in the UM and D boxes. High-BD indicates that the full sediment of the D box is include to estimate NO_3^- loss via benthic denitrification and phosphate release via phosphate regeneration. These values are estimated from Aqua-Modis satellite data.

of the NO_3^- inventories (Table 3.2). The higher sedimentary NO_3^- sink in the UM box can be attributed to the anoxic conditions and larger RRPOC there.

Our simulated biogeochemical tracer concentrations at steady state are quite robust with respect to including benthic denitrification (Fig. 3.3). There are only minor deviations of the MBD and DBD configurations from the control run. Nitrogen fixation rates increases by about 2.9% and 5.8% respectively in the MBD and DBD configurations (A-bars in panels MBD and

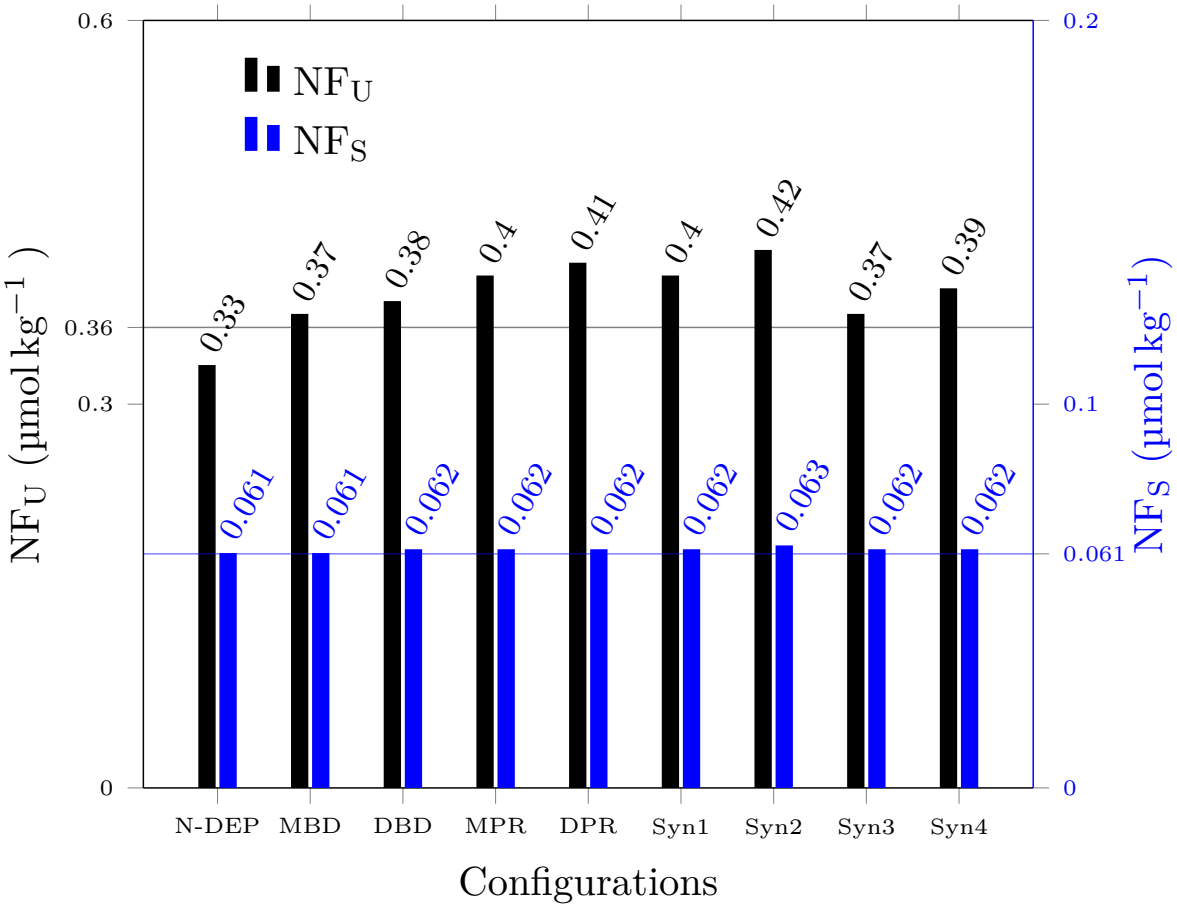

Figure 3.3: Sensitivity of simulated steady-state concentrations of nitrogen fixers NF_U and NF_S in the U and S boxes respectively. Horizontal grey and light blue lines represent the NF_U and NF_S concentrations in the control configuration respectively. Syn1, Syn2, Syn3 and Syn4 denote the "MBD+MPR", "DBD+DPR" , "MBD+MPR+N-DEP'', and "DBD+DPR+N-DEP'' synthesis configurations defined in Table. 3.1.

DBD of Fig. 3.4). Obviously, the response is stronger in the DBD configuration than in the MBD configuration, because there is an approximately 5-times larger fixed-N loss via benthic denitrification in the DBD configuration (A-bars in Fig. 3.4). The DBD configuration results in stronger responses of nitrogen fixation and lateral fluxes to benthic denitrification: the increase in nitrogen fixation can not fully compensate the nitrogen loss by benthic denitrification, thus, the model domain becomes a smaller fixed-N source, about 25% of that in the control configuration. Otherwise, the steady-state solutions of the MBD and DBD configurations are almost identical to that of the control configuration after including benthic denitrification. The temporal development of biogeochemical tracer concentrations is also insensitive to including benthic denitrification (not shown).

3.3.3 Phosphate regeneration

Phosphate release by phosphate regeneration accounts for about 0.23% and 2.2 $\times 10^{-3}$% per year, respectively, of the total phosphate inventories in the UM and D boxes (Table 3.2). The higher sedimentary PO_4^{3-} source in the UM box can be attributed to the anoxic conditions and larger RRPOC there. The phosphate release associated with benthic phosphate regeneration can stimulate nitrogen fixation and EP from the surface ocean, followed by higher water-column denitrification, owing to enhanced decomposition of exported organic matter (A-bars in MPR and DPR panels of Fig. 3.4). In the MPR configuration, nitrogen fixation and water-column denitrification increase by 12% and 11%, respectively, while in the DPR configuration, nitrogen fixation and water-column denitrification increase by about 17% and 15% (A-bars in MPR and DPR panels of Fig. 3.4). Compared with the MBD and DBD configurations, phosphate regeneration cannot turn our model domain into a smaller fixed-N source even though there is higher water-column denitrification, because nitrogen fixation can compensate for the nitrogen loss by water-column denitrification (A-bars in Fig. 3.4).

While changes in nitrogen deposition and benthic denitrification are to a large extent compensated by adjustments via simulated nitrogen fixation, phosphate is the ultimate limiting nutrient in our model domain [Su et al., 2015]. Hence the extra phosphate input into the model domain by phosphate regeneration has a more significant influence on the steady-state model results than the perturbations of the nitrogen input or loss applied in the model (Fig. 3.3). Phy concentration in the DPR configuration decreases in the U box but remains unchanged in the S box (not shown). Phy concentrations in the U and S boxes remain almost unaltered in the MPR configuration. Compared with the control configuration, NF concentrations in the U and S boxes increase by 11% and 1.6% respectively in the MPR configuration, and 14% and 1.6% respectively in the DPR configuration (Fig. 3.3). The nitrate concentration in the UM box decreases by about 4.2% in the MPR configuration and 5.2% in the DPR configuration (not shown). The temporal development of biogeochemical tracer concentrations is also robust to benthic phosphate regeneration (not shown).

3.3.4 Synthesis configurations

In the synthesis configurations (Tables 3.1), phytoplankton, nutrient and oxygen concentrations are quite robust with respect to the various fluxes associated with nitrogen input or removal and phosphate release from the sediment into the water column (Fig. 3.3). However, the interactions among nitrogen fixation, water-column denitrification, benthic denitrification, and phosphate regeneration result in different sensitivities of nitrogen fixation and the lateral flux to atmospheric N deposition in the presence of benthic denitrification and phosphate regeneration (Fig. 3.3). In contrast to the N-DEP configuration, nitrogen fixation rates in the Syn3 and Syn4 configurations increase by about 1.7% and 8.5% in spite of additional nitrogen in-

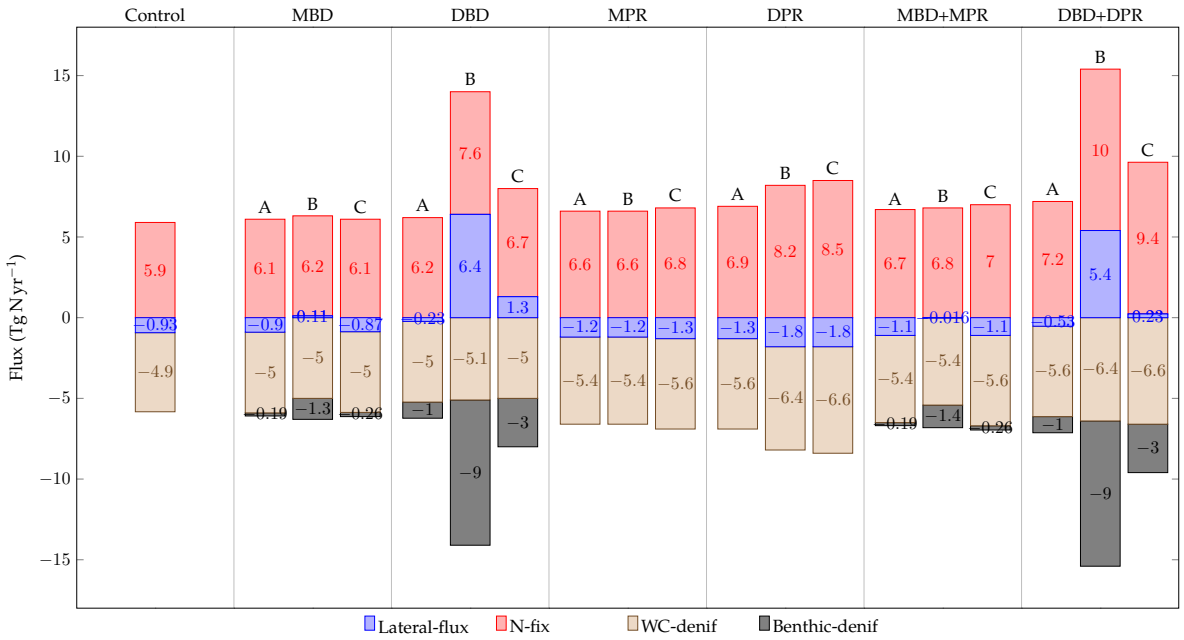

Figure 3.4: Nitrogen fluxes after including benthic denitrification or/and phosphate regeneration. Lateral-flux identifies the nitrogen efflux or influx through the southern boundary; N-fix represents the nitrogen fixation rate by NF; WC-denif is water-column denitrification; Benthic-denif represents the fixed-N loss via benthic denitrification in the model domain. Bar labels: A, main experiments; B, sensitivity experiments with high-BD; C, sensitivity experiments with Martin Curve exponent b=0.4.

put into model domain by atmospheric nitrogen deposition. The lateral flux out of the model domain (NO_3^- source) increases by about 0.97 Tg N yr^{-1} in the Syn3 configuration, which accounts for about 65% of the total nitrogen deposition, so that more than half of the extra nitrogen supplied by nitrogen deposition is not utilised locally. However, in the Syn4 configuration, the lateral NO_3^- efflux increase only accounts for about 25% of the total nitrogen deposition, with 75% of the deposited nitrogen utilised in the model domain. Less fixed-N is lost laterally from the model domain in the configurations including data-based estimates than those including model-based estimates, due to more NO_3^- loss within the model domain (Fig. 3.4). Thus, the lateral fluxes and the sensitivity to nitrogen deposition are also controlled by benthic denitrification and phosphate regeneration rather than nitrogen deposition only.

3.3.5 Model sensitivity

Fig. 3.5 shows the results of the sensitivity experiments with high-BD and high-PR. Compared with Fig. 3.3, the influence on the biogeochemical tracer concentrations at steady state is stronger, due to the larger NO_3^- loss via benthic denitrification and PO_4^{3-} release via phosphate regeneration (Table. 3.3). High-BD or high-BD together with high-PR can even turn our model

domain into a NO_3^- sink (B-bars in panels DBD and DBD+DPR of Fig. 3.4).

Applying the Martin Curve exponent b=0.4 also amplifies the influence of benthic denitrification and phosphate regeneration on phytoplankton and biogeochemical tracers, although the effect is weaker than in the high-BD and high-PR configurations. For example, NF_U increases by as much as 33% in the DBD+DPR configuration, and NF_S increase about 34% in the DBD configuration (Fig. 3.6). Compared with A-bars in Fig. 3.4, this enhanced influence results from the higher NO_3^- loss through benthic denitrification and phosphate input via phosphate regeneration (C-bars in Fig. 3.4).

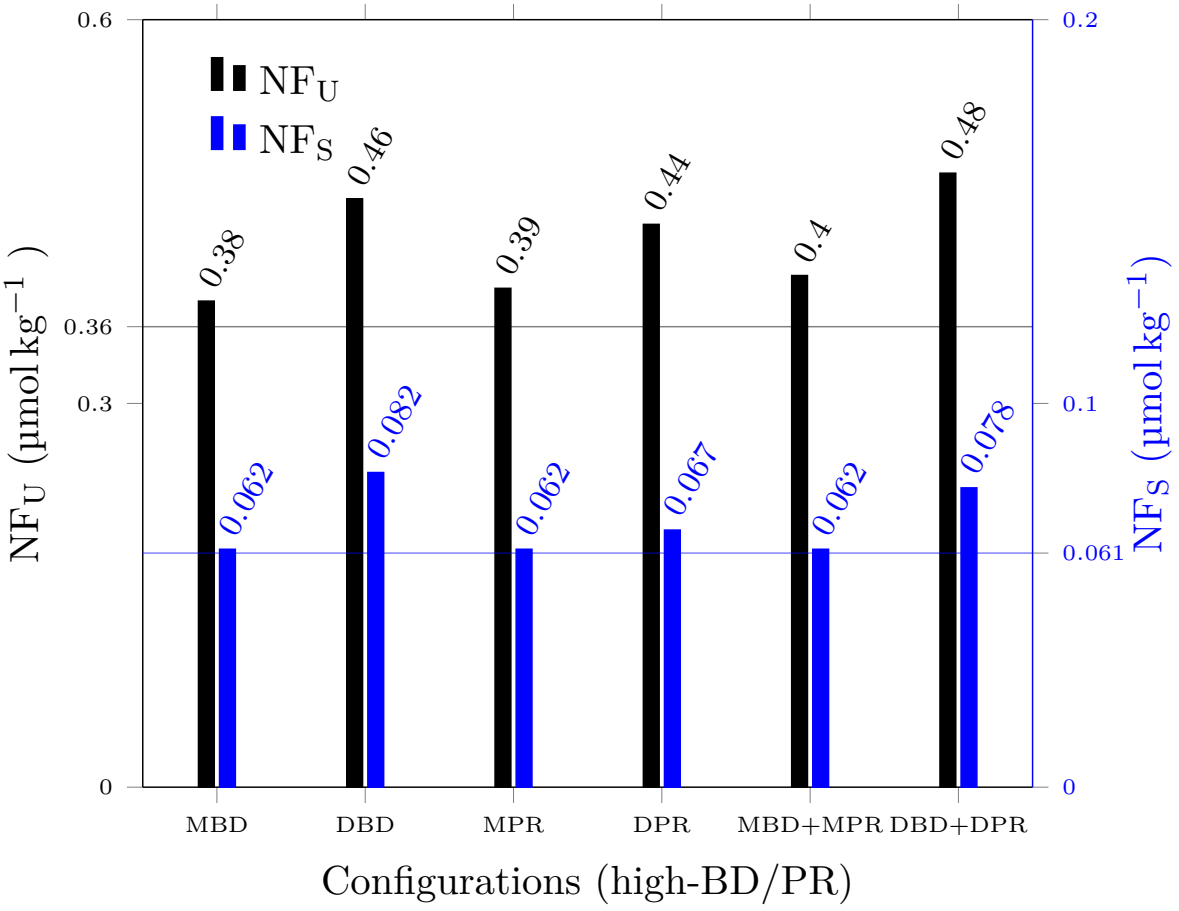

Figure 3.5: Sensitivity of simulated steady-state concentrations of nitrogen fixers (NF_U and NF_S) in the U and S boxes respectively after incorporating high-BD and high-PR. Horizontal grey and light blue lines represent the NF_U and NF_S concentrations in the control configuration.

Due to the higher RRPOC reaching the sea floor below the water column with suboxic conditions, benthic denitrification increases by about 42% and 198% (A- and C-bars of panels MBD and DBD in Fig. 3.4) and phosphate regeneration increases about 36% and 200% respec-

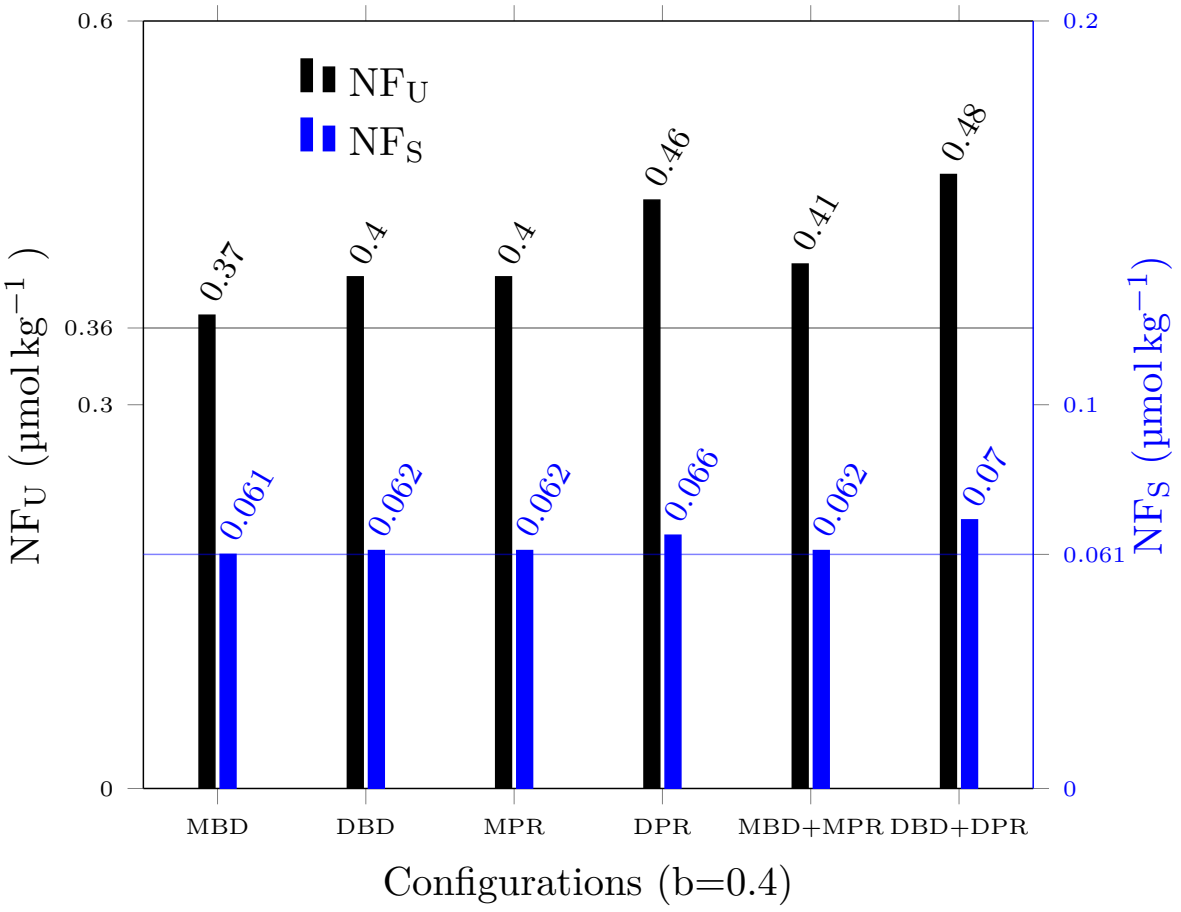

Figure 3.6: Sensitivity of simulated steady-state concentrations of nitrogen fixers (NF_U and NF_S) in the U and S boxes respectively after applying b=0.4 for Eq. 3.2. Horizontal grey and light blue lines represent the NF_U and NF_S concentrations in the control configuration.

tively in model- and data-based estimations in the sensitivity experiments with Martin Curve value b=0.4. Our model domain switches to a NO_3^- sink in the DBD and DBD+DPR configurations with b=0.4 (C-bars in Fig. 3.4). Comparing A- and C-bars of panel DBD in Fig. 3.4, we find that higher benthic denitrification can stimulate nitrogen fixation, but the water-column denitrification remains constant. However, comparing A- and C-bars of panel DBD+DPR in Fig. 3.4, we find that higher benthic denitrification can increase nitrogen fixation and water-column denitrification, indicating important role of PO_4^{3-} in the balance nitrogen inventory. This shows a positive feedback between water-column denitrification in the OMZ and benthic denitrification below, caused by slower remineralisation under anoxic conditions, which results in more RRPOC reaching the sea floor. All above comparisons indicate that phosphate limitation could be responsible for breaking this positive feedback under the assumption of our model that PO_4^{3-} is the only limiting factor for the growth of nitrogen fixers.

3.4 Discussion and conclusions

The impact of nitrogen deposition on the ETSP has rarely been investigated so far, since this region is believed to receive less atmospheric fixed-N deposition compared with the coasts of western Europe, South and East Asia [Dentener et al., 2006, Duce et al., 2008]. The influence of anthropogenic nitrogen deposition on the biogeochemical cycles of the open ocean is increasing and the increase in atmospheric nitrogen deposition will probably induce an approximately 10% rise in carbon sequestration on land and in the ocean by 2030 [Duce et al., 2008, Reay et al., 2008]. The ETSP, a typical N-deficit region due to denitrification in the OMZ, is likely to be sensitive to anthropogenic nitrogen deposition. We find that, in our model, nitrogen deposition can inhibit N_2 fixation by relieving nitrogen limitation for Phy: this counteracts the effect of atmospheric nitrogen input. This is in line with the finding that N_2 fixation decreases with increasing nitrogen deposition in global-scale models that use essentially the same assumptions about the environmental controls on marine nitrogen fixation. [Krishnamurthy et al., 2007, 2009, 2010, Zamora et al., 2010]. Another portion of the deposited nitrogen is exported out of the model domain since not all the deposited nitrogen can be taken up by Phy locally because of phosphate limitation (Fig. 3.2). Appendix A shows the model results when there is facultative N_2 fixation, which slightly enhances the strength of the negative feedback between nitrogen fixation and nitrogen deposition.

In a 3-D biogeochemical model study of the nitrogen fixation response to benthic denitrification, Somes et al. [2013] found that an increase of benthic denitrification can stimulate N_2 fixation, but this occurred under the condition that N_2 fixation was tuned to compensate for the fixed-N loss by reducing mortality and predation rates. Nitrogen fixation can also be stimulated by a N-deficit [Deutsch et al., 2007], which can result from benthic denitrification. In our 2-D model, we also find that nitrogen fixation can be enhanced by the N-deficit caused by benthic denitrification, so that nitrogen fixation can somehow compensate for the nitrogen loss.

We find a strong increase in primary production after incorporating benthic phosphate regeneration, which is mainly attributed to nitrogen fixation (Panels MPR and DPR in Fig. 3.4). Phosphate regeneration will be enhanced under O_2 deficit conditions, and the enhanced phosphate release will stimulate primary production, finally resulting in the expansion of OMZs and a possible positive feedback loop leading to more benthic phosphate regeneration [Van Cappellen and Ingall, 1994, Wallmann, 2010]. However, our model domain only represents the upper 2000 meters of the ocean and its sediments only account for a small fraction of total sediment in the ETSP. The model results incorporating benthic denitrification and phosphate regeneration for a case where all of the bottom of the D box is assumed in contact with the sediment are shown in Figs. 3.4 and 3.5. For our parameterization of nitrogen fixation being favoured in N-deficit waters, the increase of water-column denitrification can always be compensated by increased nitrogen fixation when there is only phosphate regeneration (panels

MPR and DPR in Fig. 3.4). Our model domain can only turn into a fixed-N sink after including high-BD of the full sediment.

Due to the simplicity and computational efficiency of our box model, it is relatively easy to explore model sensitivity to processes related to the nitrogen budget of the ETSP. Even though some spatial and temporal variations are missing compared with results from the global circulation models [Krishnamurthy et al., 2007, 2010, Zamora et al., 2010], we can efficiently diagnose the regional impacts at steady state. Stimulatory effects can be identified, respectively, between nitrogen fixation and water-column denitrification, phosphate regeneration and nitrogen fixation, phosphate regeneration and water-column denitrification, and atmospheric deposition and lateral NO_3^- transport (Fig. 3.4). Depressive effects occur between atmospheric deposition and nitrogen fixation, benthic denitrification and the lateral NO_3^- transport (Fig. 3.4). The model sensitivity to processes related to the nitrogen budget of the OMZ in the ETSP is illustrated in Fig. 3.7. The Nitrogen fixation rate can be enhanced by benthic denitrification, compensating for part of the NO_3^- loss. The stimulatory effect between nitrogen fixation and water-column denitrification can help to keep a fixed-N balance in the ocean. The extra fixed-N input by nitrogen deposition can be counteracted by decreased nitrogen fixation and partially removed by lateral flux. All of these local responses combined constitute a nitrogen-balancing mechanism in the ETSP. In the high-BD sensitivity experiment, our model domain turns into a NO_3^- sink (Fig. 3.4). The NO_3^- inventory in the ETSP is determined by nitrogen fixation, water-column denitrification, benthic denitrification and lateral NO_3^- flux. Since nitrogen fixation and water-column denitrification ensue only in the surface ocean and the OMZ, which are included in our model domain, we cannot rule out that the ETSP including sedimentary denitrification is a NO_3^- sink, which is consistent with many model-derived or observational results [Ganachaud and Wunsch, 2002, Kalvelage et al., 2013]. Extra phosphate input into the model domain via phosphate regeneration can increase water-column denitrification significantly due to the increase of EP from the surface ocean. However, phosphate regeneration alone can not turn our model domain into a NO_3^- sink, which corroborates that the water column of ETSP is net source of NO_3^-.

The remineralization rate of organic matter is thought to be reduced under anoxic conditions [Martin et al., 1987, Van Mooy et al., 2002], which results in more RRPOC reaching the sediments. According to the analysis of Bohlen et al. [2012], benthic denitrification is very sensitive to RRPOC, i.e., higher RRPOC results in higher benthic denitrification. Based on the findings that higher benthic denitrification can increase nitrogen fixation, higher nitrogen fixation could result in higher water-column denitrification and the expansion of OMZs and finally a positive feedback between water-column and benthic denitrification. But this positive feedback is only observed in the configurations with phosphate input via phosphate regeneration, which indicates that PO_4^{3-} limitation could prevent this positive nitrogen loss feedback.

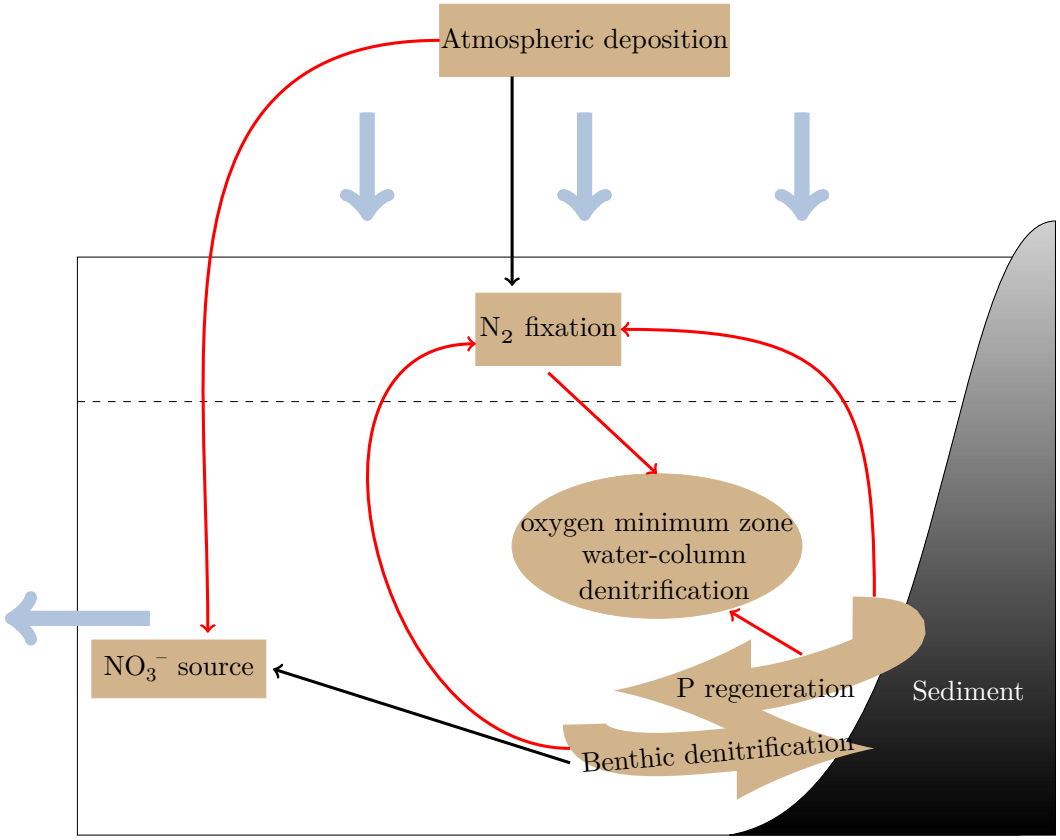

Figure 3.7: Schematic of the model sensitivity to different processes related to the nitrogen budget of the ETSP. The red solid lines present stimulatory effects, and the black solid lines represent depressive effects.

3.5 Appendix A

It is known from laboratory experiments that diazotrophic phytoplankton can also utilize DIN for growth [e.g., Holl and Montoya, 2005]. In contrast to our NF model where NF can only fix N_2 from the atmosphere, Schmittner et al. [2008] introduced a formulation to allow also NO_3^- uptake by diazotrophs. In Schmittner et al.[2008]'s model, nitrogen fixers preferentially use nitrate when available and cover only the residual N demand by N_2 fixation, denoted as facultative N_2-fixation. Thus, we explore the effect of facultative N_2-fixation on our model results with extra fixed-N input by nitrogen deposition.

Compared to results from the configurations in which NF can only fix N_2 (Fig. 3.3), both Phy and NF in the U-box are more robust to the extra nitrogen input via nitrogen deposition, for instance, Phy decreases by 1.5% (facultative N_2-fixation) vs 2.9% (N_2 fixation), and NF increases by 2.5% (facultative N_2-fixation) vs 11% (N_2 fixation). Again, the biogeochemical concentrations at steady state are relatively insensitive to nitrogen deposition (not shown).

There is a stronger negative feedback between nitrogen deposition and facultative N_2-fixation,

since nitrogen fixation is reduced by about 21% (facultative N_2-fixation) compared to 12% (obligate N_2 fixation) (Fig. 3.8). The lateral fluxes of NO_3^- only accounts for about 34% of the extra nitrogen input by nitrogen deposition (facultative N_2-fixation) compared to 50% (obligate N_2 fixation) (Fig. 3.8). Thus, facultative N_2-fixation can adjust nitrogen fixation in response to nutrient concentrations in the surface boxes and control the magnitude of our model domain being a NO_3^- source.

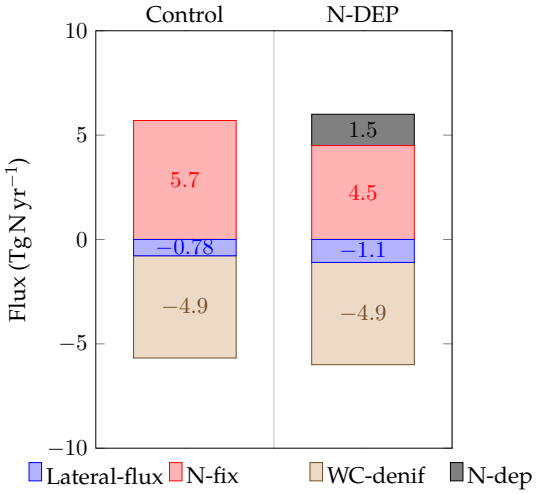

Figure 3.8: Nitrogen fluxes after including atmospheric nitrogen deposition in the model with facultative N_2-fixation. Labels are the same as those in Fig. 3.2.

3.6 Acknowledgements

The authors wish to acknowledge funding from CSC (Chinese Scholarship Council), Sonderforschungsbereich 754 'Climate-Biogeochemistry Interaction in the Tropical Ocean' (www.sfb 754.de) supported by the Deutsche Forschungsgemeinschaft, and the Cluster of Excellence 'The Future Ocean', Kiel, Germany. The authors also wish to thank Wolfgang Koeve and Paul Kähler for the great help in improving this manuscript.

Chapter 4

Coupled physical/biogeochemical modeling of the oxygen minimum zone in the eastern tropical South Pacific: sensitivity to the southern boundary conditions

Bei Su[1], Yonss José[1], Ivonne Montes[2], Markus Pahlow[1], and Andreas Oschlies[1]

[1]GEOMAR Helmholtz-Zentrum für Ozeanforschung Kiel, Marine Biogeochemical Modelling, Düsternbrooker Weg 20, 24105 Kiel, Germany.
[2]Instituto Geofísico del Perú (IGP), Lima, Peru

Correspondence to: B. Su (bsu@geomar.de)

This is a manuscript in preparation.

Abstract The impact of the southern boundary on the Oxygen Minimum Zone (OMZ) of the eastern tropical South Pacific (ETSP) is investigated with a high-resolution coupled physical-biogeochemical model. Model assessment of the realistic model configuration suggests good agreement of horizontal and vertical oxygen and nutrient distributions with observations. Comparisons among different model configurations indicate that the southern boundary is an important oxygen source to the OMZ in the ETSP, mainly influencing the southern border and the coast of the region. Lateral flux estimations show that our model domain is gaining oxygen, but losing nitrate and phosphate through the southern boundary. The southern boundary is found to have a more significant influence on O_2 concentration of the deep layer than that of the upper layer, suggesting a pathway of deep northward intrusion of well-oxygenated southern waters. The Southern Ocean is thought to be sensitive to global warming due to reductions in deep convection, resulting in a significant decrease in O_2 concentrations. This study can give some insights into the impacts of Southern Ocean variations on the O_2 cycle of the ETSP.

4.1 Introduction

The Humboldt Current System, known as the most productive eastern boundary current system, is dominant at the surface and subsurface of the eastern South Pacific. In the northern part of the Humboldt Current System, the Peru Current System (PCS) is located at the eastern tropical South Pacific (ETSP) off Peru, which hosts one of the most significant upwelling regions and permanent oxygen minimum zones (OMZs) of world ocean [Hellya and Levin, 2004, Paulmier and Ruiz-Pino, 2009]. In the OMZ, NO_3^- is converted to N_2 or N_2O by canonical denitrification or anammox, resulting in a nitrate deficit relative to phosphate [Codispoti and Christensen, 1985]. Thus, the ETSP is a location for active reactions associated with nitrogen cycle, and has significant impacts on local and even global nitrogen cycles.

The ETSP has a rich water mass structure, with water sources mainly from the equatorial Pacific and the Southern Ocean to feed waters of different depths. The surface of the PCS is the equatorward Peru Coastal Current (PCC), with a width of 500-1000 km from the coast [Strub et al., 1998]. PCC is directly associated with the coastal upwelling, thus featured by cold and salty water [Stramma et al., 2010]. It carries the subtropical water (STW) and subantarctic water (SAAW) with low NO_3^- and ${PO_4}^{3-}$ concentrations, and feeds the South Equatorial Current (SEC), which is the westward surface current of the Equatorial Current System (ECS) [Llanillo et al., 2013, references therein]. The Peru-Chile Under Current (PCUC) is a poleward flow below the PCC, which dominates the subsurface layer and extends from 50m to 700m along the western coast of South America. Its depth increases toward south and transports salty equatorial subsurface water (ESSW), which is rich in nutrients and extremely low in O_2 [Wyrtki, 1963, Penven et al., 2005, and references therein]. Since the PCUC is thought to be one of the

major sources of the upwelled water of the ETSP, the oxygen and nutrient concentrations of it are important for the study of the upwelling region and the OMZ below [Penven et al., 2005, and references therein]. As another surface current belonging to the PCS, the offshore Peru Oceanic Current (POC) extends from the surface to a depth of 700m and veers westward around 15–20°S [Wyrtki, 1963, Penven et al., 2005]. Offshore of PCC and PCUC, the Peru-Chile Counter Current (PCCC) is featured by warm water originating from the split of Equatorial Under Current (EUC), and ranges from 80°W to 84°W and 8°S to 35°S [Huyer et al., 1991, Penven et al., 2005]. The PCCC flows southward carrying ESSW and reaches a maximum speed of $0.1\,\mathrm{m\,s^{-1}}$ at 50m depth [Huyer et al., 1991].

Due to its remarkable characteristic of the PCS being in proximity and directly connected to the equatorial ocean at its northern border both in the surface ocean (0–50m) and below the surface, the ECS is one of the water sources of the PCS. PCUC is thought to originate from the eastward Equatorial Under Current (EUC), which splits when arriving at the American landmass. Both the primary South Subsurface Countercurrent (sSSCC) and secondary South Subsurface Countercurrent (pSSCC) could be complementary sources of the PCUC [Lukas, 1986, Montes et al., 2010]. The connection between the PCUC and the equatorial eastward subsurface currents (EUC, pSSCC, sSSCC) is very important for understanding the formation of the OMZ in the ETSP. However, Montes et al. [2010] find in a high-resolution regional model that only about 30% of the PCUC is fed by the three subsurface equatorial currents (EUC, pSSCC, sSSCC), among which only the two SSCCs contribute substantially. The remaining part of the PCUC comes from an alongshore recirculation associated with flows below and from the southern part of the region (south of 9°S) [Montes et al., 2010], indicating the southern border being important for the formation and maintenance of the OMZ. The box model of Su et al. [2015] for the ETSP also shows that the O_2 ventilation from the southern boundary is very important in maintaining a realistic O_2 concentration in the deep ocean and the water column of the ETSP is a source of NO_3^- and ${PO_4}^{3-}$ under its parameterization.

There are mainly two water masses in the intermediate and deep levels of the ETSP: antarctic intermediate water (AAIW) and pacific deep water (PDW). The new-found Peru-Chile Deep Coast Current (PCDCC) flows below the PCUC and carries AAIW between 700m and 1200m [Chaigneau et al., 2013]. Typically low in nutrients and high in dissolved O_2 concentrations, the northward AAIW brings oxygen into the ETSP [Schneider et al., 2003, and references therein]. Below AAIW sits the PDW, which is a vast water mass flowing southward. The PDW is thought to be homogenous and the oldest water mass in the ocean, which carries water with low O_2 but hight nutrient concentrations [Reid, 1997, Tomczak and Godfrey, 2003, Llanillo et al., 2013].

In this study, the impact of the southern boundary on the OMZ characteristics and the nutrient distributions of the ETSP is investigated in a high-resolution coupled physical-biogeochemical model. The model is set up in a climatological configuration similar to Echevin et al. [2008] and Montes et al. [2010], but with a smaller domain in order to exclude the impacts of ECS and fo-

cus on the southern boundary. The model assessments in section 4.2.5 show that our model can well reproduce both physical and biogeochemical features of this region, which provides the precondition for studying the southern boundary conditions. Then we investigate the impact of different southern boundary conditions on the OMZ and the whole ETSP in terms of (1) OMZ structure evolution, (2) O_2 and nutrient contents, (3) O_2 and nutrient distributions, and (4) lateral fluxes. We find that the southern boundary conditions have a more significant influence on the deep than on the surface ocean. The ETSP is gaining O_2 from the southern boundary, but losing both NO_3^- and ${PO_4}^{3-}$.

4.2 Methods

To investigate the role of the southern boundary on the OMZ off Peru, a coupled physical and biogeochemical model to simulate the dynamics of this region is applied. The physical model employed is the regional model ROMS (Regional Oceanic Model System). This model is coupled with the biogeochemical model PISCES (Pelagic Interaction Scheme for Carbon and Ecosystem Studies).

4.2.1 ROMS oceanic model

ROMS is a free surface and terrain-following vertical coordinate model, which is designed to enhance resolution near the sea surface [Shchepetkin and McWilliams, 2005, 2009]. As described by Shchepetkin and McWilliams [2005], this model employs a mode-splitting algorithm to separate the time-scales of barotropic and baroclinic processes, by solving the vertically-integrated barotropic momentum equations [Shchepetkin and McWilliams, 2009]. The unresolved processes involved in vertical mixing are parameterized using a non-local K-Profile (KPP) introduced by Large et al. [1994]. Its open boundary conditions provide outward radiations and nudging towards prescribed external boundaries (sponge layers). Explicit lateral viscosity is null everywhere in the simulated model domain, except in the sponge layers at open boundaries.

4.2.2 PISCES model

PISCES is a biogeochemical model which simulates the marine biological productivity and describes the biogeochemical cycles of carbon and the main nutrients (N, P, Si, Fe) [Aumont and Bopp, 2006]. It includes two phytoplankton (nanophytoplankton and diatoms), and two zooplankton (microzooplankton and mesozooplankton) size classes. The PISCES model considers phytoplankton growth limitation by five different nutrients: NO_3^-, NH_4^+, ${PO_4}^{3-}$, ${SiO_4}^{3-}$ and Fe. There are three non-living compartments: semi-labile dissolved organic matter, small

and large sinking particles. The model also simulates dissolved inorganic carbon, total alkalinity and dissolved oxygen [Aumont and Bopp, 2006]. All parameters for this region follow Echevin et al. [2014].

The nitrogen-related biogeochemical processes in PISCES include nitrogen fixation, denitrification, nitrification and ammonification [Aumont, 2005]. Diazotrophic phytoplankton can fix N_2 under the conditions that: 1) water temperature is above 20 °C, 2) there is insufficient fixed-N in the environment, 3) iron is available. Nitrogen fixation is restricted to the sea surface and annual total nitrogen fixation should balance denitrification to ensure nitrogen conservation in the model domain. Denitrification ensues only when oxygen concentration is less than 6 $\mu mol\, kg^{-1}$. Nitrification represents the conversion of NH_4^+ to NO_3^- due to bacterial activity, which is assumed to be photoinhibited and O_2 concentration dependent. Ammonification is responsible for the remineralization of particulate organic matter and dissolved organic matter to NH_4^+, which can be utilised directly by phytoplankton again.

4.2.3 Model configurations

The standard configuration

To capture the role of the southern boundary on the OMZ off Peru, we implement a regional configuration centered at the core of the eastern tropical south Pacific OMZ. This configuration allows a close comparison with the previous study by Su et al. [2015], which suggests an important role of open boundaries on preventing O_2 depletion in the deep ocean of the ETSP. The present configuration has a rectangular grid extending from 4°S to 16°S in latitude and from 72°W to 91°W in longitude. The horizontal grid has an isotropic resolution of 1/9°, corresponding to about 12 km, and contains 172x111 grid points. The vertical grid has 32 vertical sigma-levels, parameterized to allow good representation of upper layer ocean processes ($theta_s$=6, $theta_b$=0, hc=10). Thus, the vertical resolution varies according to the water column depth, from a minimum of 37.4cm to a maximum 5.04m for the surface layer and from 10.43m to 776.71m for the bottom layer.

The idealized configurations

The role of the southern boundary on the OMZ off Peru is investigated by comparing simulations with different southern boundary settings, from completely closed boundary conditions to removing all the incoming oxygen and nutrient supplies into model domain through the southern boundary. There are four configurations in total developed in this study: (1) STD is the standard configuration introduced above. (2) CLOSEBOUND is identical to the STD simulation except that the southern boundary is totally closed, suppressing the exchange of water masses properties with the southern subtropical Pacific. (3) NOO2 is identical to the STD simulation except that there is no oxygen supply into the model domain via advection from the southern boundary. (4) NOO2NO3PO4 is identical to the NOO2 simulation except that there are no NO_3^- and ${PO_4}^{3-}$ supplies into the model domain via advection from the southern

boundary. We consider the STD configuration the most realistic, and the others as the idealised experiments.

Simulations

All simulations of the four model configurations are conducted over 30 climatological years, with model outputs averaged and stored every 3 days. The simulated physical and biogeochemical dynamics reach an equilibrium after 25 years (Appendix A). Therefore, we have constructed the mean dynamics (monthly, seasonal and annual) from the last five years of the model simulation (years 26–30).

4.2.4 Data sets used for open boundary conditions, forcing and model assessments

The model grid, forcing, initial and boundary conditions are built with the ROMSTOOLS package [Penven et al., 2008]. The bottom topography and coastline of our model domain are derived from the ETOPO2 dataset [Smith and Sandwell, 1997], which provides a fine $2'$ resolution to avoid potential errors in the horizontal pressure gradient. COADS ocean surface 0.5° resolution monthly climatology data are applied for the model heat and fresh water fluxes at the ocean surface [Silva et al., 1994]. For surface wind stress, the QuickSCAT satellite scatterometer data, which is gridded at a resolution of 0.5° and calculated over 2000-2007, is employed[Liu et al., 1998]. Pathfinder, a finer SST climatology ($1/12^\circ$), is employed to replace the coarser SST dataset [Casey and Cornillon, 1999]. The initial values and boundary conditions of the biogeochemical tracers including O_2, NO_3^-, ${PO_4}^{3-}$, and SiO_4^- are interpolated from CISRO Atlas of Regional Seas [CARS, 2009, http://www.cmar.csiro.au/cars] to the model resolution. The dynamical variables (temperature, salinity and velocity fields) for ROMS open boundary conditions are provided by the monthly climatology computed from the Simple Ocean Data Assimilation (SODA) reanalysis [Carton and Giese, 2008]. The interannual variabilities such as EL-Ninõs are explicitly excluded.

AVISO satellite altimetric data (http://www.aviso.oceanobs.com/) in the period from January 1990 to December 2010 are applied to evaluate the sea surface hight variability. The CISRO Atlas of Regional Seas (Ridgway et al. [2002], Dunn) monthly climatological data with $1/2^\circ$ resolutions for nutrients, oxygen, salinity and temperature are used for comparison with model outputs to assess our model skills. The monthly climatological SeaWiFS products of level 3-binned data for Chloraphyll(Chla) over 2005-2010 are used for comparison with simulated Chla concentration at surface, which is the sum of diatom and nanophytoplankton chlorophyll.

4.2.5 Model assessment

The simulated physical and biogeochemical dynamics from the STD configuration are compared with existing observations and previous studies, in order to evaluate the realistic repro-

duction of the dynamics of this region.

Figure 4.1 shows the annual mean sea surface height from the AVISO data and the STD configuration. From this dynamic, the Peru coastal current (PCC) along the coast and the equatorward flow of the Peru Oceanic current (POC) offshore are visible. Close to the southern border, between 12 and 15°S, the westward current represents the Peru Oceanic Current (POC). Thus, our simulation can reproduce the general patterns of surface currents compared with those estimated from the AVISO data.

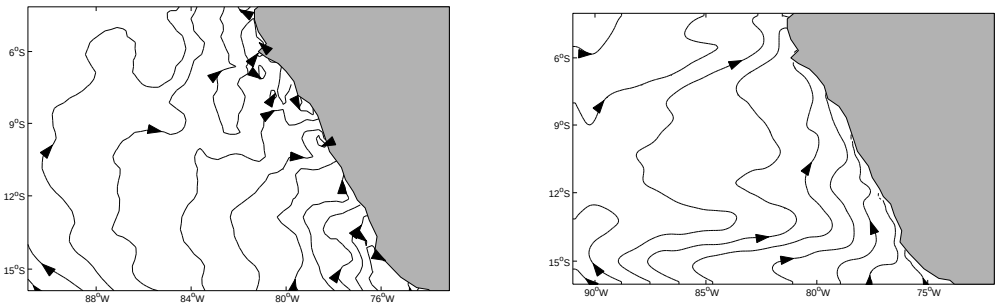

(a) AVISO (b) STD

Figure 4.1: Surface currents derived from the annual mean sea surface height for both data (a) and the STD configuration (b).

The vertical structures of the zonal and meridional velocities (Fig. 4.2) also suggest good agreement with the previous observations and model results [Penven et al., 2005, Montes et al., 2010, Czeschel et al., 2011]. The simulated westward South Equatorial current (SEC) separates the eastward flow of the subsurface counter currents (SSCC) and the South Equatorial Countercurrent (SECC) of this region, in agreement with the previous observations [Czeschel et al., 2011] and model studies [Montes et al., 2010]. The eastward flow of the SSCC is centered at around 6°S in the simulated results as documented in the observational study by Czeschel et al. [2011]. Further south, at around 12°S, the structure of the SECC is well represented in the model simulation [Czeschel et al., 2011]. Along the coast, the northward PCC is dominant at the upper layer of the onshore side, and overlaying the core of the Peru Chile Undercurrent (PCUC), which is in agreement with the previous studies [Penven et al., 2005, Montes et al., 2010, Echevin et al., 2014]. The subsurface PCUC flows poleward with the velocities up to 10 cm s^{-1}, in agreement with the previous studies [Penven et al., 2005, Montes et al., 2010, Echevin et al., 2014].

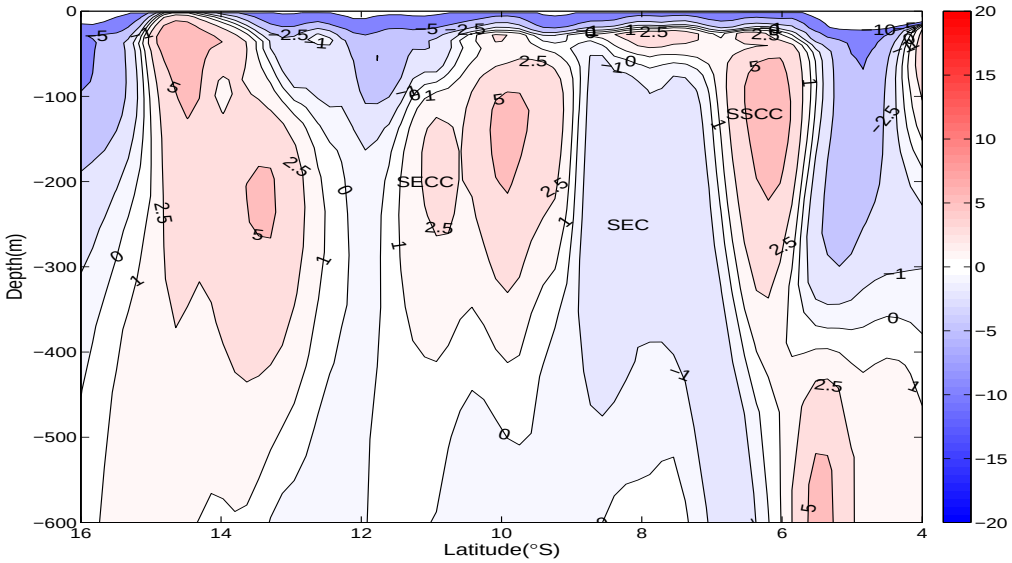

(a) u-86°W-Feb

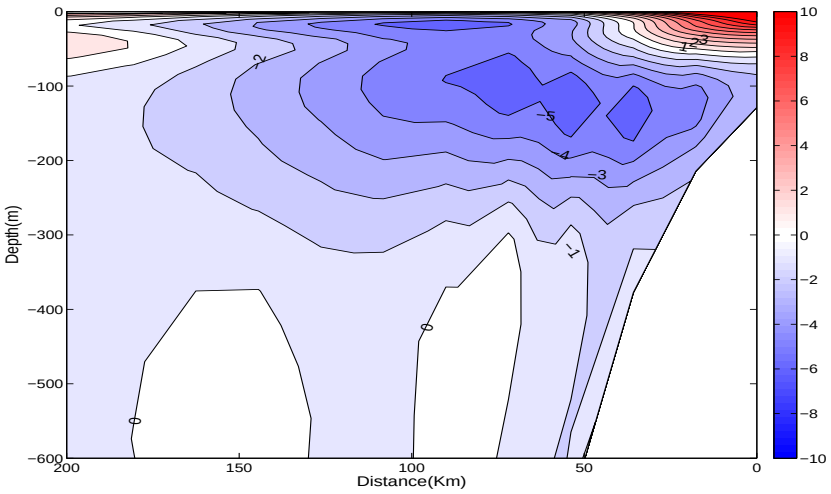

(b) v-12°S

Figure 4.2: Vertical sections of zonal and meridional velocities (cm s^{-1}). (a) mean zonal velocity at 86°W in February; (b) annual mean meridional velocity at 12°S.

A Taylor diagram is shown in Fig. 4.3 to evaluate the modeling abilities of the STD configuration in terms of both physical (temperature and salinity) and biogeochemical (oxygen, nitrate, phosphate and surface chlorophyll) fields in an annual mean time scale [Taylor, 2001]. The simulated fields of the STD configuration are compared with climatological CARS 2009 data in statistical metrics of the standard deviation, the correlation coefficient and root mean square (RMS). For the physical variables, correlation coefficients are above 0.97 for both surface and 100-600m depth of the model domain. The normalized standard deviations are very close to 1.0 and the centered RMS differences are between 0.2 and 0.3 (Fig. 4.3). The simulated bio-

geochemical variables are also in agreement with the CARS 2009 and SeaWiFS observations, with a correlation coefficient above 0.7. The RMS and standard deviation are more dispersive. The surface chlorophyll and nitrate in the ocean interior show low variations compared to observed fields. The variations in oxygen (both at surface and in ocean interior), surface nitrate and phosphate in the ocean interior are larger than observations (Fig. 4.3).

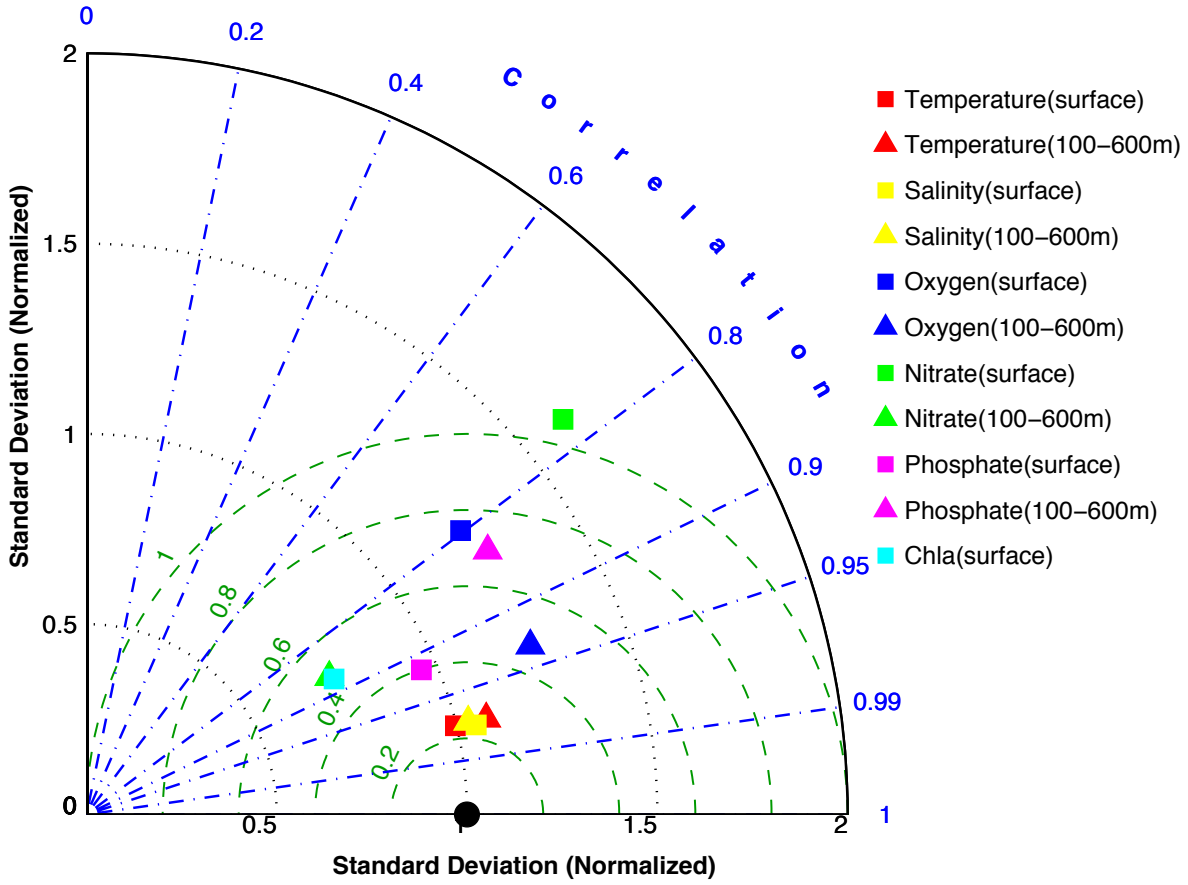

Figure 4.3: Taylor diagram for annual average temperature(red), salinity(yellow), oxygen(blue), nitrate(green), phosphate(magenta) and chlorophyll(cyan) concentrations. The radial distance from the origin (the black filled circle) is proportional to the standard deviation, which is normalized by the standard deviation of the observational data. The correlation between the model and data is shown by the angular coordinates (blue dash-dot lines). The distance of each model point from the origin represents the root-mean-square (RMS, green dashed lines). The statistics are performed for the horizontal surface slice and 100-600m depth of the model domain (to represent the core of OMZ) with both model outputs and data to evaluate the model skills. The model outputs are the last 5 years annual means; the data are from the CARS 2009 annual climatologies.

The vertical structures of simulated temperature and salinity also suggest a realistic representation of the dynamics of this region. In the upper surface layer (Figs. 4.4 and 4.5), the warmer and salty subtropical waters (STW) dominates the water mass properties in both off-

shore and coastal sections. Along the coast, the relatively low temperature and salinity suggest the upwelled subsurface waters induced by the equatorial winds along the coast ((a) and (b) in Figs. 4.4). The simulated subsurface waters are colder and fresher, characteristic of the equatorial subsurface water (ESSW). The ESSW is also characterized by extremely low oxygen and high nutrient concentrations ((c), (d) and (e) in Figs. 4.4 and 4.5). Above the less oxygenated ESSW, the simulated STW is well oxygenated and with low nutrient, which is in agreement with observation ((c) in Figs. 4.4 and 4.5). The only deficiency in the meridional section is that both temperature and salinity are slightly higher than data in the top 100m between 12 and 15°S ((a) and (b) in Fig. 4.5).

4.3 Results and discussion

To gain insights into the influence of southern boundary on the ETSP dynamics, we analyse the evolution of OMZ structures, the O_2 and nutrient contents, the volume distributions as a function of O_2 and nutrient concentrations, and the vertical profiles of average O_2, NO_3^- and PO_4^{3-} concentrations of the model domain of the four configurations defined in section 4.2. At the end, the lateral fluxes of O_2 and nutrients for our model domain are examined.

4.3.1 The effect of southern boundary on the OMZ structure

The structures of the OMZ (defined as O_2 concentration <20 µmol kg^{-1}) derived from the oxygen distribution of both realistic STD and idealized simulations are presented in Fig 4.6. The structure of the OMZ in the STD configure is comparable with that estimated from the CARS 2009 data, with extended OMZ thickness close to the continental shelf and reduced thickness in direction toward the southern border ((a) and (b) in Fig. 4.6). The maximum OMZ thicknesses are about 600m in both the estimate with CARS 2009 data and the STD configuration.

In the CLOSEBOUND configuration, the low-oxygen waters are vertically expanded in the southern part of the domain, with maximum thickness of 700m ((c) in Fig. 4.6). This expansion is pronounced in the south-western side of the domain, suggesting an important role of O_2 exchange through the southern boundary on the offshore side ((c) in Fig. 4.6). The reduced oxygen content in the NOO2 and NOO2NO3PO4 simulations induce a more significant vertical expansion of the OMZ, with a stronger impact on the southern side and inshore. Toward the southern border, the maximum thicknesses are 3950m in these two configurations ((d) and (e) in Fig. 4.6). At around 10°S, the O_2-depleted waters are observed between 200 m and 1000 m depth, showing a vertical expansion of about 200 m. These simulations suggest a strong northward transport of oxygenated waters from the south. As the O_2 concentration in the southern waters decreases, the OMZ of the ETSP might expand.

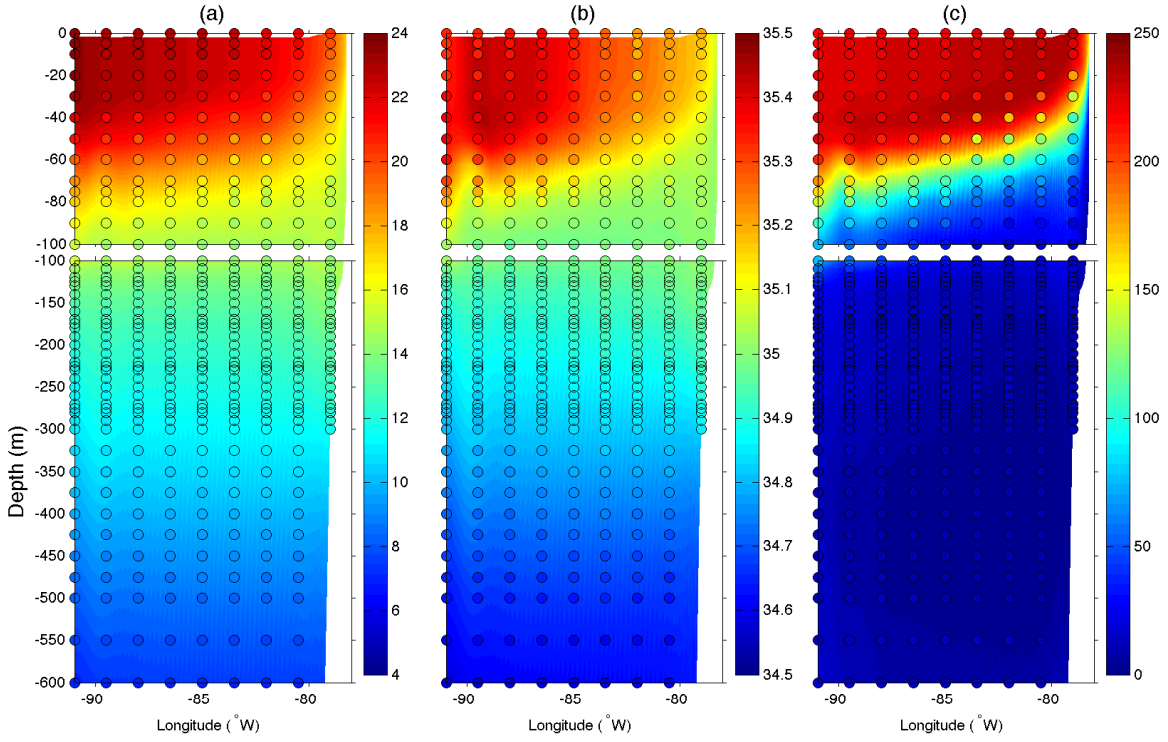

Figure 4.4: Simulated annual average (a) temperature, (b) salinity, (c) oxygen, (e) nitrate, and (d) phosphate concentrations at 10°S from surface to 600m depth, zoomed out for 0-100m depth. Colored circles represent the annual mean CARS (2009) datasets. Both model fields and data apply the same color bar in each panel.

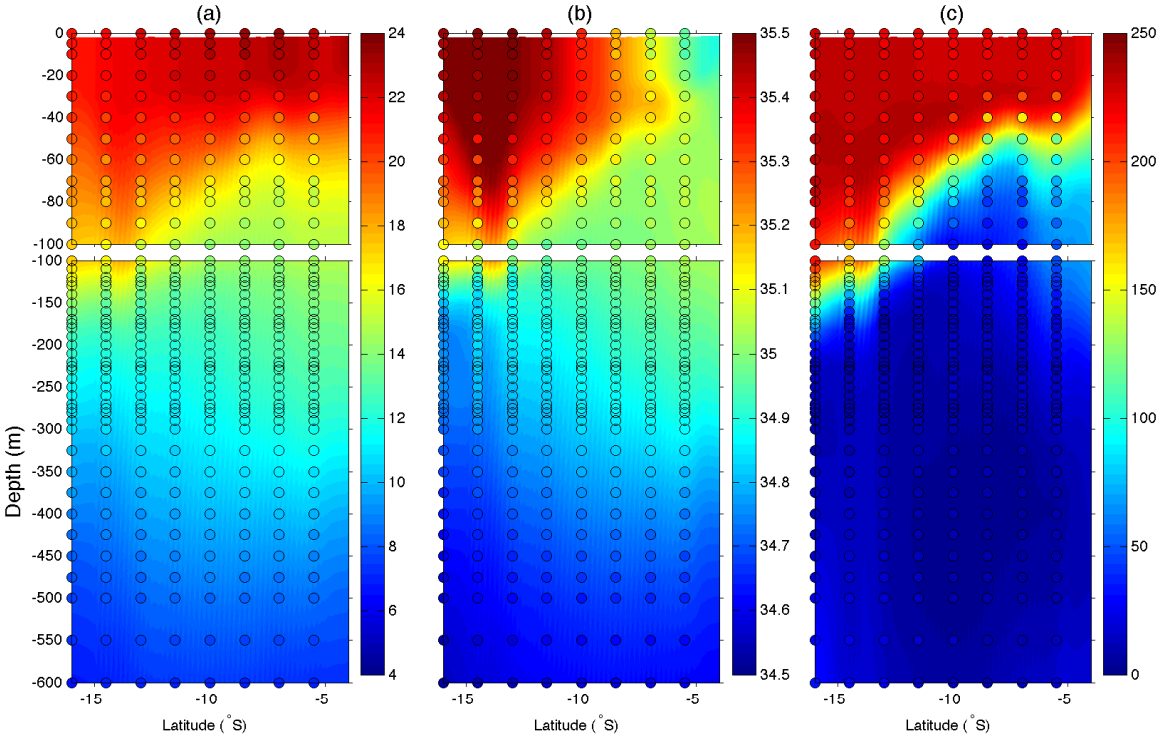

Figure 4.5: Simulated annual average (a) temperature, (b) salinity, (c) oxygen, (e) nitrate, and (d) phosphate concentrations at 85°W from surface to 600m depth, zoomed out for 0-100m depth. Colored circles represent the annual mean CARS (2009) datasets. Both model fields and data apply the same color bar in each panel.

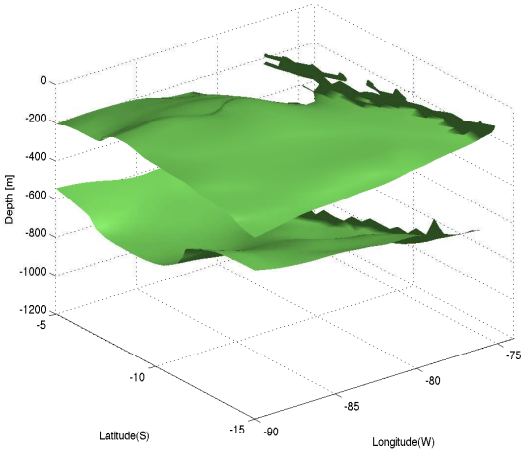

(a) CARS 2009

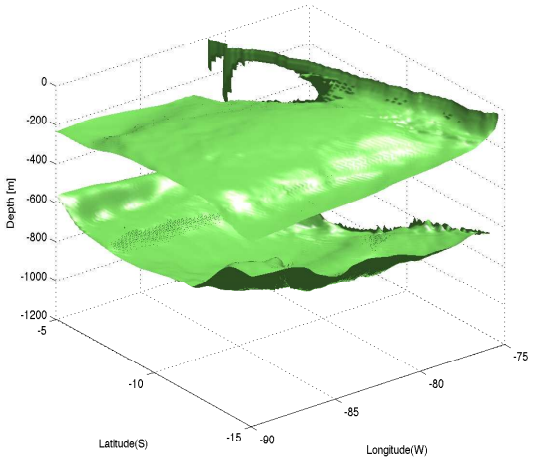

(b) STD

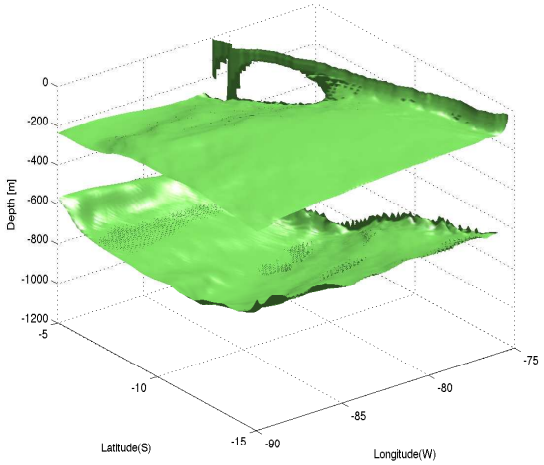

(c) CLOSEBOUND

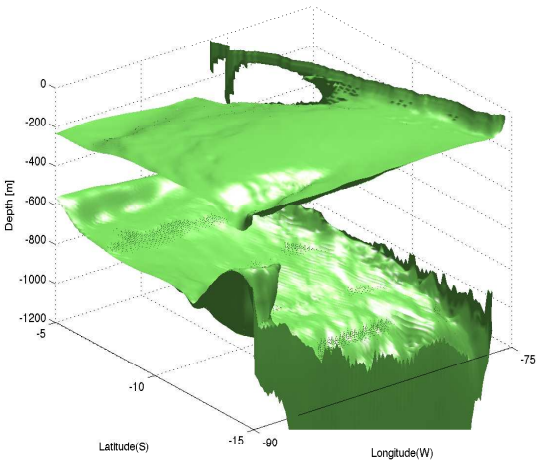

(d) NOO2

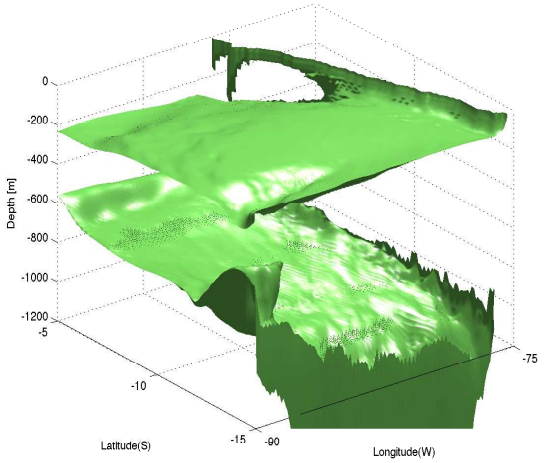

(e) NOO2NO3PO4

Figure 4.6: Structure evolution of the OMZ. Green surfaces represents isosurfaces with the annual average O_2 concentration of 20 µmol kg^{-1}.

4.3.2 O_2 and nutrient contents

The changes in the southern boundary conditions also modify the O_2 and nutrient contents of the ETSP (Fig. 4.7). We estimate both the upper 600m (to focus on the OMZ core) and the whole model domain (Fig. 4.7). The vertical profiles of the annual mean O_2, NO_3^- and ${PO_4}^{3-}$ concentrations are also presented in Fig. 4.8. Both contents and vertical profiles show good agreement with CARS 2009 data, indicative of good model skills in simulating the biogeochemical features of the region.

In the upper 600m, the O_2 and nutrient contents show generally slight changes in the idealised experiments (CLOSEBOUND, NOO2 and NOO2NO3PO4) in comparison with the STD (Figs. 4.7 and 4.8), e.g., O_2 content decreases by about 16%, 15% and 15% respectively in the CLOSEBOUND, NOO2 and NOO2NO3PO4 configurations; NO_3^- content decreases by about 4.6%, 1.4% and 13% respectively; however, ${PO_4}^{3-}$ content decreases only in NOO2NO3PO4, stays constant in NOO2, but increases by about 5.5% in CLOSEBOUND. There are very small chlorophyll a concentration differences in the surface layer of different model configurations, except in the CLOSEBOUND configuration where there is higher chlorophyll a concentration (Fig.4.9). This can be attributed to the slightly higher NO_3^- and ${PO_4}^{3-}$ concentrations at the surface of the CLOSEBOUND configuration (Fig. 4.8a).

Different from the upper layer dynamics, the net contributions of the southern boundary conditions to the oxygen and nutrient contents appear more significant in the whole water column in NOO2 and NOO2NO3PO4, but not in CLOSEBOUND ((b) in Figs. 4.7 and 4.8). For example, O_2 content decreases by about 36% respectively in NOO2 and NOO2NO3PO4; NO_3^- and ${PO_4}^{3-}$ decrease by about 29% and 28% respectively in NOO2NO3PO4. The reduction in oxygen supplies through the southern boundary reduces the O_2 content, and a stronger reduction is observed in the NOO2 and NOO2NO3PO4 configurations, suggesting that a reduction of southern-origin O_2 might impact the OMZ of the ETSP. As for the O_2 dynamics in the water column, the reduction in southern-origin nutrient in NOO2NO3PO4 induce changes in the nutrient availability in the ETSP region. It is important to highlight that these changes are stronger in the deeper layers, from 600 m down to the bottom (Fig. 4.7b).

4.3.3 Ocean volume distributions as a function of annual mean O_2 and nutrient concentrations

The volume distributions as a function of O_2 and nutrient concentrations are used as a metric for investigating the impact of the southern boundary on the biogeochemistry of the ETSP (Fig. 4.10). At the upper 600 meter, all oxygen bins between 0 and 300 $\mu mol\, l^{-1}$ show weaker responses to the reduced O_2 supplies from the southern boundary (Fig. 4.10a), which is in agreement with Figs. 4.7a and 4.8a. The most significant change is observed in the deoxygenated wa-

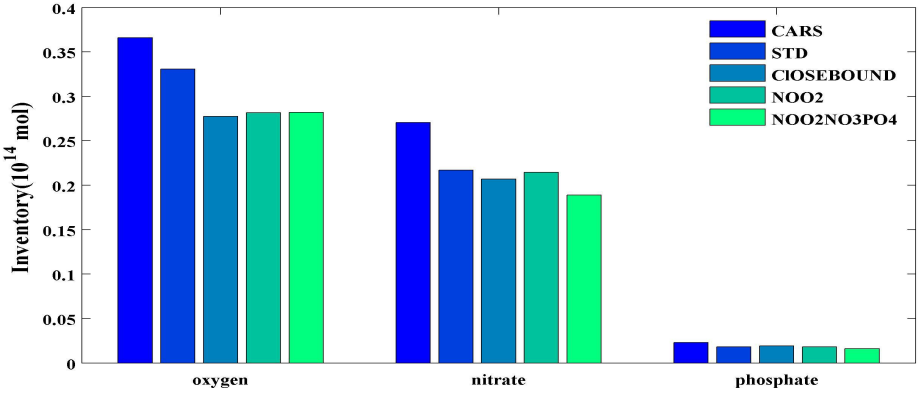

(a) 0–600m

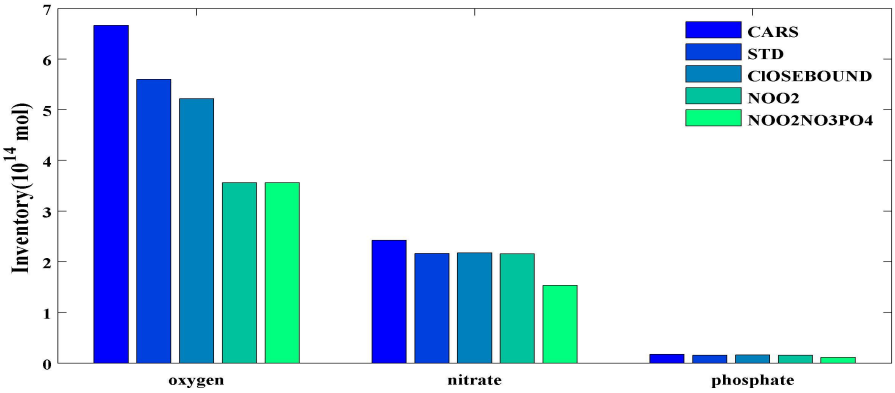

(b) surface-bottom

Figure 4.7: Annual mean contents of O_2, NO_3 and PO_4 respectively for the model domain. The contents are estimated respectively (a) above 600m and (b) the whole water column for both CARS 2009 data and model simulations.

ter volume with O_2 concentration between 0 and 20 µmol kg^{-1}, as the volumes increase about 5% in the three idealised configurations (CLOSEBOUND, NOO2 and NOO2NO3PO4). For the whole model domain, the volume changes in relation to the boundary condition changes show a stronger impact, especially for the volume bins with O_2 concentration between 100 and 200 µmol l^{-1}(Fig. 4.10b). Removing the O_2 supply from the southern boundary (in NOO2 and NOO2NO3PO4) leads to a decrease of as much as 44% for the oxygenated volume. These results support the suggestion that the southern boundary O_2 supply mainly influences the deep ocean rather than the upper 600m.

The contributions of the southern boundary to the volume distributions of NO_3^- are variable among the simulations (Figs. 4.10c and 4.10d). In the CLOSEBOUND configuration, this distribution has been mainly changed only in the upper 600m, i.e., the bin with NO_3^- concentration between 25 and 30 µmol kg^{-1} decreases by about 44% (Fig. 4.10c). There is no obvious impact

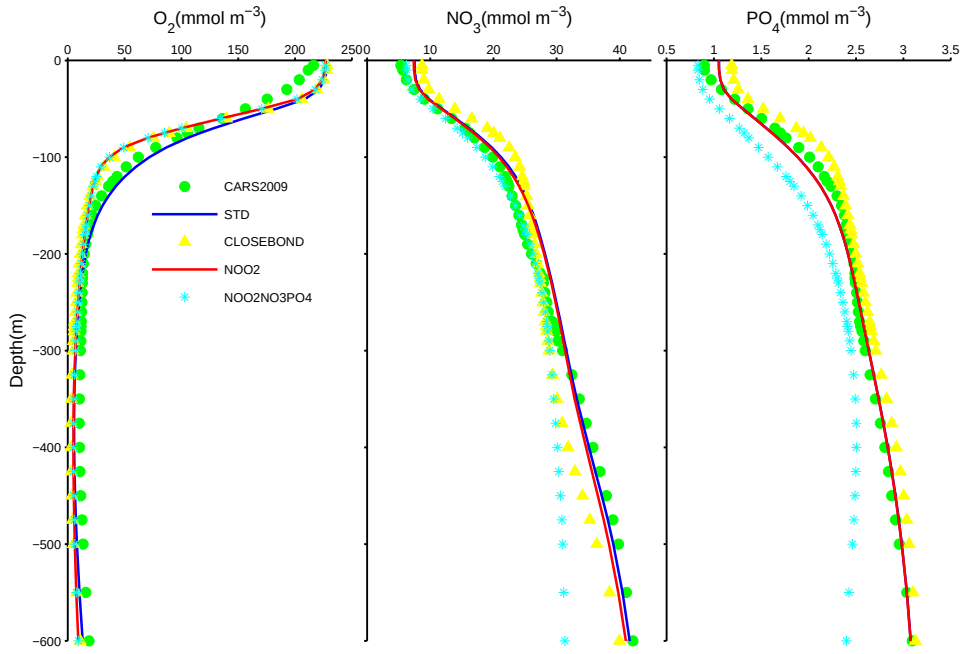

(a) 0–600m

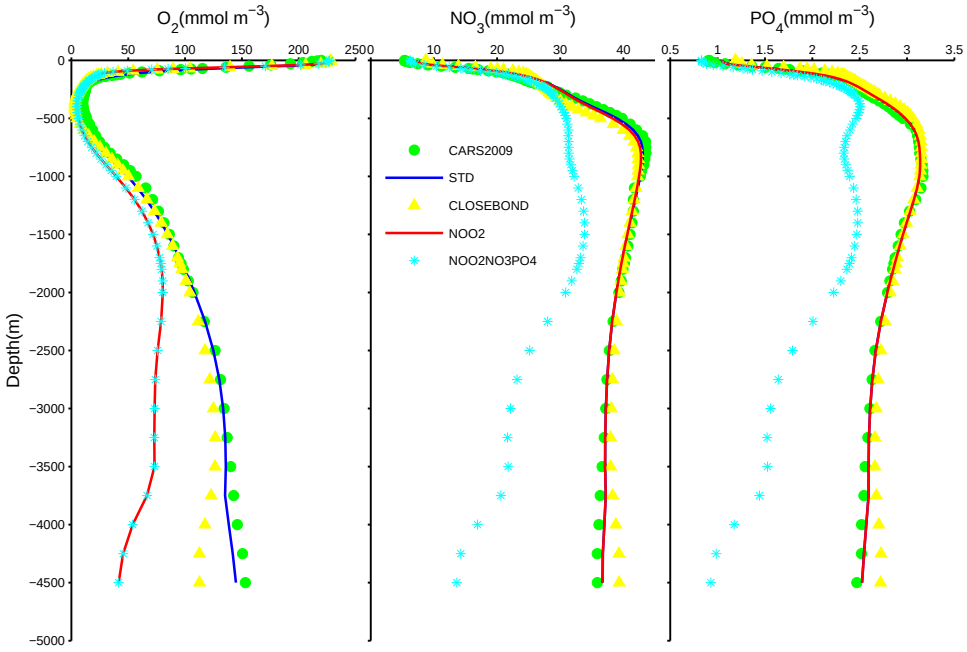

(b) Surface–bottom

Figure 4.8: Simulated annual average vertical profiles for oxygen, nitrate and phosphate concentrations from surface to (a) 600m and (b) bottom respectively. Vertical profiles are average for the region of 5–15°S and 72-90°W.

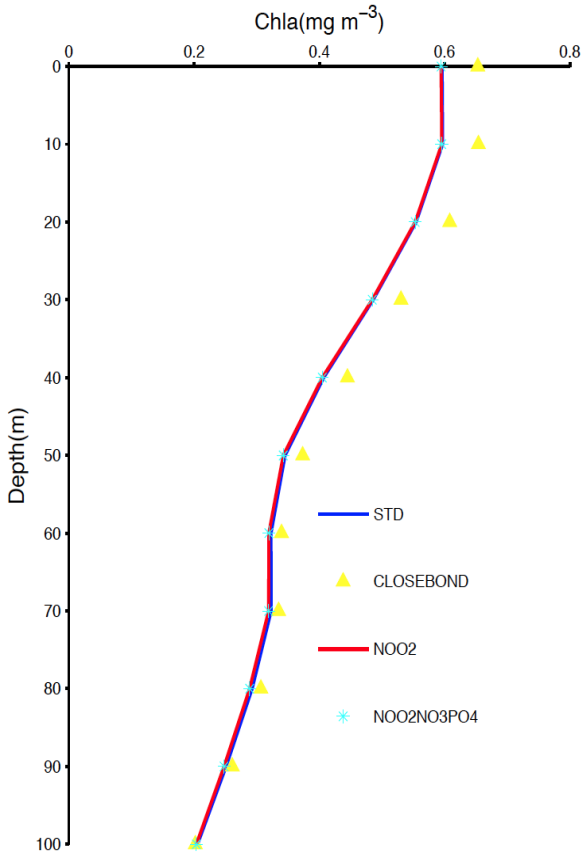

Figure 4.9: Annual mean vertical profile for chlorophyll a concentrations from the surface to 100m depth for different model configurations.

from the southern boundary conditions in the NOO2 configuration. The most significant influence is found in the NOO2NO3PO4 configuration, where the nitrate bins start to decrease from 30 and 35 µmol kg^{-1} respectively in the upper 600m and the whole water column respectively. Generally, the effect of removing the NO_3^- supply from the southern boundary is to shift the water volumes from high concentration bins to low concentration bins.

The volume distributions of PO_4^{3-} also show variable responses to the southern boundary conditions (Figs. 4.10e and 4.10f). Compared with the STD configuration, a stronger increase in the volume is observed in the phosphate bins of 2.0-2.5 µmol kg^{-1}, while a stronger decrease in volume distribution is observed in 2.5-3.0 µmol kg^{-1} in both the upper 600m and the whole water column of the NOO2 and NOO2NO3PO4 configurations. Thus, in these two idealised configurations, the impact of removing PO_4^{3-} supply from the southern boundary is to reduce water volumes with PO_4^{3-} concentration more than 2.5 µmol kg^{-1}. However, the volume increases in high PO_4^{3-} concentration bins in the CLOSEBOUND configuration, which indicates that the PO_4^{3-} content increases (Fig. 4.7). This suggests that a fully closed southern boundary can prevent PO_4^{3-} loss and subsequently increase primary production in the model domain, which is consistent with the box model result of Su et al. [2015].

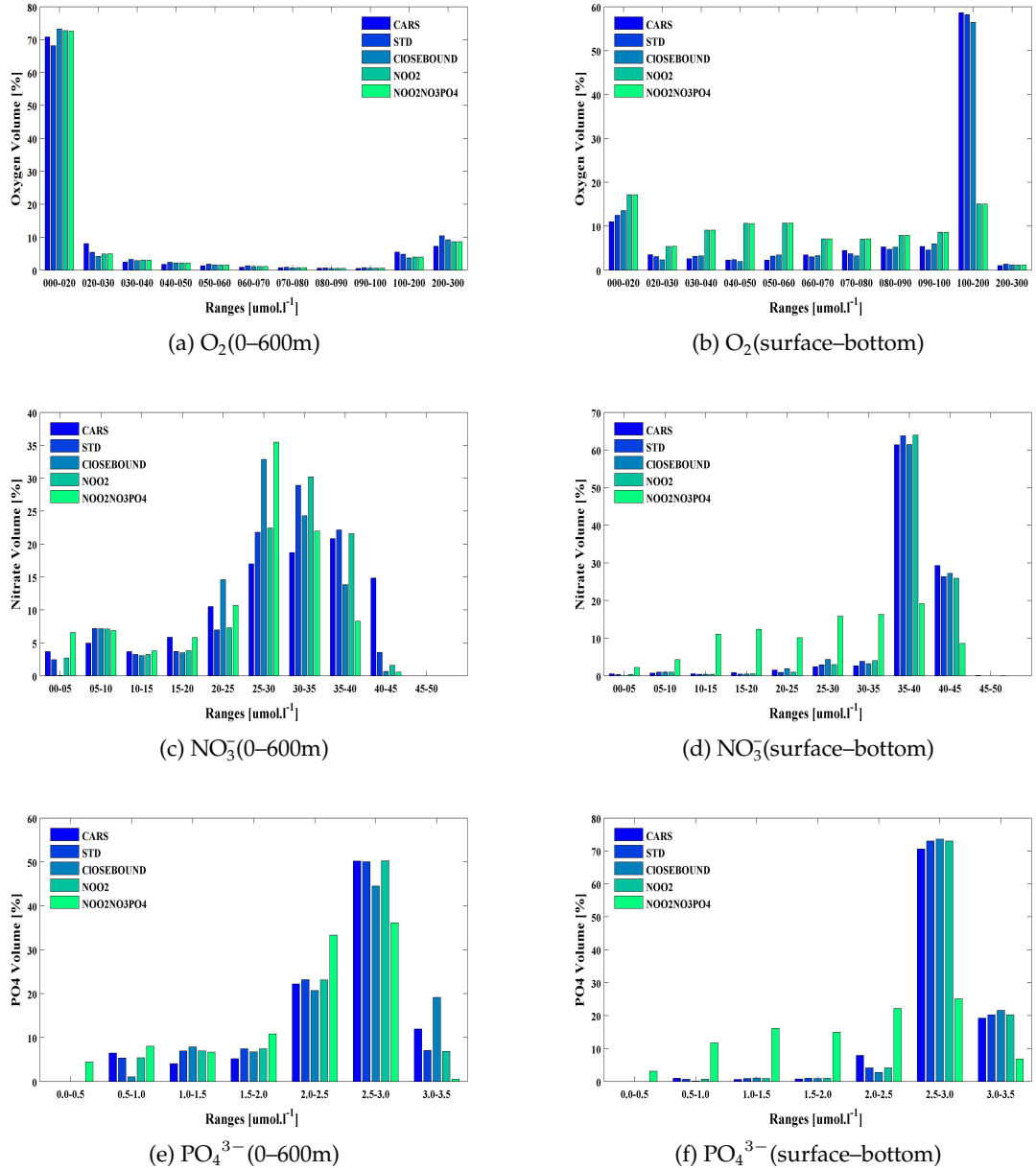

(a) O_2(0–600m) (b) O_2(surface–bottom)

(c) NO_3^-(0–600m) (d) NO_3^-(surface–bottom)

(e) PO_4^{3-}(0–600m) (f) PO_4^{3-}(surface–bottom)

Figure 4.10: Ocean volume distributions as s function of annual mean O_2, NO_3 and PO_4 concentrations respectively. The contents are estimated above the 600m depth (a, c, e) and full vertical depth (b, d, f) for both CARS 2009 data and annual model means for the domain 72–90°W/5–15°S.

4.3.4 Lateral fluxes

The above model assessment results show good model performance for the annual means of the ETSP, which provides the possibility to compare the fluxes through open boundaries in different model configurations. The focus will be on the lateral fluxes when analysing the O_2

and nutrient concentrations of different model configurations, especially for the region below 600m.

In the upper 600m of the ocean, both O_2 and nutrients are lost through the southern boundary (Table. 4.1) in the STD configuration mainly due to the combined effect of the surface equatorward PCC and subsurface southward PCUC. But only little O_2 is lost through the southern boundary, which can be attributed to the southward PCUC carrying OMZ water with low O_2 concentration. This loss term is lacking in the CLOSEBOUND configuration, which can partially explain why PO_4^{3-} concentrations are higher in this configuration than in the STD configuration (in Figs. 4.7a and 4.10e). But this does not apply to NO_3^-, probably due to the higher NO_3^- consumption via denitrification resulting from higher export production (Fig. 4.9). In the NOO2 and NOO2NO3PO4 configurations, there is much more O_2 loss through the southern boundary, but there are only slight O_2 variations (Fig. 4.8a), which can be attributed to both less loss through the western boundary and more input from the atmosphere (Table 4.1). In the NOO2NO3PO4 configuration, NO_3^- and PO_4^{3-} concentrations are lower than those in the STD configuration (Fig. 4.8a), resulting in less NO_3^- and PO_4^{3-} losses from the southern boundary.

The entire model domain gains O_2 through the southern boundary (Table 4.1). O_2 is lost through the southern boundary in the upper 600m and the PCDCC is the main equatorward current below 600m. Therefore, this gain can only be due to the equatorward PCDCC carrying O_2 rich water into the ETSP. In the CLOSEBOUND configuration in which all the connection with the southern subtropical Pacific is closed, less NO_3 and PO_4 are lost through the southern boundary (Table 4.1). Since there is more loss through the northern boundary and less input of NO_3^- and PO_4^{3-} from the western boundary (Table 4.1), the slightly higher contents of these two nutrients in the whole domain can only be attributed to the southern boundary (Fig. 4.7b). The higher concentrations in the deep ocean may be due to the nutrients imported via nutrient-rich southward PDW (Fig. 4.8b). In the NOO2 and NOO2NO3PO4 configurations, there are more O_2 losses from the southern boundaries (Table 4.1), mainly resulting in low O_2 concentrations in the model domain (Fig. 4.8b). The lower NO_3^- and PO_4^{3-} concentrations below the subsurface in the model domain (Fig. 4.8b) can be attributed to the higher NO_3 and PO_4 losses through the southern boundary (Table 4.1).

4.4 Conclusions

We used a coupled physical-biogeochemical model to investigate the impact of the southern boundary on the O_2 and nutrient variabilities in the OMZ off Peru and the ETSP. Model assessment indicates good performance of the model in simulating the main physical and biogeochemical features of the region. The influence of the southern boundary on the OMZ is investigated in terms of O_2, NO_3^- and PO_4^{3-} by analysing model configurations with different southern boundary conditions.

	STD			CLOSEBOUND			NOO2			NOO2NO3PO4		
	0-600m											
	O_2	NO_3^-	PO_4^{3-}	O_2	NO_3^-	PO_4^{3-}	O_2	NO_3^-	PO_4^{3-}	O_2	NO_3^-	PO_4^{3-}
south	-0.721	-30.2	-2.54	0	0	0	-51.9	-29.7	-2.54	-52.5	-21.7	-1.92
north	136	18.3	1.68	124	11.1	1.11	136	18.3	1.68	136	18.4	1.68
west	-247	32.3	1.96	-230	15.2	0.396	-205	32.4	1.96	-205	34.2	2.31
Atm	2.87			7.59			46.8			46.6		
sum	-109	20.5	1.10	-98.5	26.3	1.50	-74.1	21.0	1.11	-74.7	30.9	2.07
	surface-bottom											
	O_2	NO_3^-	PO_4^{3-}	O_2	NO_3^-	PO_4^{3-}	O_2	NO_3^-	PO_4^{3-}	O_2	NO_3^-	PO_4^{3-}
south	45.4	-26.8	-2.38	0	0	0	-78.4	-26.4	-2.38	-78.9	-33.8	-2.79
north	46.5	-7.07	-0.120	48.4	-13.7	-0.666	49.5	-7.06	-0.120	49.5	-6.21	-0.0598
west	-159	52.9	3.49	-102	39.0	2.09	-99.7	53.1	3.49	-99.5	58.5	4.07
Atm	2.87			7.59			46.8			46.6		
sum	-64.6	19.1	0.996	-45.8	25.3	1.43	-81.7	19.7	0.996	-82.4	18.4	1.22

Table 4.1: Oxygen and nutrient fluxes through boundaries via horizontal advections and air-sea gas exchange (10^{11}mol yr^{-1}). "Atm"is the oxygen flux through sea surface. Positive values indicate gains into the model domain, while negative values losses.

The southern boundary conditions appear to have significant influence on the O_2 distribution in the ETSP. Even though the lack of O_2 input from the southern subtropical Pacific can enlarge the OMZ, the impacts on critical O_2 distribution and concentration changes are mainly in the ocean deeper than 600m (Figs. 4.10b and 4.8b). The O_2 input from atmosphere plays an important role in compensating for lack of O_2 input from the southern boundary at the upper layer (Table 4.1).

The ETSP is a gaining both NO_3^- and PO_4^{3-} from the adjacent ocean. But both NO_3^- and PO_4^{3-} are lost to the adjacent subtropical ocean through the southern boundary. Compared with the CLOSEBOUND configuration, our model domain loses NO_3^- and PO_4^{3-} in the realistic STD configuration when the southern boundary is open. This corroborates each other with the box model of Su et al. [2015]. In the upper layer, removing NO_3^- and PO_4^{3-} supplies from the southern boundary can also reduce the net loss in all idealised model configurations.

By changing the boundary conditions, it is evident that the northward water originating from

south into the OMZ off Peru can induce changes in the OMZ thickness and O_2 and nutrient distributions. The stronger changes of oxygen are mainly observed in the deeper layers, suggesting a pathway of deep northward intrusion of well-oxygenated southern waters.

O_2 concentrations are critical for fish and marine animals. The ETSP is thought to contribute more than 10% of the global fish catches [Chavez et al., 2008], thus the O_2 concentrations are very important for maintaining the high fish production. Expansion of the OMZs will narrow down the habitable depth range of fishes and, together with overfishing, may threaten the sustainability of pelagic fisheries and marine ecosystems [Stramma et al., 2012]. The Southern Ocean is thought to be sensitive to global warming due to reductions in deep convection, resulting in a significant decrease in O_2 concentrations [Keeling and Garcia, 2002, and references therein]. The Southern Ocean is an important source of water masses in the ETSP. Thus, this study can give some insights into the impacts of Southern Ocean variation on the oxygen cycle of the ETSP.

4.5 Appendix A

A 30-year simulation is conducted to attain a nearly repeating annual cycle. Figures 4.11 and 4.12 depicts the time variations of both physical and biogeochemical variables. For each of these variables, after a spin-up of 25 years, the model exhibits no temporal drift, especially the volume-averaged kinetic energy (Fig. 4.11) and nitrate concentrations (Fig. 4.12). Afterwards, they stay stable.

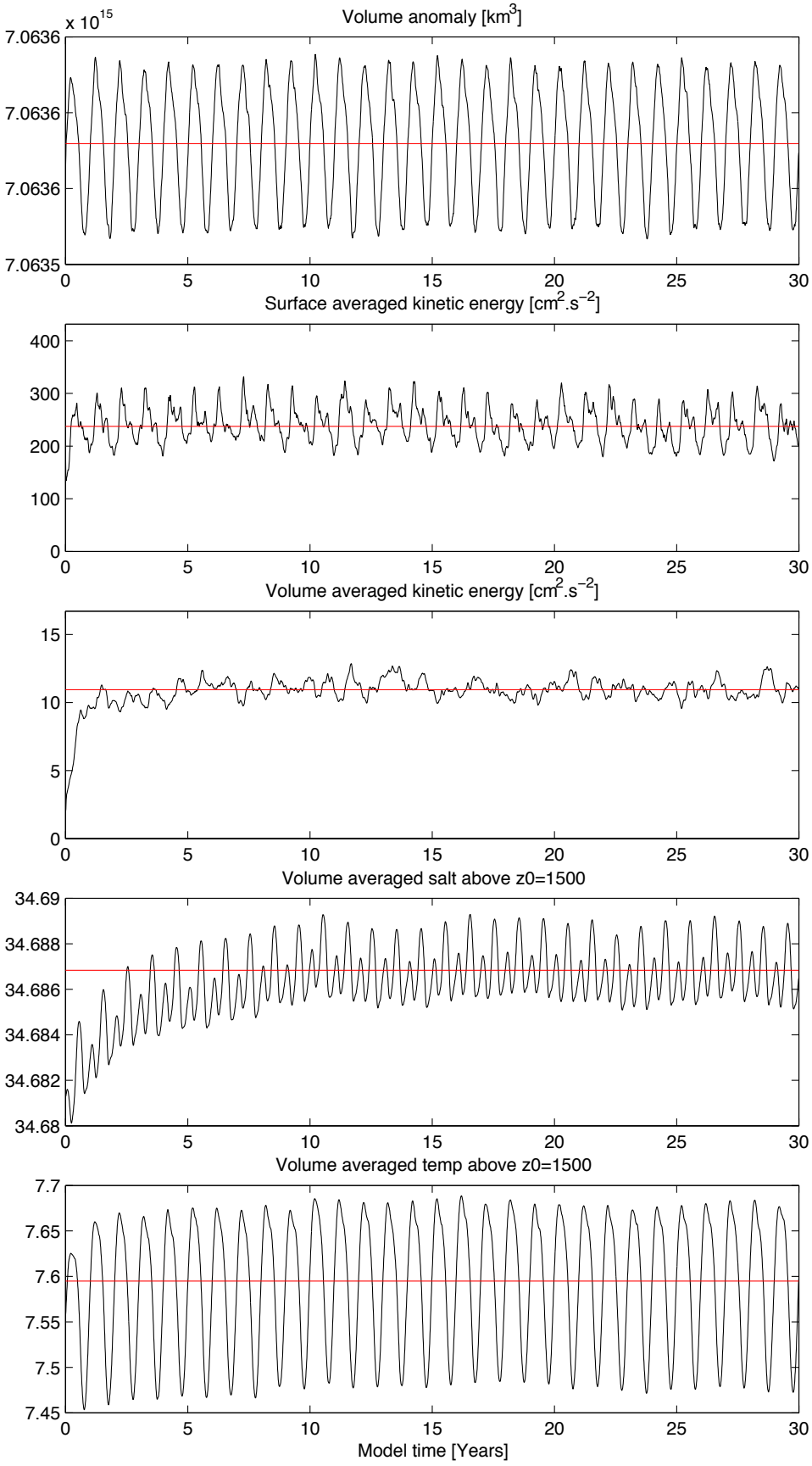

Figure 4.11: Time evolution of simulated physical variables.

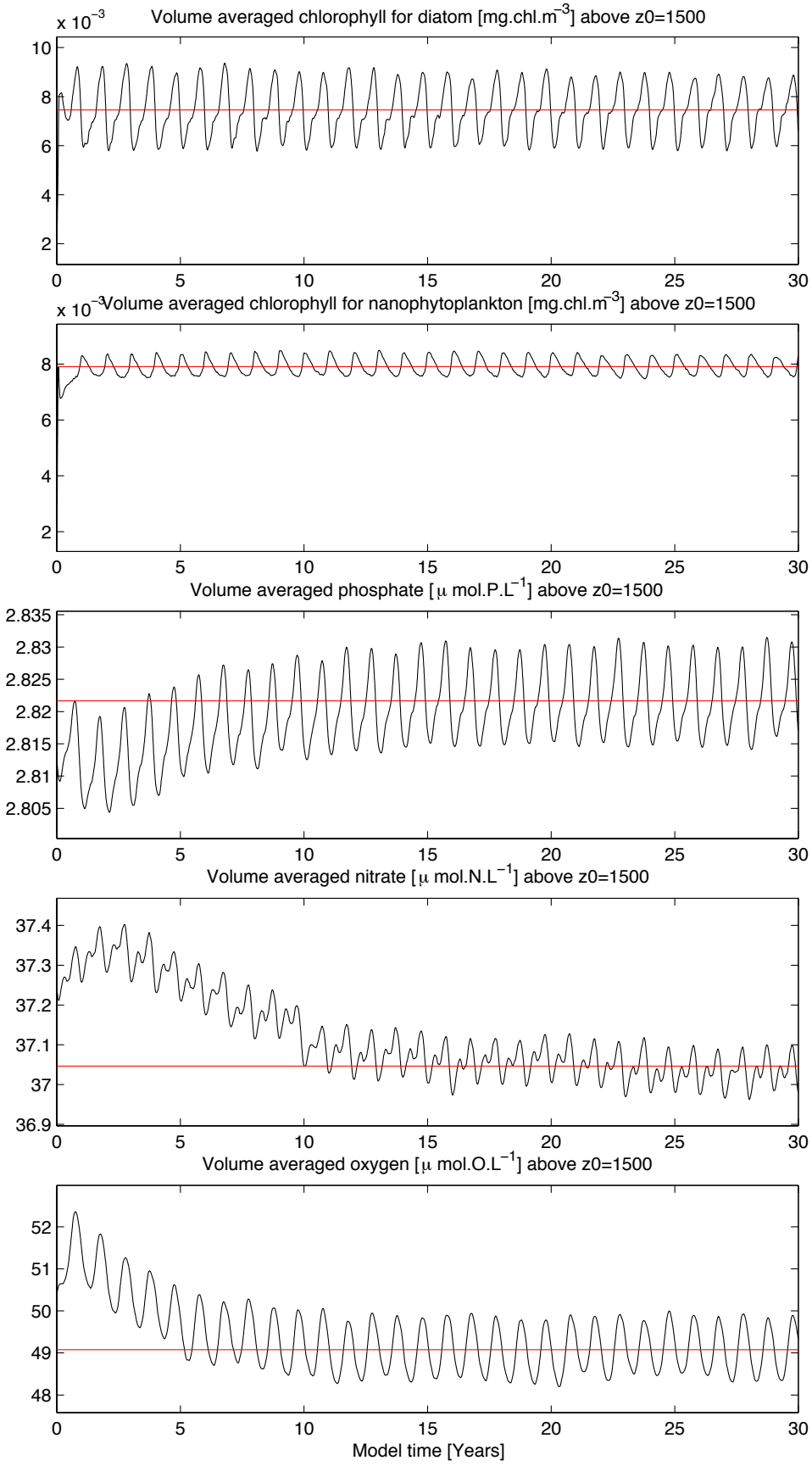

Figure 4.12: Time evolution of simulated biogeochemical variables.

Chapter 5

Summary and outlook

The nitrogen cycle in the Oxygen Minimum Zone (OMZ) of the eastern tropical South Pacific (ETSP) has been simulated with both 2-D box and 3-D coupled physical-biogeochemical models. In the 2-D box model, reduced remineralization by denitrification under anoxic conditions is found to be responsible for preventing nitrogen depletion in the OMZ of the ETSP [Su et al., 2015]. After including the atmospheric deposition and benthic remineralisation, the local responses indicate dominant stabilizing feedbacks in the ETSP, tending to keep a balanced nitrogen inventory. All of these results indicate possible mechanisms that are responsible for keeping a stabilized nitrogen inventory in the OMZ of the ETSP. Under the current notion of nitrogen fixation being favoured in nitrogen-deficit waters, the model domain of the ETSP is a NO_3^- source. After including benthic denitrification, the ETSP might become a NO_3^- sink. We also find in the box model that O_2 supply into the model domain from the southern boundary is very important in retrieving the realistic O_2 concentration in the deep ocean.

Based on the important role of the southern boundary on the oxygen and nutrient contents of the ETSP found in the box model [Su et al., 2015], a model configuration of the same region is built with the high-resolution hydrodynamic model ROMS (*Regional Ocean Modelling System*) [Shchepetkin and McWilliams, 2005], coupled with the biogeochemical model PISCES (*Pelagic Interaction Scheme for Carbon and Ecosystem Studies*) [Aumont and Bopp, 2006]. A validation against in situ observations shows a realistic simulation of the horizontal and vertical oxygen and nutrient distributions by the standard configuration. Comparisons among different model configurations indicate that the southern boundary has significant influence on O_2 and nutrient contents and distributions of this region. Lateral fluxes estimations indicate that our model domain is gaining O_2 and losing NO_3^- and PO_4^{3-} through the southern boundary. The southern boundary is found to have more significant influence on O_2 concentration of the deep layer than that of the upper layer, suggesting a pathway of deep northward intrusion of well-oxygenated southern waters. The Southern Ocean is thought to be sensitive to global warming due to reductions in deep convection, resulting in significant decrease in O_2 con-

centrations. This study can give insights into the impacts of Southern Ocean variations due to climate change on the O_2 changes of the ETSP.

In the high-resolution coupled physical-biogeochemical model, a stabilised nitrogen inventory is observed in the OMZ of the ETSP even though remineralisation rates are identical under oxic and anoxic conditions. Dissolved organic matter (DOM) is found to be exported out of model domain. This could explain the stabilised nitrogen inventory, because DOM cycling is thought to be capable of promoting the spacial decoupling of nitrogen fixation and denitrification, and allowing for negative feedbacks stabilising the nitrogen inventory [Landolfi et al., 2013]. A future research topic could be to further investigate the mechanisms capable of preventing the essential complete drawdown of NO_3^- in the high-resolution coupled physical-biogeochemical model.

The interannual variations in the Pacific (i.e., El Niño-Southern Oscillation, ENSO) have an important role on the climate and marine primary production of the ETSP [Wang and Fiedler, 2006]. The circulation and water-mass connections are also found to change during the ENSO period [Montes et al., 2011]. How dose the nitrogen inventory in this region vary corresponding to the ENSO-induced variations? What is the nitrogen stabilising mechanism in the ENSO period? These questions can potentially also be answered using the high-resolution coupled physical-biogeochemical model applied in this dissertation.

To have better understanding of the full nitrogen cycle in the ETSP, benthic remineralization processes can be included using Bohlen et al. [2012]'s transfer function and the relation for phosphate regeneration following Wallmann [2010] in the high-resolution model. The interactions among nitrogen fixation, water-column and benthic denitrification, and the question whether the ETSP is a fixed-nitrogen source or sink can be further investigated.

Bibliography

L. A. Anderson and J. L. Sarmiento. Redfield ratios of remineralization determined by nutrient data analysis. *Global Biogeochem. Cycles*, 8(1):65–80, Mar. 1994. doi: 10.1029/93GB03318.

A.-S. Auguéres and M. Loreau. Regulation of Redfield ratios in the deep ocean. *Global Biogeochem. Cycles*, 2015. doi: 10.1002/2014GB005066.

O. Aumont. *PISCES biogeochemical model*. Chargé de Recherche of IRD at the research centre of Brest, France, Oct. 2005.

O. Aumont and L. Bopp. Globalizing results from ocean in situ iron fertilization studies. *Global Biogeochem. Cycles*, 20(GB2017):1–15, June 2006. doi: 10.1029/2005GB002591.

O. Aumont, E. Maier-Reimer, S. Blain, and P. Monfray. An ecosystem model of the global ocean including fe, si, p colimitations. *Global Biogeochem. Cycles*, 17(2):1–29, June 2003. doi: 10.1029/2001GB00174.

A. Bakun and S. J. Weeks. The marine ecosystem off peru: What are the secrets of its fishery productivity and what might its future hold? *Prog. Oceanogr.*, 79:290–299, Nov. 2008.

M. J. Behrenfeld, E. Boss, D. A. Siegel, and D. M. Shea. Carbon-based ocean productivity and phytoplankton physiology from space. *Global Biogeochem. Cycles*, 19(GB1006):1–14, Jan. 2005. doi: 10.1029/2004GB002299.

W. M. Berelson. The flux of particulate organic carbon into the ocean interior: A comparison of four U. S. JGOFS regional studies. *Oceanography*, 14(4):59–67, 2001.

J. P. Bethoux. Oxygen consumption, new production, vertical advection and environmental evolution in the Mediterranean Sea. *Deep-Sea Res.*, 36(5):769–781, 1989. doi: 10.1016/0198-0149(89)90150-7.

D. Bianchi, J. P. Dunne, J. L. Sarmiento, and E. D. Galbraith. Data-based estimates of suboxia, denitrification, and N_2O production in the ocean and their sensitivities to dissolved O_2. *Global Biogeochem. Cycles*, 26(GB2009), May 2012.

L. Bohlen, A. W. Dale, S. Sommer, T. Mosch, C. Hensen, A. Noffke, F. Scholz, and K. Wallmann. Benthic nitrogen cycling traversing the Peruvian oxygen minimum zone. *Geochim. Cosmochim. Acta*, 75:6094–6111, Aug. 2011.

L. Bohlen, A. W. Dale, and K. Wallmann. Simple transfer functions for calculating benthic fixed nitrogen losses and c:n:p regeneration ratios in global biogeochemical models. *Global Biogeochem. Cycles*, 26(GB3029):1–16, Sep. 2012. doi: 10.1029/2011GB004198.

E. W. Boyer, R. W. Howarth, J. N. Galloway, F. J. Dentener, P. A. Green, and C. J. Vörösmarty. Riverine nitrogen export from the continents to the coasts. *Global Biogeochem. Cycles*, 20 (GB1S91):1–9, Mar. 2006. doi: 10.1029/2005GB002537.

J. A. Brandes and A. H. Devol. A global marine-fixed nitrogen isotopic budget: Implications for holocene nitrogen cycling. *Global Biogeochem. Cycles*, 16(4):1–14, Dec. 2002. doi: 10.1029/2001GB001856.

J. A. Brandes, A. H. Devol, and C. Deutsch. New developments in the marine nitrogen cycle. *J. Am. Chem. Soc.*, 107(2):577–589, 2007.

E. Breitbarth, A. Oschlies, and J. LaRoche. Physiological constrains on the global distribution of *Trichodesmium*-effect of temperature on diazotropy. *Biogeosciences*, 4:53–61, Jan. 2007. doi: 10.5194/bg-4-53-2007.

S. E. Bulow, J. J. Rich, H. S. Naik, A. K. Pratihary, and B. B. Ward. Denitrification exceeds anammox as a nitrogen loss pathway in the Arabian Sea oxygen minimum zone. *Deep-Sea Res. I*, 57(3):384–393, 2010. doi: 10.1016/j.dsr.2009.10.014.

D. E. Canfield. Models of oxic respiration, denitrification and sulfate reduction in zones of coastal upwelling. *Geochimica et Cosmochimica Acta*, 70(23):5753 – 5765, 2006. doi: 10.1016/j.gca.2006.07.023.

D. G. Capone and J. M. Budin. Nitrogen fixation associated with rinsed roots and rhizomes of the eelgrass zostera marina. *Plant Physiol.*, 70:1601–1604, 1982.

D. G. Capone and A. N. Knapp. A marine nitrogen cycle fix? *Nature*, 445:159–160, Jan. 2007. doi: 10.1038/445159a.

D. G. Capone, J. P. Zehr, H. W. Paerl, B. Bergman, and E. J. Carpenter. *Trichodesmium*, a globally significant marine cyanobacterium. *Science*, 276:1221–1229, May 1997. doi: 10.1126/science.276.5316.1221.

E. J. Carpenter. *Nitrogen in the Marine Environment*, chapter Nitrogen fixation by marine Oscillatoria (Trichodesmium) in the world's ocean, pages 65–103. Achdemie Press, New York, 1983.

E. J. Carpenter and D. G. Capone. *Nitrogen in the Marine Environment*, chapter Nitrogen fixation in the marine evironment, pages 141–198. Number 4. Elsevier Inc., Amsterdam, second edition, 2008. doi: 10.1016/B978-0-12-372522-6.00004-9.

J. A. Carton and B. S. Giese. A reanalysis of ocean climate using simple ocean data assimilation (SODA). *Mon. Weather Rev.*, 136:2999–3017, May 2008. doi: http://dx.doi.org/10.1175/2007MWR1978.1.

K. S. Casey and P. Cornillon. A comparison of satellite and in situ–based sea surface temperature climatologies. *J. Clim.*, 12:1848—1863, June 1999. doi: http://dx.doi.org/10.1175/1520-0442(1999)012<1848:ACOSAI>2.0.CO;2.

A. Chaigneau, N. Dominguez, G. Eldin, L. Vasquez, R. Flores, C. Grados, and V. Echevin. Near-coastal circulation in the northern humboldt current system from shipboard adcp data. *J. Geophys. Res.*, 118:1–16, July 2013. doi: 10.1002/jgrc.20328.

B. X. Chang, A. Devol, and S. R. Emerson. Denitrification and the nitrogen gas excess in the eastern tropical south pacific oxygen deficient zone. *Deep-Sea Res. I*, 57:1092–1101, June 2010.

F. P. Chavez, A. Bertrand, Guevara-Carrasco, Renato, Soler, Pierre, and J. Csirke. The northern Humboldt Current System: Brief history, present status and a view towards the future. *Prog. Oceanogr.*, 79:95–105, 2008. doi: 10.1016/j.pocean.2008.10.012.

J. P. Christensen, J. W. Murray, A. Devol, and L. A. Codispoti. Denitrification in the continental shelf sediment has major impact on the oceanic nitrogen budget. *Global Biogeochem. Cycles*, 1(2):97–116, June 1987.

S. P. Chu. The utilization of organic phosphorus by phytoplankton. *J. Mar. Biol. Assoc. U. K.*, 26(3):285–295, July 1946.

J. D. Cline and F. A. Richards. Oxygen deficient conditions and nitrate reduction in the Eastern Tropical North Pacific Ocean. *Limnol. Oceanogr.*, 17(6):885–900, Nov. 1972.

L. A. Codispoti. Is the ocean losing nitrate? *Nature*, 376:724, Aug. 1995. doi: 10.1038/376724a0.

L. A. Codispoti. An oceanic fixed nitrogen sink exceeding 400 Tg N a^{-1} vs the concept of homeostasis in the fixed-nitrogen inventory a^{-1} vs the concept of homeostasis in the fixed-nitrogen inventory. *Biogeosciences*, 4:233–253, May 2007. doi: 10.5194/bg-4-233-2007.

L. A. Codispoti and J. P. Christensen. Nitrification, denitrification and nitrous oxide cycling in the Eastern Tropical South Pacific Ocean. *Mar. Chem.*, 16:277–300, 1985. doi: 10.1016/0304-4203(85)90051-9.

L. A. Codispoti and T. Packard. Denitrification rates in the eastern tropical South Pacific. *J. Mar. Res*, 38(3):453–477, 1980.

L. A. Codispoti and F. A. Richards. An analysis of the horizontal regime of denitrification in the eastern tropical North Pacific. *Limnol. Oceanogr.*, 21(3):379–388, May 1976.

L. A. Codispoti, J. Brandes, J. Christensen, A. Devol, S. W. Naqvi, H. Paerl, and T. Yoshinari. The oceanic fixed nitrogen and nitrous oxide budgets: Moving targets as we enter the anthropocene? *Sci. Mar.*, 65(S2), 2001. doi: 10.3989/scimar.2001.65s285.

S. E. Cornella, T. D. Jickells, J. N. Cape, A. P. Rowland, and R. A. Duce. Organic nitrogen deposition on land and coastal environments: a review of methods and data. *Atmos. Environ.*, 37:2173–2191, 2003. doi: 10.1016/S1352-2310(03)00133-X.

J. B. Cotner, Jr. and R. G. Wetzel. Uptake of dissolved inorganic and organic bphosphorus compounds by phytoplankton and bacterioplankton. *Limnol. Oceanogr.*, 37(2):232–243, 1992. doi: 10.4319/lo.1992.37.2.0232.

R. Czeschel, L. Stramma, F. U. Schwarzkopf, B. S. Giese, A. Funk, and J. Karstensen. Middepth circulation of the eastern tropical south pacific and its link to the oxygen minimum zone. *J. Geophys. Res.*, 116(C01015):1–13, Jan. 2011. doi: 10.1029/2010JC006565.

T. Dalsgaard, B. Thamdrup, and D. E. Canfield. Anaerobic ammonium oxidation (anammox) in the marine environment. *Res. Microbiol.*, 156(4):457 – 464, 2005. doi: 10.1016/j.resmic.2005.01.011.

F. Dentener, J. Drevet, J. F. Lamarque, I. Bey, B. Eickhout, A. M. Fiore, D. Hauglustaine, L. W. Horowitz, M. Krol, U. C. Kulshrestha, M. Lawrence, C. Galy-Lacaux, S. Rast, D. Shindell, D. Stevenson, T. V. Noije, C. Atherton, N. Bell, D. Bergman, T. Butler, J. Cofala, B. Collins, R. Doherty, K. Ellingsen, J. Galloway, M. Gauss, V. Montanaro, J. F. Müller, G. Pitari, J. Rodriguez, M. Sanderson, F. Solmon, S. Strahan, M. Schultz, K. Sudo, S. Szopa, and O. Wild. Nitrogen and sulfur deposition on regional and global scales: A multimodel evaluation. *Global Biogeochem. Cycles*, 20(GB4003):1–21, Oct. 2006. doi: 10.1029/2005GB002672.

C. Deutsch, N. Gruber, R. M. Key, J. L. . Sarmiento, and A. Ganachaud. Denitrification and N_2 fixation in the Pacific Ocean. *Global Biogeochem. Cycles*, 15(2):483–506, June 2001.

C. Deutsch, D. M. Sigman, R. C. Thunell, A. N. Meckler, and G. H. Haug. Isotopic constraints on glacial/interglacial changes in the oceanic nitrogen budget. *Global Biogeochem. Cycles*, 18 (GB4012):1–22, Oct. 2004. doi: 10.1029/2003GB002189.

C. Deutsch, J. L. Sarmiento, D. M. Sigman, N. Gruber, and J. P. Dunne. Spatial coupling of nitrogen inputs and losses in the ocean. *Nature*, 445(05392):163–167, Jan. 2007. doi: 10.1038/nature05392.

A. H. Devol. Direct measurement of nitrogen gas fluxes from continental shelf sediments. *Nature*, 349:319–321, Jan. 1991.

A. H. Devol. Solution to a marine mystery. *Nature*, 422:575–576, Apr. 2003.

A. H. Devol and H. E. Hartnett. Role of the oxygen-deficient zone in transfer of organic carbon to the deep ocean. *Limnol. Oceanogr.*, 46(7):1684–1690, 2001. doi: 10.4319/lo.2001.46.7.1684.

T. DeVries, C. Deutsch, F. Primeau, B. Chang, and A. Devol. Global rates of water-column denitrification derived from nitrogen gas measurements. *Nature*, 5:547–550, Aug. 2012. doi: 10.1038/NGEO1515.

T. DeVries, C. Deutsch, P. A. Rafter, and F. Primeau. Marine denitrification rates determined from a global 3-d inverse model. *Biogeosciences*, 10:2481–2496, Apr. 2013. doi: 10.5194/bg-10-2481-2013.

C. M. Duarte, J. Dachs, M. Llabrés, P. Alonso-Laita, J. M. Gasol, A. Tovar-Sánchez, S. S. nudo Wilhemy, and S. Agustí. Aerosol inputs enhance new production in the subtropical northeast atlantic. *J. Geophys. Res.*, 111(G04006):1–8, Nov. 2006.

R. A. Duce. The impact of atmospheric nitrogen, phosphorus, and iron species on marine biological productivity. In P. Buat-Ménard, editor, *The Role of Air-Sea Exchange in Geochemical Cycling*, volume 185 of *NATO ASI Series*, pages 497–529. Springer, 1986.

R. A. Duce, P. S. Liss, J. T. Merrill, E. L. Atlas, P. Buat-Menard, B. B. Hicks, J. M. Miller, J. M. Prospero, R. . Arimoto, T. M. Church, W. Ellis, J. N. Galloway, L. Hansen, T. D. Jickells, A. H. Knap, K. H. Reinhardt, B. Schneider, A. Soudine, J. J. Tokos, S. Tsunogai, R. . Wollast, and M. Zhou. The atmospheric input of trace species to the world ocean. *Global Biogeochem. Cycles*, 5(3):193–259, Sep. 1991.

R. A. Duce, J. LaRoche, K. Altieri, K. R. Arrigo, A. R. Baker, D. G. Capone, S. Cornell, F. Dentener, J. Galloway, R. S. Ganeshram, R. J. Geider, T. Jickells, M. M. Kuypers, R. Langlois, P. S. Liss, S. M. Liu, J. J. Middelburg, C. M. Moore, S. Nickovic, A. Oschlies, T. Pedersen, J. Prospero, R. Schlitzer, S. Seitzinger, L. L. Sorensen, M. Uematsu, O. Ulloa, M. Voss, B. Ward, and

L. Zamora. Impacts of atmospheric anthropoganic nitrogen on the open ocean. *Science*, 320 (5878):893–897, May 2008.

J. Dunn. Cisro atlas of regional seas.

J. P. Dunne, R. A. Armstrong, A. Gnanadesikan, and J. L. Sarmiento. Empirical and mechanistic models for the particle export ratio. *Global Biogeochem. Cycles*, 19(GB4026):1–16, Dec. 2005. doi: 10.1029/2004GB002390.

V. Echevin, O. Aumont, J. Ledesma, and G. Flores. The seasonal cycle of surface chlorophyll in the peruvian upwelling system: A modelling study. *Prog. Oceanogr.*, 79:167–176, Oct. 2008.

V. Echevin, A. Albert, M. Lévy, M. Graco, O. Aumont, A. Piétri, and G. Garric. Intraseasonal variability of nearshore productivity in the northern humboldt current system: The role of coastal trapped waves. *Cont. Shelf Res.*, 73:14–30, 2014. doi: http://dx.doi.org/10.1016/j.csr.2013.11.015.

R. W. Eppley, J. N. Rogers, and J. J. McCarthy. Half-saturation constants for uptake of nitrate and ammonium by marine phytoplankton. *Limnol. Oceanogr.*, 14(6): 912–920, Nov. 1969. doi: 10.4319/lo.1969.14.6.0912CumulativeAnnual10.4319/lo.1969.14.6.0912CumulativeAnnual10.4319/lo.1969.14.6.0912.

O. Eugster and N. Gruber. A probabilistic estimate of global marine N-fixation and denitrification. *Global Biogeochem. Cycles*, 26(GB4013):1–15, Nov. 2012. doi: 10.1029/2012GB004300.

P. G. Falkowski. Evolution of the nitrogen cycle and its influence on the biological sequestration of CO_2 in the ocean. *Nature*, 387:272–275, May 1997.

P. G. Falkowski, R. T. Barber, and V. Smetacek. Biogeochemical Controls and Feedbacks on Ocean Primary Production. *Science*, 281:200–206, July 1998.

K. Fennel, J. Wilkin, J. Levin, J. Moisan, J. O'Reilly, , and D. Haidvogel. Nitrogen cycling in the Middle Atlantic Bight: Results from a three-dimensional model and implications for the North Atlantic nitrogen budget. *Global Biogeochem. Cycles*, 20(GB3007):1–14, July 2006. doi: 10.1029/2005GB002456.

C. Fernandez, L. Farías, and O. Ulloa. Nitrogen fixation in denitrified marine waters. *PLoS ONE*, 6(6):1–9, June 2011. doi: 10.1371/journal.pone.0020539.

S. Flögel, K. Wallmann, C. J. Poulsen, J. Zhou, A. Oschlies, S. Voigt, and W. Kuhnt. Simulating the biogeochemical effects of volcanic CO_2 degassing on the oxygen-state of the deep ocean during the Cenomanian/Turonian Anoxic Event (OAE2). *Earth Planet. Sci. Lett.*, 305:371–384, Apr. 2011.

R. A. Foster and J. P. Zehr. Characterization of diatom–cyanobacteria symbioses on the basis of nifH , hetR and 16s rRNA sequences. *Environ. Microbiol.*, 8(11):1913–1925, 2006. doi: 10.1111/j.1462-2920.2006.01068.x.

R. A. Foster, M. M. Kuypers, T. Vagner, R. W. Paerl, N. Musat, and J. P. Zehr. Nitrogen fixation and transfer in open ocean diatom–cyanobacterial symbioses. *Nature*, 5:1484–1493, Mar. 2011. doi: 10.1038/ismej.2011.26.

J. M. S. Franz, H. Hauss, U. Sommer, T. Dittmar, and U. Riebesell. Production, partitioning and stoichiometry of organic matter under variable nutrient supply during mesocosm experiments in the tropical Pacific and Atlantic Ocean. *Biogeosciences*, 9:4629–4643, Nov. 2012. doi: 10.5194/bg-9-4629-2012.

M. J. Furnas. In situ growth rates of marine phytoplankton: Approaches to measurement, community and species growth rates. *J. Plankton Res.*, 12(6):1117–1151, 1990. doi: 10.1093/plankt/12.6.1117.

J. N. Galloway, F. J. Dentener, D. G. Capone, E. W. Boyer, R. W. Howarth, S. P. Seitzinger, G. P. Asner, C. C. Cleveland, P. A. Green, E. A. Holland, D. M. Karl, A. F. Michaels, J. H. Porter, A. R. Townsend, and C. J. Vörösmarty. Nitrogen cycles: past, present and future. *Biogeochem.*, 70:153–226, 2004. doi: 10.1007/s10533-004-0370-0.

A. Ganachaud and C. Wunsch. Oceanic nutrients and oxygen transports and bounds on export production during the world ocean circulation experiment. *Global Biogeochem. Cycles*, 16(4): 1–14, Oct. 2002. doi: 10.1029/2000GB001333.

H. E. Garcia, R. A. Locarnini, T. P. Boyer, J. I. Antonov, O. K. Baranova, M. M. Zweng, and D. R. Johnson. Volume 3: Dissolved oxygen, apparent oxygen utilization, and oxygen saturation. In S. Levitus, editor, *World Ocean Atlas 2009*, page 344. NOAA Atlas NESDIS 70, U.S. Government Printing Office, Washington, D.C., 2010a.

H. E. Garcia, R. A. Locarnini, T. P. Boyer, J. I. Antonov, M. M. Zweng, O. K. Baranova, and D. R. Johnson. Volume 4: Nutrients (phosphate, nitrate, silicate). In S. Levitus, editor, *World Ocean Atlas 2009*, page 398. NOAA Atlas NESDIS 71, U.S. Government Printing Office, Washington, D.C., 2010b.

P. A. Green, C. J. Vörösmarty, M. Meyback, J. N. Galloway, B. J. Peterson, and E. W. Boyer. Pre-industrial and contemporary fluxes of nitrogen through rivers: a global assessment based on typology. *Biogeochem.*, 68:71–105, 2004.

T. Großkopf, W. Mohr, T. Baustian, H. Schunck, D. Gill, M. M. M. Kuypers, G. Lavik, R. A. Schmitz, D. W. R. Wallace, and J. LaRoche. Doubling of marine dinitrogen-fixation rates based on direct measurements. *Nature*, 488:361–364, Aug. 2012.

N. Gruber. The dynamics of the marine nitrogen cycle and its influence on atmospheric CO_2 variations. In M. Follows and T. Oguz, editors, *The Ocean Carbon Cycle and Climate*, volume 40 of *NATO Science Series*, chapter 4, pages 97–148. Kluwer Academic, P.O.Box 17,3300 AA Dordrecht, The Netherlands, 2004.

N. Gruber. *Nitrogen in the Marine Environment*, chapter The Marine Nitrogen Cycle: Overview and Challenges, pages 1–50. Elsevier Science Publishers, Amsterdam, 2008a. doi: 10.1016/B978-0-12-372522-6.00001-3.

N. Gruber. *Nitrogen in the Marine Environment*, chapter Coastal upwelling, pages 771–806. Elsevier Science Publishers, Amsterdam, 2008b. doi: 10.1016/B978-0-12-372522-6.00001-3.

N. Gruber and J. L. Sarmiento. Global patterns of marine nitrogen fixation and denitrification. *Global Biogeochem. Cycles*, 11:235–266, 1997. doi: 10.1029/97GB00077.

N. Gruber and J. L. Sarmiento. Large-scale biogeochemical-physical interactions in elemental cycles. In A. R. Robinson, J. J. Macarthy, B. J. Rothschild, J. Wiley, and Sons, editors, *Biogeochemical/physical interactions in elemental cycles*, volume 12 of *The sea*, chapter 9, pages 337–399. Harward University Press, 2002.

M. R. Hamersley, G. Lavik, D. Woebken, J. E. Rattray, P. Lam, E. C. Hopmans, J. S. S. Damsté, S. Krüger, M. Graco, D. Gutiérrez, and M. M. M. Kuypers. Anaerobic ammonium oxidation in the Peruvian oxygen minimum zone. *Limnol. Oceanogr.*, 52(3):923–933, May 2007. doi: 10.4319/lo.2007.52.3.0923.

J. Hellya and L. A. Levin. Global distribution of naturally occurring marine hypoxia on continental margins. *Deep-Sea Res. I*, 51:1159–1168, 2004. doi: 10.1016/j.dsr.2004.03.009.

C. M. Holl and J. P. Montoya. Interactions between nitrate uptake and nitrogen fixation in continuous cultures of the marine diazotroph *Trichodesmium* (cyanobacteria). *J. Phycol.*, 41: 1178–1183, 2005. doi: 10.1111/j.1529-8817.2005.00146.x.

B. Z. Houlton, Y.-P. Wang, P. M. Vitousek, and C. B. Field. A unifying framework for dinitrogen fixation in the terrestrial biosphere. *Nature*, 454:327–331, July 2008. doi: doi:10.1038/nature07028.

A. Huyer, M. Knoll, T. Paluszkiewicz, and R. L. Smith. The peru undercurrent: a study in variability. *Deep-Sea Res.*, 38:S247–S271, 1991. doi: 10.1016/S0198-0149(12)80012-4.

E. D. Ingall and R. Jahnke. Evidence for enhanced phosphorus regeneration from marine sediments overlain by oxygen depleted waters. *Geochim. Cosmochim. Acta*, 58(11):2671–2575, Mar. 1994.

E. D. Ingall, R. M. Bustin, and P. V. Cappellen. Influence of column anoxia on the burial and preservation of carbon and phosphorus in marine shales. *Geochim. Cosmochim. Acta*, 57: 303–316, June 1993.

X. Jin and N. Gruber. Offsetting the radiative benefit of ocean iron fertilization by enhancing N_2O emissions. *Geophys. Res. Lett.*, 30(24):1–4, Dec. 2003. doi: 10.1029/2003GL018458.

T. Kalvelage, G. Lavik, P. Lam, S. Contreras, L. Arteaga, C. R. Löscher, A. Oschlies, A. Paulmier, L. Stramma, and M. M. M. Kuypers. Nitrogen cycling driven by organic matter export in the South Pacific oxygen minimum zone. *Nature Geosci.*, 6:228–234, Mar. 2013. doi: 10.1038/NGEO1739.

D. Karl, R. Letelier, L. Tupas, J. Dore, J. Christian, and D. Hebel. The role of nitrogen fixation in biogeochemical cycling in the subtropical North Pacific Ocean. *Nature*, 388:533–536, Aug. 1997.

D. Karl, A. Michaels, B. Bergman, D. Capone, E. Carpenter, R. Letelier, F. lipschultz, H. P. D. Sigman, and L. Stal. Dinitrogen fixation in the world's oceans. *Biogeochemistry*, 57/58:47–98, 2002.

J. Karstensen, L. Stramma, and M. Visbeck. Oxygen minimum zones in the eastern tropical Atlantic and Pacific oceans. *Prog. Oceanogr.*, 77:331–350, Apr. 2008. doi: 10.1016/j.pocean.2007.05.009.

A. Kasai, S. Kimura, H. Nakata, and Y. Okazaki. Entrainment of coastal water into a frontal eddy of the kuroshio and its biological significance. *J. Mar. Syst.*, 37:185–198, Jan. 2002.

R. F. Keeling and H. E. Garcia. The change in oceanic O_2 inventory associated with recent global warming. *Proc. Natl. Acad. Sci. USA*, 99(12):7848–7853, June 2002.

R. M. Key, A. Kozyr, C. L. Sabine, K. Lee, R. Wanninkhof, J. L. Bullister, R. A. Feely, F. J. Millero, C. Mordy, and T.-H. Peng. A global ocean carbon climatology: Results from Global Data Analysis Project (GLODAP). *Global Biogeochem. Cycles*, 18(GB4031):1–23, Dec. 2004. doi: 10.1029/2004GB002247.

W. Koeve and P. Kähler. Heterotrophic denitrification vs. autotrophic anammox – quantifying collateral effects on the oceanic carbon cycle. *Biogeosciences*, 7:2327–2337, Aug. 2010.

A. Krishnamurthy, J. K. Moore, C. S. Zender, and C. Luo. Effects of atmospheric inorganic nitrogen deposition on ocean biogeochemistry. *J. Geophys. Res.*, 112(G02019):1–10, May 2007. doi: 10.1029/2006JG000334.

A. Krishnamurthy, J. K. Moore, N. Mahowald, C. Luo, S. C. Doney, K. Lindsay, and C. S. Zender. Impacts of increasing anthropogenic soluble iron and nitrogen deposition on ocean biogeochemistry. *Global Biogeochem. Cycles*, 23(GB3016):1–15, Aug. 2009. doi: 10.1029/2008GB003440.

A. Krishnamurthy, J. K. Moore, N. Mahowald, C. Luo, , and C. S. Zender. Impacts of atmospheric nutrient inputs on marine biogeochemistry. *J. Geophys. Res.*, 115(G01006):1–13, Feb. 2010. doi: 10.1029/2009JG001115.

M. M. M. Kuypers, A. O. Sliekers, G. Lavik, M. Schmid, B. B. Jørgensen, J. G. Kuenen, J. S. S. Damste, M. Strous, and M. S. M. Jetten. Anaerobic ammonium oxidation by anammox bacteria in the Black Sea. *Nature*, 422(10):608–611, Apr. 2003.

M. M. M. Kuypers, G. Lavik, D. Woebken, M. Schmid, B. M. Fuchs, R. Amann, B. B. Jørgensen, and M. S. M. Jetten. Massive nitrogen loss from the Benguela upwelling system through anaerobic ammonium oxidation. *Proc. Natl. Acad. Sci. USA*, 102(18):6478–6483, May 2005. doi: 10.1073/pnas.0502088102.

P. Lam, G. Lavika, M. M. Jensena, J. van de Vossenberg, M. Schmidb, D. Woebkena, D. Gutiérrezc, R. Amanna, M. S. M. Jettenb, and M. M. M. Kuypersa. Revising the nitrogen cycle in the Peruvian oxygen minimum zone. *Proc. Natl. Acad. Sci. USA*, 106(12):4752–4757, Mar. 2009. doi: 10.1073/pnas.0812444106.

J.-F. Lamarque, G. P. Kyle, M. Meinshausen, K. Riahi, S. J. Smith, D. P. van Vuuren, A. J. Conley, and F. Vitt. Global and regional evolution of short-lived radiatively-active gases and aerosols in the Representative Concentration Pathways. *Climatic Change*, 109:191–121, Aug. 2011. doi: 10.1007/s10584-011-0155-0.

A. Landolfi, H. Dietze, W. Koeve, and A. Oschlies. Overlooked runaway feedback in the marine nitrogen cycle: the vicious cycle. *Biogeosciences*, 10:1351–1363, Mar. 2013. doi: 10.5194/bg-10-1351-2013.

W. G. Large, J. C. McWilliams, and S. C. Done. Oceanic vertical mixing: A review and a model with a nonlocal boundary layer. *Rev. Geophys.*, 32:363–403, Nov. 1994. doi: 10.1029/94RG01872.

J. LaRoche and E. Breitbarth. Importance of the diazotrophs as a source of new nitrogen in the ocean. *J. Sea Res.*, 53:67–91, 2005. doi: 10.1016/j.seares.2004.05.005.

E. A. Laws, P. G. Falkowski, W. O. S. Jr., H. Ducklow, and J. J.McCart. Temperature effects on export production in the open ocean. *Global Biogeochem. Cycles*, 14(4):1231–1246, Dec. 2000.

T. M. Lenton and A. J. Watson. Redfield revisited 1. Regulation of nitrate, phosphate, and oxygen in the ocean. *Global Biogeochem. Cycles*, 14(1):225–248, March 2000. doi: 10.1029/1999GB900065.

W. F. Libby. Radiocarbon dating. *Amer. Sci.*, 44(1):98–112, Jan. 1956.

K.-K. Liu and I. R. Kaplan. Denitrification rates and availability of organic matter in marine environments. *Earth Planet. Sci. Lett.*, 68:88–100, 1984. doi: 10.1016/0012-821X(84)90142-0.

W. T. Liu, W. Tang, and P. S. Polito. Nasa scatterometer provides global ocean-surface wind fields with more structures than numerical weather prediction. *Geophys. Res. Lett.*, 25(6):761–764, 1998. doi: 10.1029/98GL00544.

P. J. Llanillo, J. Karstensen, J. L. Pelegrí, and L. Stramma. Physical and biogeochemical forcing of oxygen and nitrate changes during El Niño/El Viejo and la niã/la Vieja upper-ocean phases in the tropical eastern South Pacific along 86°w. *Biogeosciences*, 10:6339–6355, Oct. 2013. doi: 10.5194/bg-10-6339-2013.

R. A. Locarnini, A. V. Mishonov, J. I. Antonov, T. P. Boyer, H. E. Garcia, O. K. Baranova, M. M. Zweng, and D. R. Johnson. Volume 1: Temperature. In S. Levitus, editor, *World Ocean Atlas 2009*, page 184. NOAA Atlas NESDIS 68, U.S. Government Printing Office, Washington, D.C., 2010.

R. Lukas. The termination of the equatorial undercurrent in the Eastern Pacific. *Prog. Oceanogr.*, 16:63–90, 1986. doi: 10.1016/0079-6611(86)90007-8.

N. Mahowald, T. D. Jickells, A. R. Baker, P. Artaxo, C. R. Benitez-Nelson, G. Bergametti, T. C. Bond, Y. Chen, D. D. Cohen, B. Herut, N. Kubilay, R. Losno, C. Luo, W. Maenhaut, K. A. McGee, G. S. Okin, R. L. Siefert, , and S. Tsukuda. Global distribution of atmospheric phosphorus sources, concentrations and deposition rates, and anthropogenic impacts. *Global Biogeochem. Cycles*, 22(GB4026):1–19, Dec. 2008. doi: 10.1029/2008GB003240.

J. H. Martin, G. A. Knauer, D. M. Karl, and W. W. Broenkow. VERTEX: carbon cycling in the northeast pacific. *Deep-Sea Res.*, 34(2):267–285, 1987.

C. D. McAllister, N. Shah, and J. D. H. Strickland. Marine phytoplankton photosynthesis as a function of light intensity: A comparison of methods. *J. Fish. Res. Board Can.*, 21:159–181, 1964. doi: 10.1139/f64-010.

M. M. Mills and K. R. Arrigo. Magnitude of oceanic nitrogen fixation influenced by the nutrient uptake ratio of phytoplankton. *Nature Geosci.*, 3:412–416, June 2010. doi: 10.1038/NGEO856.

M. M. Mills, C. Ridame, M. Davey, J. LaRoche, and R. J. Geider. Iron and phosphorus co-limit nitrogen fixation in the eastern tropical North Atlantic. *Nature*, 429:292–232, May 2004. doi: 10.1038/nature02550.

V. Molina and L. Farás. Aerobic ammonium oxidation in the oxycline and oxygen minimum zone of the eastern tropical South Pacific off northern Chile (∼20 °S). *Deep-Sea Res. II*, 56(16): 1032–1041, 2009. doi: 10.1016/j.dsr2.2008.09.006.

F. M. Monteiro, M. J. Follows, and S. Dutkiewicz. Distribution of diverse nitrogen fixers in the global ocean. *Global Biogeochem. Cycles*, 24(GB3017):1–16, Sep. 2010. doi: 10.1029/2009GB003731.

I. Montes, F. Colas, X. Capet, and W. Schneider. On the pathways of the equatorial subsurface currents in the eastern equatorial Pacific and their contributions to the Peru-Chile Undercurrent. *J. Geophys. Res.*, 115(C09003):1–16, Sep. 2010. doi: 10.1029/2009JC005710.

I. Montes, W. Schneider, F. Colas, B. Blanke, and V. Echevin. Subsurface connections in the eastern tropical pacific during la niña 1999–2001 and el niño 2002–2003. *J. Geophys. Res.*, 116 (C12022):1–18, Dec. 2011. doi: doi:10.1029/2011JC007624.

J. P. Montoya, C. M. Holl, J. P. Zehr, A. Hansen, T. A. Villareal, and D. G. Capone. High rates of N_2 fixation by unicellular diazotrophs in the oligotrophic Pacific Ocean. *Nature*, 430: 1027–1031, Aug. 2004. doi: 10.1038/nature02824.

C. M. Moore, M. M. Mills, K. R. Arrigo, I. Berman-Frank, L. Bopp, P. W. Boyd, E. D. Galbraith, R. J. Geider, C. Guieu, S. L. Jaccard, T. D. Jickells, J. LaRoche, T. M. Lenton, N. M. Mahowald, E. Marañón, I. Marinov, J. K. Moore, T. Nakatsuka, A. Oschlies, M. A. Saito, T. F. Thingstad, A. Tsuda, and O. Ulloa. Processes and patterns of oceanic nutrient limitation. *Nature Geosci.*, pages 1–10, Mar. 2013. doi: 10.1038/NGEO1765.

J. K. Moore and O. Braucher. Sedimentary and mineral dust sources of dissolved iron to the world ocean. *Biogeosciences*, 5:631–656, May 2008. doi: 10.5194/bg-5-631-2008.

J. K. Moore and S. C. Doney. Iron availability limits the ocean nitrogen inventory stabilizing feedbacks between marine denitrification and nitrogen fixation. *Global Biogeochem. Cycles*, 21(GB2001):1–12, Apr. 2007. doi: 10.1029/2006GB002762.

J. Morrison, L. Codispoti, S. L. Smith, K. Wishner, C. Flagg, W. D. Gardner, S. Gaurin, S. Naqvi, V. Manghnani, L. Prosperie, and J. S. Gundersen. The oxygen minimum zone in the Arabian Sea during 1995. *Deep-Sea Res. II*, 46:1903–1931, Aug. 1999.

J. M. Morrison, L. A. Codispoti, S. Gaurin, B. Jones, V. Manghnani, and Z. Zheng. Seasonal variation of hydrographic and nutrient fields during the US JGOFS Arabian Sea Process Study. *Deep-Sea Res. II*, 45:2053–2101, 1998. doi: 10.1016/S0967-0645(98)00063-0.

B. Mouriño-Carballido, M. Pahlow, and A. Oschlies. High sensitivity of ultra-oligotrophic marine ecosystems to atmospheric nitrogen deposition. *Geophys. Res. Lett.*, 39(L05601):1–6, March 2012. doi: 10.1029/2011GL050606.

G. S. Okin, A. R. Baker, I. Tegen, N. M. Mahowald, F. J. Dentener, R. A. Duce, J. N. Galloway, K. Hunter, M. Kanakidou, N. Kubilay, J. M. Prospero, M. Sarin, V. Surapipith, M. Uematsu, and T. Zhu. Impacts of atmospheric nutrient deposition on marine productivity: Roles of nitrogen, phosphorus, and iron. *Global Biogeochem. Cycles*, 25(GB2022):1–10, June 2011.

H. W. Paerl and D. R. Whitall. Anthropogenically-derived atmospheric nitrogen deposition, marine eutrophication and harmful algal bloom expansion: Is there a link? *Ambio*, 28: 307–311, 1999.

M. Pahlow and A. F. Vézina. Adaptive model of dom dynamics in the surface ocean. *J. Mar. Res.*, 61:127–146, 2003.

J. R. Palmer and I. J. Totterdell. Production and export in a global ocean ecosystem model. *Deep-Sea Res. I*, 48:1169–1198, 2001. doi: 10.1016/S0967-0637(00)00080-7.

A. Paulmier and D. Ruiz-Pino. Oxygen minimum zones (OMZs) in the modern ocean. *Prog. Oceanogr.*, 80:113–128, 2009. doi: 10.1016/j.pocean.2008.08.001.

A. Paulmier, D. Ruiz-Pino, V. Garçon, and L. Farías. Maintaining of the Eastern South Pacific Oxygen Minimum Zone (OMZ) off Chile. *Geophys. Res. Lett.*, 33(L20601):1–6, Oct. 2006. doi: 10.1029/2006GL026801.

P. Penven, V. Echevin, J. Pasapera, F. Colas, and J. Tam. Average circulation, seasonal cycle, and mesoscale dynamics of the peru current systems: A modeling approach. *J. Geophys. Res.*, 110 (C10021):1–21, Oct. 2005. doi: 10.1029/2005JC002945.

P. Penven, P. Marchesiello, L. Debreu, and J. Lefèvre. Software tools for pre- and post-processing of oceanic regional simulations. *Environ. Model. Softw.*, pages 1–3, July 2008. doi: 10.1016/j.envsoft.2007.07.004.

P. Penven, G. Cambon, T.-A. Tan, P. Marchesiello, and L. Debreu. *ROMS_AGRIF/ROMSTOOLS User's Guide*. Institut de Recherche pour le Développement (IRD), 44 Boulevard de Dunkerque CS 90009 13572 Marseille cedex 02 France, July 2010.

D. S. Reay, F. Dentener, P. Smith, J. Grace, and R. A. Feely. Global nitrogen depisition and carbon sinks. *Nature Geosci.*, 1:430–437, July 2008.

A. C. Redfield. On the proportions of organic derivations in sea water and their relation to the composition of plankton. *University Press of Liverpool*, James Johnstone Memorial:177–192, 1934.

A. C. Redfield, B. H. Ketchum, and F. A. Richards. *The influence of organisms on the composition of sea-water*. Interscience, 1963.

J. L. Reid. On the total geostrophic circulation of the pacific ocean: flow patterns, tracers, and transports. *Prog. Oceanogr.*, 39(4):263–252, 1997.

K. R. Ridgway, J. R. Dunn, and J. L. Wilkin. Ocean interpolation by four-dimensional least squares -application to the waters around australia. *J. Atmos. Ocean. Technol.*, 19(9): 1357–1375, 2002.

R. D. Robarts and T. Zohary. Temperature effects on photosynthetic capacity, respiration, and growth rates of bloom forming cyanobacteria. *N. Z. J. Mar. Freshwat. Res.*, 21(3):391–399, 1987. doi: 10.1080/00288330.1987.9516235.

K. C. Ruttenberg. *The global phosphorus cycle*, volume 8, chapter The global phosphorus cycle, pages 585–643. Elsevier, 2003.

A. Schmittner, A. Oschlies, H. D. Matthews, and E. D. Galbraith. Future changes in climate, ocean circulation, ecosystems, and biogeochemical cycling simulated for a business-as-usual CO_2 emission scenario until year 4000 AD. *Global Biogeochem. Cycles*, 22(GB1013):1–21, 2008. doi: 10.1029/2007GB002953.

W. Schneider, R. Fuenzalida, E. Rodrǵuez-Rubio, and J. Garcés-Vargas. Characteristics and formation of Eastern South Pacific Intermediate Water. *Geophys. Res. Lett.*, 30(11):1–4, June 2003. doi: 10.1029/2003GL017086.

S. P. Seitzinger and R. W. Sanders. Atmospheric inputs of dissolved organic nitrogen stimulate estuarine bacteria and phytoplankton. *Limnol. Oceanogr.*, 44:721–730, 1999.

S. P. Seitzinger, J. A. Harrison, E. D. Arthur, H. W. Beusen, and A. F. Bouwman. Sources and delivery of carbon, nitrogen, and phosphorus to the coastal zone: An overview of global nutrient export from Watersheds (NEWS) models and their application. *Global Biogeochem. Cycles*, 19(GB4S01):1–11, Dec. 2005. doi: 10.1029/2005GB002606.

S. P. Seitzinger, E. Mayorga, A. F. Bouwman, C. Kroeze, A. H. W. Beusen, G. Billen, G. V. Drecht, E. Dumont, B. M. Fekete, J. Garnier, , and J. A. Harrison. Global river nutrient export: A scenario analysis of past and future trends. *Global Biogeochem. Cycles*, 24(GB0A08):1–16, May 2010.

G. Shaffer and J. L. Sarmiento. Biogeochemical cycling in the global ocean 1. A new, analytical model with continuous vertical resolution and high-latitude dynamics. *J. Geophys. Res.*, 100 (C2):2659–2672, Feb. 1995. doi: 10.1029/94JC01167.

A. F. Shchepetkin and J. C. McWilliams. The regional oceanic modeling system (ROMS): a split-explicit, free-surface, topography-following-coordinate oceanic model. *Ocean Model.*, 9:347–404, Sep. 2005. doi: 10.1016/j.ocemod.2004.08.002.

A. F. Shchepetkin and J. C. McWilliams. Correction and commentary for "ocean forecasting in terrain-following coordinates: Formulation and skill assessment of the regional ocean modeling system" by haidvogel et al., j. comp. phys. 227, pp. 3595–3624. *J. Comput. Phys.*, 228: 8985–9000, 2009. doi: 10.1016/j.jcp.2009.09.002.

A. M. D. Silva, C. C. Young, and S. Levitus, editors. *Atlas of Surface Marine Data 1994*, volume 1, chapter Atlas of Surface Marine Data 1994. NOAA Atlas NESDIS 6. U.S. Department of Commerce, NOAA, NESDIS., 1994.

C. P. Slomp and P. Van Cappellen. The global marine phosphorus cycle: sensitivity to oceanic circulation. *Biogeosciences*, 4:155–171, Feb. 2007. doi: 10.5194/bg-4-155-2007.

W. H. F. Smith and D. T. Sandwell. Global sea floor topography from satellite altimetry and ship depth soundings. *Science*, 277(5334):1956–1962, Sep. 1997. doi: 10.1126/science.277.5334.1956.

C. J. Somes, A. Schmittner, E. D. Galbraith, M. F. Lehmann, M. A. Altabet, J. P. Montoya, R. M. Letelier, A. C. Mix, A. Bourbonnais, and M. Eby. Simulating the global distribution of nitrogen isotopes in the ocean. *Global Biogeochem. Cycles*, 24(GB4019):1–16, Nov. 2010.

C. J. Somes, A. Oschlies, and A. Schmittner. Isotopic constraints on the pre-industrial oceanic nitrogen budget. *Biogeosciences*, 10:5889–5910, Sep. 2013.

J. H. Steele. Incorporating the microbial loop in a simple plankton model. *Proc. R. Soc. Lond. B*, 265:1771–1777, June 1998.

L. Stramma, G. C. Johnson, J. Sprintall, and V. Mohrholz. Expanding Oxygen-Minimum Zones in the Tropical Oceans. *Science*, 320:655–658, May 2008.

L. Stramma, G. C. Johnson, E. Firing, and S. Schmidtko. Eastern Pacific oxygen minimum zones: Supply paths and multidecadal changes. *J. Geophys. Res.*, 115(C09011):1–12, Sep. 2010. doi: 10.1029/2009JC005976.

L. Stramma, A. Oschlies, and S. Schmidtko. Mismatch between observed and modeled trends in dissolved upper-ocean oxygen over the last 50 yr. *Biogeosciences*, 9:4045–4057, Oct. 2012. doi: 10.5194/bg-9-4045-2012.

P. T. Strub, J. M. Mesías, V. Montecino, J. Rutllant, and S. Salinas. Coastal ocean circulation off western south america coast segment. In A. R. Robinson and K. H. Brink, editors, *The Sea*, volume 11, chapter 10, pages 273–313. John Wiley and Sons, 1998.

B. Su, M. Pahlow, H. Wagner, and A. Oschlies. What prevents nitrogen depletion in the oxygen minimum zone of the eastern tropical South Pacific? *Biogeosciences*, 12:1113–1130, February 2015. doi: 10.5194/bg-12-1113-2015.

E. Suess. Particulate organic carbon flux in the oceanssurface productivity and oxygen utilization. *Nature*, 288:260–263, Nov. 1980. doi: 10.1038/288260a0.

K. E. Taylor. Summarizing multiple aspects of model performance in a single diagram. *J. Geophys. Res.*, 106(D7):7183–7192, Apr. 2001. doi: 10.1029/2000JD900719.

J. R. Toggweiler, K. Dixon, and K. Bryan. Simulations of radiocarbon in a coarse-resolution world ocean model 1. Steady state prebomb distributions. *J. Geophys. Res.*, 94(C6):8217–8242, June 1989. doi: 10.1029/JC094iC06p08217.

M. Tomczak and J. S. Godfrey. *Regional Oceanography: an Introduction*. Daya Publishing House, Delhi, 2nd edition, 2003.

T. Tyrrell. The relative influences of nitrogen and phosphorus on oceanic primary production. *Nature*, 400:525–531, Aug. 1999.

P. Van Cappellen and E. D. Ingall. Benthic phosphorus regeneration, net primary production, and ocean anoxia: A model of the coupled marine biogeochemical cycles of carbon and phosphorus. *Paleoceanography*, 9(5):677–692, Oct. 1994.

B. A. S. Van Mooy, R. G. Keil, and A. H. Devol. Impact of suboxia on sinking particulate organic carbon: Enhanced carbon flux and preferential degradation of amino acids via denitrification. *Geochim. Cosmochim. Acta*, 66(3):457–467, 2002. doi: 10.1016/S0016-7037(01)00787-6.

M. Voss, J. W. Dippner, and J. P. Montoya. Nitrogen isotope patterns in the oxygen-deficient waters of the Eastern Tropical North Pacific Ocean. *Deep-Sea Res. I*, 48:1905–1921, 2001. doi: 10.1016/S0967-0637(00)00110-2.

K. Wallmann. Feedbacks between oceanic redox states and marine productivity: A model perspective focused on benthic phosphorus cycling. *Global Biogeochem. Cycles*, 17(3):1–10, Aug. 2003.

K. Wallmann. Phosphorus imbalance in the global ocean. *Global Biogeochem. Cycles*, 24 (GB4030):1–12, December 2010. doi: 10.1029/2009GB003643.

C. Wang and P. C. Fiedler. Enso variability and the eastern tropical pacific: A review. *proc*, 69: 239–266, May 2006. doi: 10.1016/j.pocean.2006.03.004.

B. B. Ward, A. H. Devol, J. J. Rich, B. X. Chang, S. E. Bulow, H. Naik, A. Pratihary, and A. Jayakumar. Denitrification as the dominant nitrogen loss process in the Arabian Sea. *Nature*, 461: 78–81, 2009. doi: 10.1038/nature08276.

P. Warneck. *Chemistry of the natural atmosphere*, volume 71 of *International geophysics series*. Elsevier, 1988.

J. Wu, W. Sunda, E. A. Boyle, and D. M. Karl. Phosphate depletion in the western north atlantic ocean. *Science*, 289:759–762, Aug. 2000. doi: 10.1126/science.289.5480.759.

K. Wyrtki. *The horizontal and vertical field of motion in the Peru Current*, volume 8 of *Bulletin of the Scripps Institution of Oceanography, La Jolla, California*. Berkeley : University of California Press, 1963.

Y. Ye, C. Völker, A. Bracher, BettinaTaylor, and D. A.Wolf-Gladrow. Environmental controls on N_2 fixation by Trichodesmium in thetropical eastern North Atlantic Ocean—A model-based study. *Deep-Sea Res. I*, 64:104–117, Jan. 2012. doi: 10.1016/j.dsr.2012.01.004.

L. Zamora, D. Hansell, and J. Prospero. The organic nitrogen deposition fraction of deposition over the North Atlantic. *Geochim. Cosmochim. Acta*, 73((13, Supplement 1)), 2009.

L. M. Zamora, A. Landolfi, A. Oschlies, D. A. Hansell, H. Dietze, and F. Dentener. Atmospheric deposition of nutrients and excess N formation in the North Atlantic. *Biogeosciences*, 7:777–793, February 2010. doi: 10.5194/bg-7-777-2010.

L. M. Zamora, J. M. Prospero, and D. A. Hansell. Organic nitrogen in aerosols and precipitation at Barbados and Miami: Implications regarding sources, transport and deposition to the western subtropical North Atlantic. *J. Geophys. Res.*, 116(D20309):1–17, Oct. 2011. doi: 10.1029/2011JD015660.

List of Figures

List of Tables

Acknowledgement

When coming to the end of this long, fantastic, and challenging journey, I can not and never forget all those who have helped, supported and encouraged me during accomplishing this thesis.

I am very grateful to Andreas Oschlies for accepting me as a PhD-student in his group, and fulfilling my wish to do research in GEOMAR. I would also like to thank for all the scientific and financial supports during my PhD whenever they are needed, which give me chances to experience the beauty and interest of science. Special thanks to him for giving me support when I have difficulties in work.

Special thanks to Markus Pahlow for many things. Firstly, for always having time and patience for my questions and discussions; secondly, for the huge encouragement, guidance and advice whenever I need or ask for; thirdly, for all the contributions to my thesis and technical help which is always in time; fourthly, for sharing the lunch time with me in the last few years.

Many thanks to Friedrike Prowe, Yonss Jose, Alexandra Marki and Ivonne Montes for the emotional and scientific help during my journey, and being good friends and colleagues of me. I also would like to thank Hannes Wagner for the scientific discussion and encouragement during the revision of my first publication during PhD. Thanks to Christoph Somes, Wolfgang Koeve, Lauren Zamora, Paul Kahler and Lionel Arteaga for the immediate help in work when needed.

Thanks to Jan Taucher, Fabian Reich, Annika Eisele, Daniel Romero-Mujalli and Helene Krieg for providing friendly atmosphere as my lovely officemates. Also many thanks to Helene Krieg for helping translate my summary into german.

Thank you, my dear parents and friends, Naicheng, Shuchan, Antje, Klaus, Shihao, Yong and Jiajun, for all your support during finishing this dissertation.

I am grateful to Chinese Scholarship Council (CSC), SFB754 (Sonderforschungsbereich 754,"Climate-Biogeochemistry Interactions in the Tropical Ocean") and ISOS (Integrated school of Ocean Science) for the financial support.

At the end, I would like to thank all members of the Biogeochemical Modeling Department at GEOMAR in kiel, for being friendly and professional colleagues during my PhD.

Declaration

Bei Su, declares that the design and content of this thesis, apart from my supervisors' guidance, are my own work except as stated below:
Computation setting in the computing-station of the Kiel University, scientific suggestions from all my coauthors for the published and submitted manuscripts.

The thesis has not been submitted either partially or wholly to apply for doctoral degree to any other examining body. And it has been prepared following the Rules of Good Scientific Practice of the German Research Foundation.

Kiel, April 27, 2015

Bei Su